SNAKE BIOMECHANICS AND LOCOMOTION

A Dissertation

Presented to

The Graduate Faculty of The University of Akron

In Partial Fulfillment

Of the Requirements for the Degree

Doctor of Philosophy

Derek Jurestovsky

May, 2022

SNAKE BIOMECHANICS AND LOCOMOTION

Derek Jurestovsky

Dissertation

Approved:

_____
Advisor
Dr. Henry Astley

_____
Committee Member
Dr. Peter Niewiarowski

_____
Committee Member
Dr. Joel Duff

_____
Committee Member
Dr. Janna Andronowski

_____
Committee Member
Dr. Chen Li

Accepted:

_____
Program Director, Integrated Bioscience
Dr. Hazel Barton

_____
Dean of the College
Dr. Mitchell McKinney

_____
Interim Director, Graduate School
Dr. Marnie Saunders

_____
Date

ABSTRACT

Snakes are one of the most successful and speciose extant reptiles on the planet. Despite this success, our knowledge of their biomechanics, musculature, and locomotion in these limbless vertebrates is surprisingly limited. This dissertation was undertaken to fill in some of these gaps in the literature. We analyzed snake vertebral range of motion, measured sarcomere lengths of their muscles, determined a new method of propulsion in limbless locomotion, and measured forces and kinematics during snake strikes.

The zygosphene is a unique process in snake vertebrae with an unknown function. We found that the zygosphene prevents the vertebrae from reaching positions where roll would occur across all species analyzed. This process, in combination with the pre- and postzygapophyses, acts to allow snakes a wide range of motion while maintaining structural stability. Vertebral stability is exceedingly important in limbless taxa that rely upon their vertebral column to interact with the natural world.

Sarcomeres are the fundamental component of muscle. We found that despite variations in mass, position along the body, and muscle analyzed, the sarcomere lengths were remarkably consistent across all variables in corn snakes (*P. guttatus*). The sarcomeres were positioned along the descending limb and ended on the ascending limb with only a handful ending on the plateau of the length-tension curve. These values

are consistent with being advantageous for constricting snakes allowing maximal force generation at contracted muscle positions making it difficult for a prey item to escape.

The natural world is full of complex three dimensional landscapes. Snakes have developed multiple modes of locomotion that are well described to navigate this complex world. However, we found a new method of limbless locomotion in corn snakes that makes use of vertical bends to generate forward propulsion. These vertical waves allow snakes to interact with their world in a new dimension, previously undescribed, to take advantage of vertical asperities and interact with the environment in a more dynamic way.

Finally, to capture prey snakes strike quickly which is indispensable to their survival. We found that snake strikes in blood pythons, *P. brongersmai*, between an open and walled setup did not differ significantly in any metrics we analyzed excepting lateral force. Snakes achieved similar performance between the two setups by using their posterior body segments swinging backwards to overcome limitations imposed by static friction between the substrate and their scales.

In conclusion, my research provides a detailed investigation into the biomechanics and locomotion of a variety of aspects of limbless locomotion. My research includes vertebral range of motion, sarcomere lengths in relation to the length-tension curve, vertical undulation to generate forward propulsion, and the forces during snake strikes. This work is designed to fill in some of the gaps in the limbless locomotion literature and provide the groundwork for future analyses to better understand limbless locomotion.

DEDICATION

This dissertation is dedicated to my wife and son who helped support me and keep me sane throughout my PhD. Additionally, I dedicate this to my family and friends who encouraged and supported me throughout my education.

ACKNOWLEDGEMENTS

I would like to thank multiple people who have assisted me in these projects. I am thankful for the contributions made by multiple coauthors including Bruce Jayne for providing bending measurements in a variety of snake species and helpful comments, Logan Usher for assisting the calibration of the force sensors and help with running vertical undulation trials, and finally Sid Joy for assistance with strike trials. I would like to thank Dr. Katelyn Sondereker for help with analyzing μCT scans. I was able to take multiple μCT scans with the assistance of Drs. George Nikolov and Andrew Knoll. Museum specimens were kindly loaned to us from both the American Museum of Natural History and the University of Michigan. I would also like to thank Dr. Jim Mead and Sandy Swift for their encouragement and getting me started with the enigmatic group of snakes. This dissertation has been improved by helpful and thoughtful comments and feedback from my committee. I would like to thank my fellow graduate students during my time at The University of Akron and fellow students in the Astley Lab for their help with multiple aspects of these projects and general discussions productive or otherwise. This work was partially supported by an NSF award #2045581.

TABLE OF CONTENTS

Page

LIST OF TABLES x

LIST OF FIGURES xi

CHAPTER

I. INTRODUCTION 1

II. EXPERIMENTAL MODIFICATION OF MORPHOLOGY REVEALS THE EFFECTS OF THE ZYGOSPHENE-ZYGANTRUM JOINT ON THE RANGE OF MOTION OF SNAKE VERTEBRAE 13

Introduction 13

Materials & Methods 17

Results 25

Discussion 31

III. ONTOGENETIC SERIES OF SARCOMERE MEASUREMENTS IN THE CORN SNAKE (*Pantherophis guttatus*) ARE PREDOMINANTLY ON THE DESCENDING LIMB OF THE LENGTH-TENSION CURVE 38

Introduction 38

Materials & Methods 40

Results 42

Discussion 45

IV. GENERATION OF PROPULSIVE FORCE VIA VERTICAL UNDULATIONS IN SNAKES 50

Introduction 50

Materials & Methods 51

Results 58

Discussion 62

V. BLOOD PYTHONS (*Python brongersmai*) STRIKE KINEMATICS AND FORCES ARE ROBUST TO VARIATIONS IN SUBSTRATE GEOMETRY 65

Introduction 65

Materials & Methods 67

Results 70

Discussion 74

VI. CONCLUSION 77

LITERATURE CITED 80

APPENDICES 95

APPENDIX A. NORMAL (GRAY) AND ALTERED (RED) VERTEBRAE OF SNAKES 96

APPENDIX B. OVERLAP OF THE YAW-PITCH ROM BETWEEN THE NORMAL VERTEBRA AND THE HIGH ROLL OF ITS CORRESPONDING ALTERED VERTEBRA 97

APPENDIX C. OVERLAP OF YAW-PITCH ROM BETWEEN SPECIES NORMAL VERTEBRAE 98

APPENDIX D. OVERLAP OF YAW-PITCH ROM BETWEEN SPECIES ALTERED VERTEBRAE 99

APPENDIX E. PERCENT OVERLAP OF NORMAL YAW-PITCH ROM 100

APPENDIX F. PERCENT OVERLAP OF ALTERED YAW-PITCH ROM 101

APPENDIX G. SUMMARY OF THE FORCE PLOTS IN ALL SNAKE TRIALS 102

APPENDIX H. SUMMARY OF THE FORCE PLOTS IN ALL ROPE TRIALS 103

APPENDIX I. TRIALS WITH MINIMAL-TO-NO PROPULSIVE FORCE..... 104

APPENDIX J. REACTION FORCES OF THE CORN SNAKES ON TWO WEDGES.... 105

APPENDIX K. SNAKE STRIKING PLATFORM..... 106

APPENDIX L. SNAKE STRIKE DATA FROM THE OPEN SETUP FOR ALL INDIVIDUALS 107

APPENDIX M. SNAKE STRIKE DATA FROM THE WALLED SETUP FOR ALL INDIVIDUALS 109

LIST OF TABLES

Table Page

2.1 Values (Figs 5-8) of vertebral range of motion 26

3.1 Sarcomeres in the corn snake showing contracted, resting, and extended lengths with mean±s.d. for all seven muscles analyzed here. Measurements are combined for all masses and positions (i.e., anterior, middle, and posterior) 43

3.2 ANOVA for snake sarcomere measurements without random linked to mass (or individual). All variables came out significant 43

3.3 ANOVA for snake sarcomere measurements with random linked to mass (or individual). Bolded variables denote significance..... 44

4.1 Summary of the maximum forces and average impulses obtained during our experiments..... 61

5.1 Average values for each variable by setup (open versus walled) and pooled alongside statistical model values showing significant variables based on a stepdown Bonferroni test (bold denotes significance)..... 71

5.2 Coefficient of variation by setup (open versus walled) based on a one-way ANOVA (bold denotes significance)..... 74

LIST OF FIGURES

Figure Page

1.1 Lateral undulation (A), roman numerals denote vertebrae, concertina locomotion (B), letters denote body markers, rectilinear locomotion (C) showing progression in cm over time (s), and sidewinding (D-E), direction of travel is oblique (D), and different segments are held stationary or active (E) 7

1.2 Snake Muscles from anterior (A) and lateral (B-C) views. Larger muscles shown are the *M. spinalis* (blue), *M. semispinalis* (dark purple), *M. multifidus* (light purple), *M. longissimus dorsi* (green), *M. iliocostalis* 1-upper (red), *M. iliocostalis* 2-lower (light red), and the *M. levator costae* (orange) 9

1.3 Length-tension curve showing the ascending limb, plateau, and descending limb. Image modified from Lieber and Boakes, (1988) 11

2.1 Anatomy and articulation of snake vertebrae 15

2.2 Unaltered μCT-scanned vertebrae of the four species used in this study in oblique anterior/lateral view 18

2.3 Examples of mobility and articulation of snake vertebrae 20

2.4 Vertebrae showing the 'red component' and its attachment in the 3D-printed vertebrae and the different axes 23

2.5 Vertebral range of motion (ROM) of the brown tree snake (*B. irregularis*) 27

2.6 Vertebral range of motion (ROM) of the prairie rattlesnake (*C. viridis*) 27

2.7 Vertebral range of motion (ROM) of the boa constrictor (*B. constrictor*) 28

2.8 Vertebral range of motion (ROM) of the corn snake (*P. guttatus*) 28

3.1 Corn snake with three maximal bends at 25%, 50%, and 75% SVL 42

3.2 Length-tension curve showing all snake muscles analyzed in this study from five corn snakes 46

4.1 The experimental setup and still images from trials 52

4.2 Analysis of snake movement through the apparatus 59

5.1 A-D stills of the snake strike in the open setup at various stages of the strike including the beginning (A), point of maximum fore-aft force (B), point when the snake's neck is straight (C), and point when forward progress ends (D)..... 72

5.2 A-D stills of the snake strike in the walled setup at various stages of the strike including the beginning (A), point of maximum fore-aft force (B), point when the snake's neck is straight (C), and point when forward progress ends (D)..... 73

CHAPTER I

INTRODUCTION

Limbs are considered one of the milestones of evolution (Clack, 2012) and yet multiple groups have never evolved limbs (e.g. worms and fish), greatly reduced their limbs (e.g., the salamander and skink *Amphiuma* and *Lerista*), or lost them entirely (e.g., most Amphisbaenians, Caecilians, and snakes) (Gans, 1975). Animals that are limbless benefit in cluttered, fossorial, and aquatic environments where limbs would incur increased resistance and drag (Gans, 1975; Kelley et al., 1997; Sharpe et al., 2015). While the majority of limbless animals exploit almost exclusively aquatic or fossorial habitats (owing to the sheer number of worm species), limb-reduced and limbless squamates exploit multiple environments including terrestrial, arboreal, fossorial, and aquatic habitats (both freshwater and marine) (Gans, 1975). Only endothermic taxa lack limbless species (Gans, 1975) likely because thermal losses from an elongate body plan are too great (Pough, 1980).

Limb-reduced clades have evolved at least 25 times within squamates (Wiens et al., 2006). Multiple authors have discussed correlations between body elongation and limb reduction (Bergmann and Irschick, 2010; Camp, 1923; Caputo et al., 1995; Gans, 1975). Gans (1975) hypothesized that elongation was the first step, followed by digit reduction, then limb reduction once lateral undulation was possible. However, Wiens

and Slingluff (2001) showed squamates become limbless gradually through concurrent reduction of the limbs and elongation of the body (through increased vertebral numbers) and concurrent reduction of limbs and digits. Head and Polly (2015) showed vertebral division into cervical, thoracic, sacral, and lumbar (as well as caudal, though these authors do not discuss it) are conserved in snake vertebrae and their increase in number is not an artifact of malfunctioning hox genes. Vertebral number varies dramatically among limbless taxa and even within species (Arnold, 1988; Gans, 1970). Thus, some of the mechanisms as to how animals reduce or lose their limbs can be explained, but the question remains why become limbless at all?

Limb-reduced squamates typically inhabit dense environments (e.g., grasslands or brush) or burrow (Gans, 1975). Dense environments appear to be logical places to become limbless because limbs will hypothetically get caught on brush, resulting in slower speeds (Astley, 2020; Gans, 1975). Unfortunately, few studies analyze the effects of locomotor performance in variably dense environments using limbed, limb-reduced, and limbless species. One study (Kelley et al., 1997) shows that snakes get faster in more cluttered or dense environments (up to some maximum density, beyond which undulation is not possible), providing support for limblessness evolving to adapt to cluttered environments. Additionally, Sharpe et al. (2015) showed *Chionactis* had less body slipping during burrowing than the sandfish lizard (*Scincus*) in part due to its longer, and more slender, body shape. Multiple authors (Branch, 1988; Camp, 1923; Caputo et al., 1995; Cogger, 2000; Klemmer; Wiens and Slingluff, 2001) discuss two 2ctomorphs of limb-reduced vertebrates that appear: burrowers appear to be

consistently short-tailed and small, while grass-swimmers appear to be consistently larger with relatively long tails. It remains unknown why limbless species are split into these two 3ctomorphs but Wiens and Slingluff (2001) suggest three hypotheses: 1) performance advantages for short tail length in burrowers and long tail length in grass-swimmers, 2) increased predation pressure in grass-swimmers might drive selection for longer tail lengths due to damage to the tail being less likely to be fatal than damage to the trunk, and 3) limitations in females due to small size to bear young requiring increased body lengths. Another hypothesis is that tails are relatively useless for generating propulsion when burrowing but are useful for generating propulsion in grass where more space is available. Further analyses are needed to discern the role of tail length in fossorial and epigean (or on the surface) habitats.

Limbless squamate taxa include multiple families: Amphisbaenidae, Anguidae, Anniellidae, Cordylidae, Dibamidae, Gymnopthalmidae, Pygopodidae, Rhineuridae, Scincidae, all families within Serpentes, and Trogonophidae (Pough et al., 2004; Vitt and Caldwell, 2009). The majority of these taxa, excluding Serpentes, are small fossorial species with small geographic ranges, while the surface-dwelling species are less diverse but typically occupy larger geographic ranges (Wiens et al., 2006). Interestingly, snakes are the only limbless taxa within squamates that have exploited fossorial, terrestrial, arboreal, and aquatic environments (Zug et al., 2001) and have a near-global range.

The origins of snakes are hotly debated as either fossorial or aquatic (Caldwell and Lee, 1997; Camp, 1923). Multiple morphological characteristics snakes share with amphisbaenians and dibamids support a fossorial origin (Coates and Ruta, 2000) while

the aquatic origin for snakes is associated with similar jaw structures present within Mosasaurs an extinct group of giant marine lizards (Caldwell and Lee, 1997). The last two decades has seen a surprising number of fossil snakes from the Cretaceous shedding light on the origins of this group. Some of these fossil snakes (e.g., *Coniophis*, *Dinilysia*, and *Najash*) support a fossorial origin for snakes (Apesteguía and Zaher, 2006; Longrich et al., 2012; Yi and Norell, 2015) and are consistent with modern basal snakes (i.e., Scolecophidians) and their fossorial habits. However, others (e.g., *Eupodophis*, *Haasiophis*, and *Pachyrachis*) support an aquatic (marine) origin (Caldwell and Lee, 1997; Rage and Escuillié, 2000; Rieppel et al., 2003; Tchernov et al., 2000). More recently, fossil snakes have been found as far back as the Jurassic period (Caldwell et al., 2015 (i.e. *Diablophis*, *Eophis*, *Parviraptor*, and *Portugalophis*)) and were found in multiple environments. Some were terrestrial, but others were found on what would have been isolated islands, requiring over-water dispersal and thus complicating the origins of snakes. Recent genetic and morphological work shows snakes are not closely related to Mosasaurs as was previously thought (Conrad, 2008; Vidal and Hedges, 2004; Wiens et al., 2010), though other analyses suggest a close relationship between Mosasaurs and snakes (Lee, 2005) making this debate far from settled. Regardless of the environment snakes originated in, they appear to have evolved in Gondwana (Hsiang et al., 2015). In North America and Europe, snakes remained a relatively minor group of mostly boids and small snakes until the Miocene when colubrids started to radiate and replace boids (Holman, 2000; Szyndlar and Rage, 2003). This shift appears to be correlated with increasingly arid environments and the transition to open grasslands in

North America (Cerling et al., 1997; Pagani et al., 1999) and possibly Europe (Bruch et al., 2011; Pagani et al., 1999). Colubroidea is thought to have originated in Asia and dispersed to Africa, Europe, and North and South America due to Eocene localities in Myanmar and Thailand containing colubroids and the subsequent appearance of these snakes on other continents at later dates (Head et al., 2005; Rage et al., 1992). Africa has the oldest colubroid-dominated fauna (from the Oligocene) suggesting the transition from boids to colubroids happened earlier in Africa than in Europe and North America (McCartney et al., 2014) likely following the same climactic shift to more arid environments around the globe during this time (Cerling et al., 1997). South Americas fossil record requires more study but the record in Brazil suggests a radiation of colubrid snakes around the Miocene but with booid snakes retaining some diversity even to the present day (Onary et al., 2017). Thus, between the Oligocene and Miocene, colubroid snakes began to dominate assemblages worldwide (Holman, 2000) where snakes currently number over 3,500 species (Burbrink and Crother, 2011).

Because they are limbless snakes must rely on their axial skeleton to generate propulsion and navigate the environment using their vertebrae either as movable components (i.e., lateral undulation, concertina, sidewinding) or as rigid structures to pull on (i.e., rectilinear). Snake biomechanics and locomotion have been studied by a range of authors (e.g., Astley and Jayne, 2007; Gans, 1970; Gray, 1946; Gray and Lissmann, 1950; Hu et al., 2009; Jayne, 1985; Jayne, 1988; Marvi et al., 2014; Mosauer, 1935; Sharpe et al., 2015). These studies highlight four types of snake locomotion (lateral undulation, concertina, rectilinear, and sidewinding) and have shown snakes can

perform multiple modes of locomotion at the same time (Gans, 1974). However, Jayne (2020) described a litany of locomotor variations in snakes beyond the simplistic characterization of these four modes. For simplicity's sake, we will focus on these four modes for the time being until the new modes of locomotion are better understood under a new paradigm for snake locomotion. Lateral undulation (Fig. 1.1A) uses posteriorly propagating lateral waves that push against asperities in the environment, generating forward propulsion. It is the most common, and it is the fastest locomotor mode alongside sidewinding (Gans, 1962; Jayne, 1986) for the majority of snakes. Lateral undulation is seen in almost all limbless vertebrates (Gans, 1986) and has energetic costs similar to limbed locomotion (Walton et al., 1990). Concertina locomotion (Fig. 1.1B) relies on areas of static contact with the substrate to anchor portions of the body while other regions are pushed or pulled forwards and is primarily used in tunnels (Astley and Jayne, 2009; Gans, 1970; Gans, 1986) and arboreal environments (Astley and Jayne, 2007; Astley and Jayne, 2009; Gans, 1962). Concertina requires the largest net cost of transport (Walton et al., 1990). Rectilinear locomotion (Fig. 1.1C) is a unique mode of locomotion which relies entirely on skin and associated musculature (Gans, 1970; Marvi et al., 2014), with slow speeds and an unknown net cost of transport. The vertebrae and ribs do not have to move during rectilinear locomotion (Bogert, 1947; Lissmann, 1950) and it is primarily utilized by larger and thick-bodied snakes (Lillywhite, 2014), but also allows snakes to move in a straight line and through small openings (Gans, 1962). Sidewinding (Fig. 1.1D-E) is the final mode of locomotion

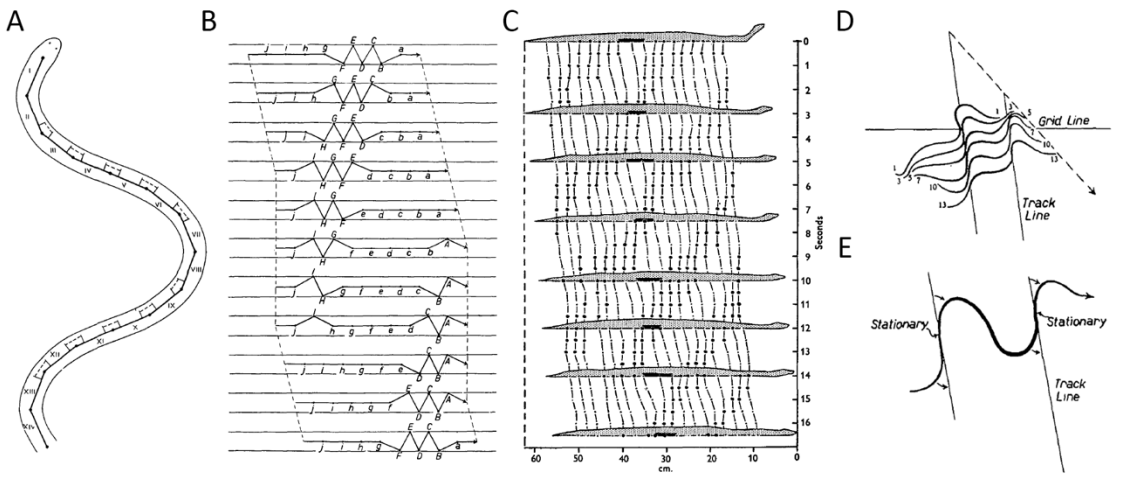

Figure 1.1: Lateral undulation (A), roman numerals denote vertebrae, concertina locomotion (B), letters denote body markers, rectilinear locomotion (C) showing progression in cm over time (s), and sidewinding (D-E), direction of travel is oblique (D), and different segments are held stationary or active (E). Images modified from Gray (1946).

discussed here and has the lowest net cost of transport compared to the modes of locomotion listed above (Secor et al., 1992). Two posteriorly propagating waves, one vertical and one horizontal, allow the snake to lift its body but also advance using a combination of static and moving body segments primarily used in sandy environments (Jayne, 1986; Marvi et al., 2014). Sidewinding typically uses two regions of static contact to prevent slipping while the moving segments lift and advance the snake (Jayne, 1986; Marvi et al., 2014). However, there are still open questions including how the modes described by Jayne (2020) compare with these four modes described above, whether snakes can perform additional modes of locomotion.

The skeletal structure of snakes, and all limbless vertebrates, is essentially comprised of vertebrae and ribs. Snake osteology is a fundamental component of how they navigate the world. Studies of the bones of snakes has focused on vertebrae and

the skull (e.g., Cundall and Irish, 2008; Hoffstetter and Gasc, 1969; Holman, 2000; Romer, 1956) because of taphonomic bias and snakes kinetic skulls are relatively unique within squamata. However, these studies concerning snake osteology tend to focus on regional differences in the vertebral column, systematic morphology, phylogeny, and fossil identification (e.g., Head and Polly, 2015; Hoffstetter and Gasc, 1969; Holman, 2000; Lee and Scanlon, 2002; Mead and Schubert, 2013; Szyndlar and Rage, 2003). While this body of literature is expansive, functional consequences of morphological variations in snake vertebrae such as range of motion remain open areas for research. Additionally, how the variation in morphology affects locomotion and muscle function is unknown. This is surprising considering how diverse snake vertebral shape is and that it can be diagnostic for snake identification to genus level (Holman, 2000). For example, constricting snakes tend to have anteroposteriorly shorter vertebrae while arboreal snakes typically have anteroposteriorly elongate vertebrae (Pough and Groves, 1983).

In addition to elongate body plans, elongate structures occur frequently in vertebrates (e.g., vertebral columns, digits, tails). These structures and organisms (e.g. fish, legless lizards, and snakes) have to balance tradeoffs between flexibility and stability (Anderson et al., 2001; Johnston and Smidt, 1970; Kazar and Relovszky, 1969; Scopp and Moorman, 2001; Sumida, 1997; Veeger and Van Der Helm, 2007; Zakani et al., 2017). Different limbless taxa (within and beyond snakes) may tend towards stability or flexibility based on the consequences for movement, prey capture, and self-defense. Tradeoffs are likely to be present between all of these demands on the vertebral column, ribs, and skulls of these animals.

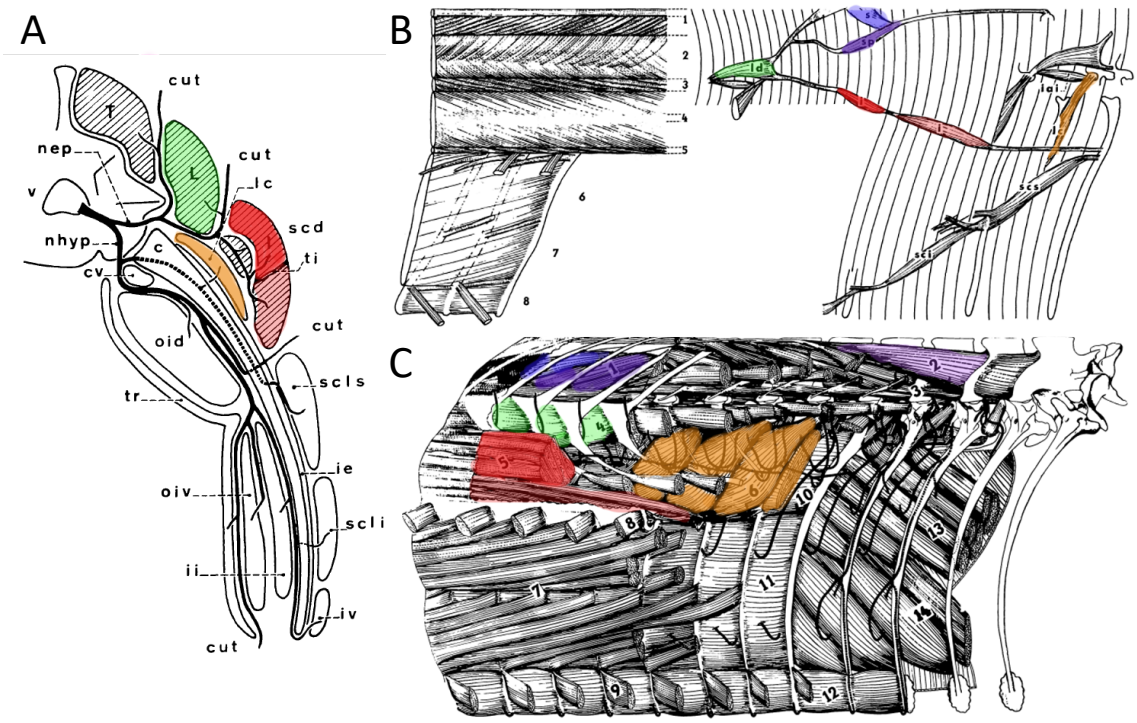

Figure 1.2: Snake Muscles from anterior (A) and lateral (B-C) views. Larger muscles shown are the *M. spinalis* (blue), *M. semispinalis* (dark purple), *M. multifidus* (light purple), *M. longissimus dorsi* (green), *M. iliocostalis* 1-upper (red), *M. iliocostalis* 2-lower (light red), and the *M. levator costae* (orange). Images modified from Gasc (1981).

The complex axial musculature of snakes (Fig. 1.2) shows both qualitative consistency across snakes and architectural changes between groups (Gasc, 1981). While there are many studies describing snake musculature (e.g., Gasc, 1981; Jayne, 1982; Lourdais et al., 2005; Penning, 2018; Ridge, 1971), few studies have examined variation in muscle anatomy between snakes with different lifestyles and prey acquisition methods. Jayne's (1982) analysis and Tingle's (2017) reanalysis remain the only two studies that extensively and quantitatively analyze a muscle group, specifically the semispinalis-spinalis complex. These studies revealed up to a four-fold difference in length of the muscle-tendon unit between species and correlations to both environment and prey capture techniques. For example, arboreal snakes typically have longer

semispinalis-spinalis muscle-tendon units than terrestrial species enhancing cantilever ability while constricting snakes tend to have shorter semispinalis-spinalis muscle-tendon units facilitating flexibility (Jayne, 1982; Tingle et al., 2017). Thus, even though we only have detailed muscle length data from one muscle group, it is clear snake musculature can vary dramatically between taxa, and more studies are needed to determine whether this pattern is prevalent in other muscles. While we have some data on muscle and tendon lengths (Gasc, 1981; Jayne, 1982), cross-sectional area (Jayne and Riley, 2007; Moon and Candy, 1997; Penning, 2018), and masses (Penning, 2018) of snakes muscle lever arms and their effects on snake locomotion are entirely unknown. Additionally, there is no data on where snake muscles operate on the length-tension curve (Fig. 1.3), and this can affect whether a muscle functions primarily for propulsion or is primarily used in stability and control (Burkholder and Lieber, 2001).

The elongate body of snakes is used in locomotion, but it is also used to capture prey. Snake strikes have to be quick but also accurate. The body needs muscles fast enough to move rapidly but also strong enough to potentially incapacitate prey. The head and neck are typically lightweight, which could potentially increase the speed during strikes, but also need to be robust enough to endure the forces of strikes and contact with prey. Strike performance in snakes has been analyzed in terms of velocity, acceleration, scaling, and temperature effects (e.g., Greenwald, 1974; Herrel et al., 2011; Kardong and Bels, 1998; LaDuc, 2002; Penning et al., 2016). Additionally, attacking and defensive strikes have been analyzed (Araújo and Martins, 2007; Kardong, 1986; LaDuc, 2002; Penning et al., 2016). However, forces (kinetics) have never been

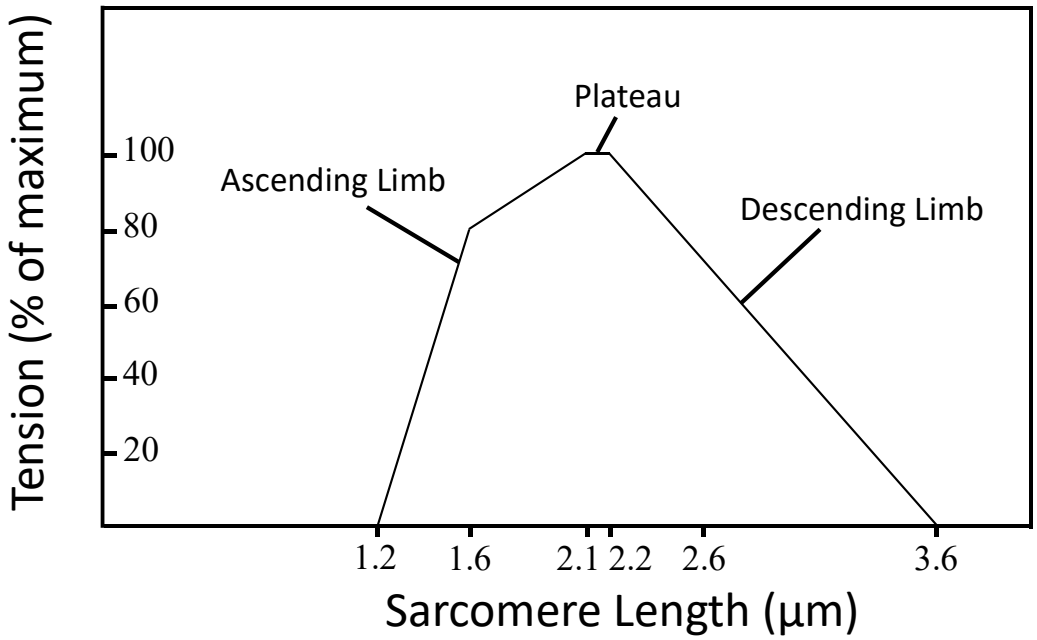

Figure 1.3: Length-tension curve showing the ascending limb, plateau, and descending limb. Image modified from Lieber and Boakes, (1988).

measured during a snake strike. The kinetics of the body can inform the amount of recoil during the strike, whether the body slips during strikes, and it can potentially even allow the calculation of joint moments during a strike.

Snakes are one of the most widespread and speciose terrestrial vertebrate groups on the planet and have exploited every continent on Earth with the exception of Antarctica (Vitt and Caldwell, 2009). Despite their incredible diversity in form, size, and environments occupied, snakes remain an understudied group (Astley, 2020). Specifically, we understand little about their biomechanics, musculature, and locomotion. In this dissertation, we aim to understand multiple unknown factors from

microscopic sarcomeres to whole animal biomechanics. These studies were conducted to better understand multiple components of how snakes' function in the natural world. Snakes traverse the world using their vertebrae, all of which have a unique bony process called the zygosphene. Despite the prevalence of this process across Serpentes, its function remains unclear. We sought to understand how this process (1) affects their range of motion and (2) whether it plays a role in limiting vertebral roll/twisting. Snake sarcomeres have never been measured despite their importance in force generation. As such, we sought to understand how snake sarcomeres have an impact on locomotion. Most locomotor modes in snakes predominantly interact with the environment through lateral forces. However, the environment is structurally complex and we hypothesized that snakes can interact and propel themselves using vertical waves to take advantage of vertical asperities. Finally, we sought to understand what forces are generated during snake strikes, which have never been previously measured. These projects together expand our knowledge of multiple aspects of snake biomechanics, incorporating a variety of aspects including vertebral range of motion, musculature, locomotor modes, and predation. Together they give a more holistic understanding of how snakes have diversified and exploited almost every natural environment on the planet.

CHAPTER II

EXPERIMENTAL MODIFICATION OF MORPHOLOGY REVEALS THE EFFECTS OF THE ZYGOSPHENE-ZYGANTRUM JOINT ON THE RANGE OF MOTION OF SNAKE VERTEBRAE

Introduction

Trade-offs between the mobility and stability of skeletal joints are determined by many factors including bone geometry, cartilage, and soft tissues such as ligaments and muscles. The shape of joints are highly variable, both across and within species, as well as within individuals, and it depends on both evolutionary history and the function of a joint in the body which can result in variable shapes (e.g., ball and socket, hinge, and saddle) (Andersson, 2004; Johnston and Smidt, 1970; Kazar and Relovszky, 1969; Veeger and Van Der Helm, 2007; Zakani et al., 2017). For example, canine limbs provide stability during running but are unable to pronate and supinate to the same degree as in felids, reflecting the canine hunting strategy of chasing prey rather than ambushing and grappling prey as cats do (Andersson, 2004). Depending on the joint, soft tissue and bone geometry can have different contributions to the stability and ROM of the joint. Joints with minimal bony constraints, such as the human shoulder, have a high range of motion (ROM) but also rely upon soft tissue for support, resulting in a higher injury risk

(Kazar and Relovszky, 1969; Veeger and Van Der Helm, 2007). By contrast, joints with substantial bony constraints, such as the human hip, have moderate to minimal soft tissue support and a correspondingly lower ROM and injury rate (Anderson et al., 2001; Johnston and Smidt, 1970; Scopp and Moorman, 2001; Zakani et al., 2017).

The vertebral column is part of the axial skeleton and essential for protecting the spinal cord and joining the cranial and appendicular parts of the skeleton together. All extant tetrapod vertebrae articulate via the centra and pre- and post-zygapophysis joints that maintain vertebral connection and provide stability (Sumida, 1997). As in other joints, there is a trade-off between stability and flexibility, depending on the needs of the animal (Anderson et al., 2001; Johnston and Smidt, 1970; Kazar and Relovszky, 1969; Scopp and Moorman, 2001; Veeger and Van Der Helm, 2007; Zakani et al., 2017). Limbless species often rely on the vertebral column for propulsion, and enhanced axial flexibility probably benefits the locomotion of terrestrial limbless animals by allowing them to contact and conform to a wide variety of shapes and sizes of surfaces that are used to generate propulsive forces.

Snakes, the most speciose limbless tetrapods, have vertebrae with variable shape, but consistently possess three articulations: 1) the cotyle-condyle joint at the centrum, 2) the pre- and post-zygapophysis joint, and 3) a distinctive joint formed by the zygosphene and zygantrum (Fig. 2.1; Hoffstetter and Gasc, 1969; Johnson, 1955; Romer, 1956). This zygosphene-zygantrum joint is large and prominent in all snakes, diagnostic for their vertebrae, and absent or minimal in all other vertebrates (Hoffstetter and Gasc, 1969; Romer, 1956). Furthermore, snakes are the only clade of limbless squamates that

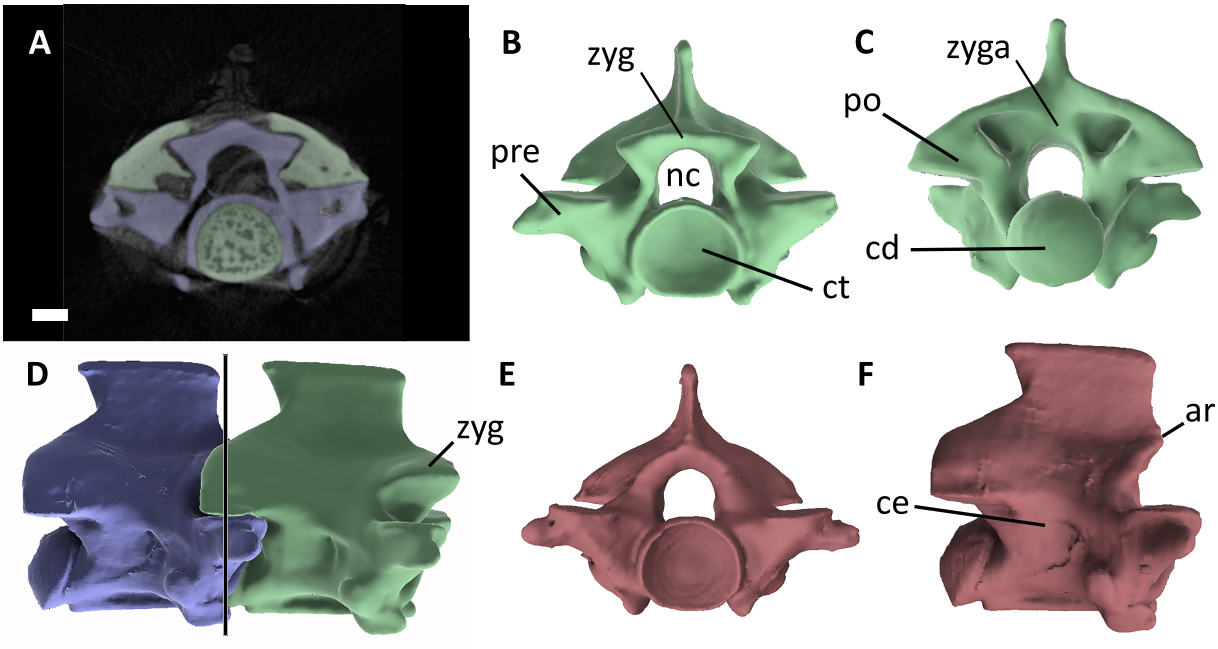

Figure 2.1: Anatomy and articulation of snake vertebrae. (A) µCT scan slice showing the anterior (green) and posterior vertebrae (blue) of a corn snake (*Pantherophis guttatus*). Note the zygosphene-zygantrum, pre- and post-zygapophyses, and cotyle-condyle articulations have narrow gaps. (B) Normal vertebra in anterior view. (C) Normal vertebra in posterior view. (D) Right lateral view with anterior and posterior vertebrae articulated. Note how deeply the zygosphene inserts into the zygantrum. Vertical bar represents the µCT scan location. (E) Altered vertebra in anterior view. (F) Altered vertebra in right lateral view. Terms: ar-altered region, ce-centrum, cd-condyle, ct-cotyle, nc-neural canal, po-postzygapophysis, pre-prezygapophysis, zyg-zygosphene, zyga-zygantrum. Scale bar = 1 mm.

possess a zygosphene-zygantrum joint, despite many other independent evolutionary origins of limblessness (Wiens et al., 2006). Although the morphology of the zygosphene-zygantrum joint is well described (Auffenberg, 1963; Gasc, 1974; Hoffstetter and Gasc, 1969; Holman, 2000; Johnson, 1955), its function is poorly understood. The zygosphene has long been postulated to prevent axial torsion (Gasc, 1976; Romer, 1956), but empirical tests of the function of this distinctive joint are lacking. However, because all snakes have the zygosphene-zygantrum joint, determining the

consequences of its presence or absence is not possible by comparing different snake taxa, and comparisons with other squamate vertebrae lacking a zygosphene would be confounded by other morphological differences.

Methods such as finite element analysis, CT scanning, and 3D printing offer the ability to experimentally alter morphology to test hypothetical alternatives providing a new way to test the function of existing morphology. For example, caecilians have two types of skulls (solid and fenestrated), one of which was hypothesized to enhance burrowing by reducing bone strain, but no extant species have an intermediate anatomy suitable for testing this hypothesis (Kleinteich et al., 2012). Thus, Kleinteich et al. (2012) digitally altered the skulls of multiple caecilians from fenestrated to solid and vice-versa, and used finite element analysis during loading revealed no significant difference between the performance of altered and unaltered skulls. This clever use of digital manipulation of morphology solved the problem of isolating the functional consequences of morphological variation not found in extant species. These methods are a way of experimentally manipulating morphology instead of relying only on natural variation and existing biological species to test functional consequences.

In this chapter, we provide the first empirical test of the hypothesis that the function of the zygosphene is prevention of roll (Gasc, 1976; Romer, 1956) by experimentally manipulating the morphology of the vertebrae by digitally deleting the zygosphene of four species of snakes. Although we primarily tested the hypothesis that removing the zygosphene will increase roll (torsion), we also examined the broader consequences of the zygosphene-zygantrum joint on ROM.

Materials & Methods

To digitally reconstruct and experimentally manipulate vertebral morphology, we used specimens of four phylogenetically diverse species of snakes from three families. We dissected and cleaned vertebrae from the mid-body of the following four specimens (Fig. 2.2): boa constrictor (Boidae, *Boa constrictor*, American Museum of Natural History, AMNH-R176819, snout vent length (SVL)= 54.3 cm), corn snake (Colubridae, *Pantherophis guttatus*, AMNH-R176816, SVL= 96.7 cm), brown tree snake (Colubridae, *Boiga irregularis,* BCJ pers. collection, SVL= 184.0 cm), and prairie rattlesnake (Viperidae, *Crotalus viridis*, University of Michigan-no specimen number, SVL= 83.4 cm).

During prior fieldwork, two authors (HCA and BCJ) gathered data on maximal lateral and dorsoventral bending from a freshly euthanized but otherwise intact brown tree snake. We photographed the mid-body while it was maximally bent laterally, dorsally, and ventrally, and images were analyzed in FIJI (Schindelin et al., 2012, ImageJ 1.8.0_66 64 bit, 3D Viewer, Wayne Rasband, NIH, Bethesda, MD). We calculated intervertebral ROM by determining the total angular displacement over 8-14 vertebrae along an arc with a uniformly minimal radius of curvature and then divided this quantity by the number of intervening joints. For the brown tree snake, these data were obtained from the same snake and body segments as were used during µCT scanning and digital rendering. Using procedures similar to those for the brown tree snake, we

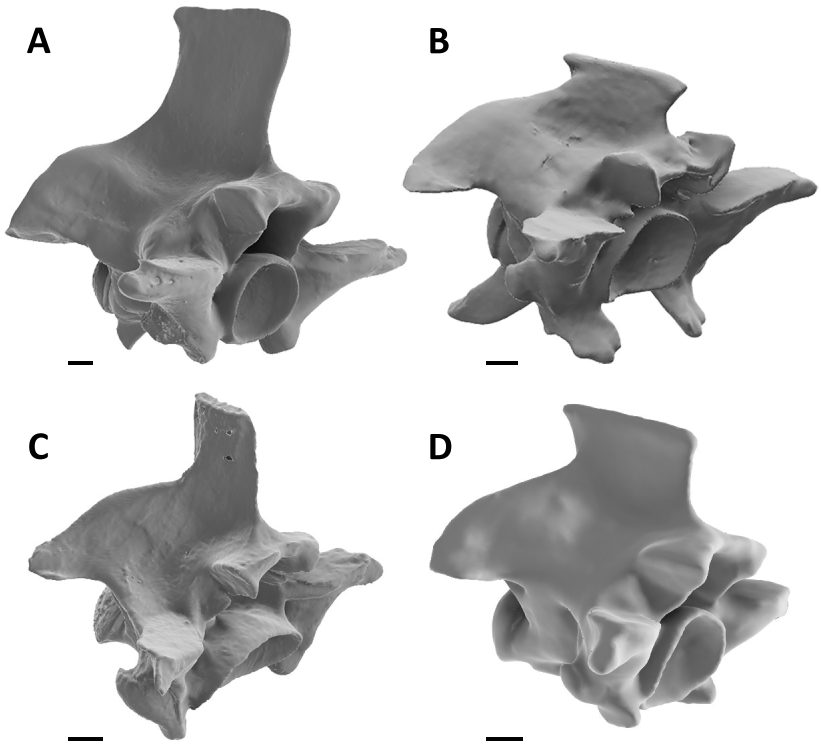

Figure 2.2: Unaltered CT scanned vertebrae of the four species used in this study in oblique anterior/lateral view. (A) *Boiga irregularis*. (B) *Crotalus viridis*. C) *Boa constrictor*. (D) *Pantherophis guttatus*. Scale bars = 1 mm.

also determined the ROM for one intact, freshly euthanized corn snake specimen (SVL = 107) and a boa constrictor specimen (SVL = 135 cm), although these were different individuals than those used to create the 3D prints of vertebrae. Hereafter we use "intact" to refer to all measurements from these fresh specimens.

For each species, two sequential vertebrae from mid-body were isolated, dissected, and µCT scanned (SkyScan 1172, Bruker, Billerica, MA), segmented manually with Adobe Photoshop (CC 2015 Adobe Inc., San Jose, CA), and digitally rendered with FIJI (Fig. 1A-F). Voxel size was 26.16 µm for all snakes except *Boiga irregularis* for which it was 19.88 µm. We used the following settings during our scans: voltage was 80 kV,

amperage was 120 μA, rotation step was 0.4, frame averaging of eight, with an aluminum filter. After segmentation, the vertebrae were smoothed in MeshLab (v. 2016.12 ISTI-CNR, Pisa, Italy) with a Laplacian Smooth method (coefficient of three). Two copies were made of the posterior vertebra for each species, one of which was unaltered and the other was edited digitally to remove the zygosphene (Fig. 2.1E-F) using Meshmixer (v.3.4.35 Autodesk, Inc., San Rafael, CA), referred to as the altered vertebra henceforth. All vertebrae were then 3D printed (Lulzbot TAZ 6, Fargo Additive Manufacturing Equipment 3D, Fargo, ND, layer height-0.18 mm, xy resolution-0.05 mm, ABS) at 14x their actual size (7-16 mm) to limit the effects of print resolution and the expanding plastic as the vertebrae are printed.

To determine ROM during manual manipulations of the 3D-printed vertebrae, we used four motion capture cameras (Flex 13, 120 images s^{-1}, NaturalPoint, Inc. Corvallis, OR). We attached six or more adhesive reflective markers to the anterior vertebra and we affixed four reflective spherical markers to the posterior vertebra. The anterior vertebra was fixed in place to prevent movement. We tracked the markers using Motive Optitrack V2.0.2 (NaturalPoint, Inc. Corvallis, OR), and the markers on each vertebra were used to define a rigid body. The software uses a non-linear least squares solver to reconstruct rigid body position, and computes rotations using quaternions, which are then decomposed into yaw, pitch, and roll relative to the external frame of reference. Because the computation is initially in quaternions, the order of rotations which can affect Euler angles is not problematic for this methodology (Richards, 2019; Richards and Porro, 2018). Dorsal pitch is defined as dorsal motion of the vertebra due

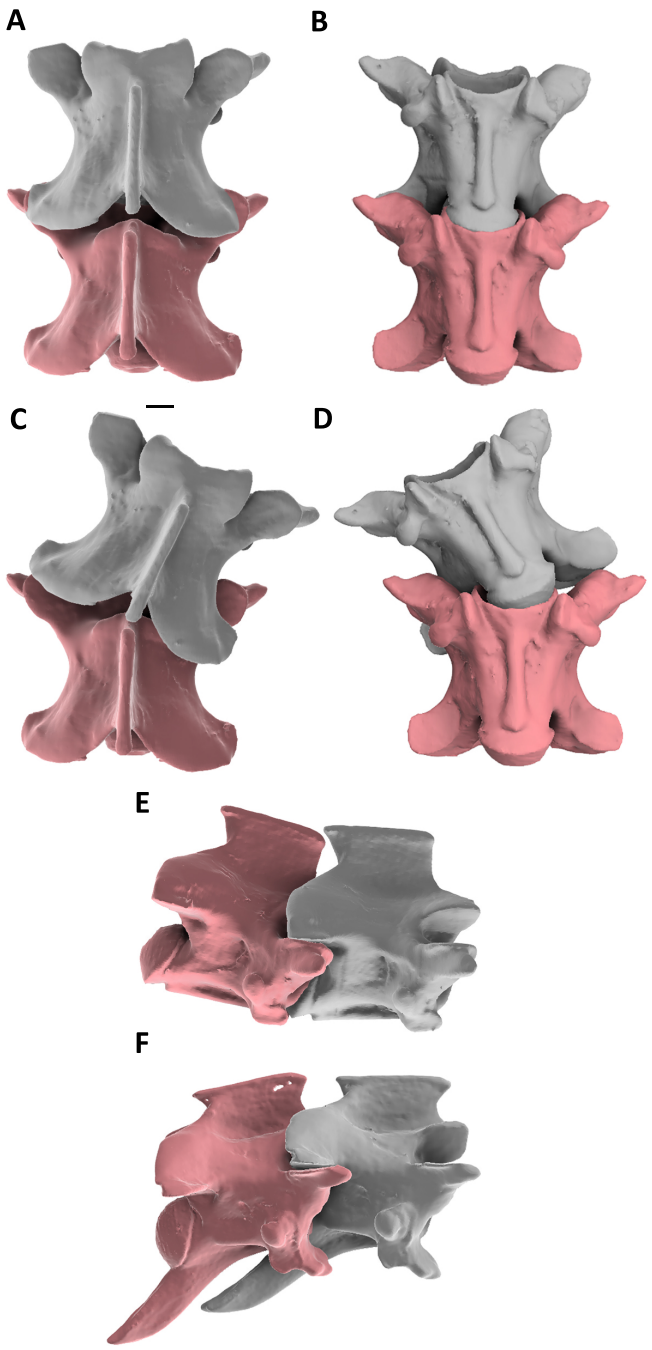

Figure 2.3: Examples of mobility and articulation of snake vertebrae. (A-E) Corn snake (*P. guttatus*) vertebrae (anterior is normal and gray, posterior is altered and red). (A) Dorsal view, straight. (B) Ventral view, straight. (C) Dorsal view, maximal yaw = 27 deg. (D) Ventral view maximal yaw = 27 deg, note lack of overlap of pre- and post-zygapophyses. (E) Right lateral view dorsal pitch = 12 deg. Note lack of contact of neural spines. (F) Prairie rattlesnake (*C. viridis*) vertebrae (anterior is normal and gray, posterior is altered and red) in right lateral view ventral pitch = -12 deg. Note lack of contact of hypapophyses. Scale bar = 1 mm for all images.

to rotation about a horizontal transverse axis (Fig. 2.3E), whereas ventral pitch is ventral motion of the vertebra due to rotation about the same axis (Fig. 2.3F). Yaw is defined as lateral motion of the vertebra due to rotation about a dorso-ventral axis, while roll is defined as rotation of the vertebrae about an antero-posterior axis. In all cases, the center of rotation was considered to be the cotyle-condyle joint. We calibrated cameras via a wanding procedure in the Motive software and advanced to trials only if the calibration error was below 0.1 mm. Vertebrae were manually manipulated over the ROM for a minimum of 11,000 frames of data to ensure thorough coverage of the possible ROM, including intermediate values. When manipulating the vertebrae, the cotyle-condyle joint remained articulated (Fig. 2.3), as disarticulation may damage living snakes. To achieve full coverage in kinematic space, the graphed data were analyzed quantitatively for gaps, and subsequent trials were performed to achieve full coverage. Certain postures at which roll was effectively unlimited would likely damage a living snake; hence we excluded all data when roll was beyond 40 deg. Because we used natural vertebrae, we note that morphological asymmetries could be present and produce asymmetries in ROM (Appendix A: F-G), though none of these asymmetries appeared to affect yaw at zero pitch. The yaw, pitch and roll angles were not smoothed or filtered.

We used a custom-written script in MATLAB (MathWorks, Natick, MA) to analyze data. Due to the imprecision of manually centering the vertebrae, we calculated the 1^{st} and 99^{th} percentile values of yaw at zero pitch, and assumed that these values would be symmetrical about the neutral axis of the vertebrae in yaw. Thus, we subtracted half of

the difference between these percentile values from all yaw values to center the data. Because our data were not smoothed, we used percentile values to ensure that isolated high values due to error did not unduly bias our data. We analyzed a subset of data from the fixed vertebra to determine error for yaw, pitch, and roll in all four species. The errors from the fixed vertebrae (n=11,000 data points minimum per fixed vertebra) for yaw, pitch, and roll ranged from 0.6-1.2 deg, 1.1-1.9 deg, and 0.4-1.4 deg, respectively, showing high precision and accuracy.

To determine the anatomically neutral pitch (true zero), we constructed a line between the centers of the circles of curvature of the cotyle and condyle in a transverse µCT scan (Fig. 2.4A). After determining this line independently for each vertebra, we locked custom, 3D-printed parts onto the condyle and projected the reference line outward (Fig. 2.4A). This gave us the orientation in 'lab space' of the true zero for pitch of the anterior (fixed) vertebra. The corresponding 3D-printed part was attached to the posterior (mobile) vertebra (Fig. 2.4C), which was then raised to maximum dorsal pitch. The resultant difference between the slopes of the true zero axes of each vertebra in world space was used to determine true maximum pitch. We used this value to re-zero the pitch of the datasets measured from Motive Optitrack. Roll was oriented in 'lab space' by making a line with the pre- and post-zygapophyses and making this line parallel to the table line (Fig. 2.4B, E). Yaw was oriented by making the neural spines line up in dorsal view (Fig. 2.4D, E).

The hypapophyses of both the brown tree snake and prairie rattlesnake created a bony limit on ventral pitch. However, the boa constrictor and corn snake lacked

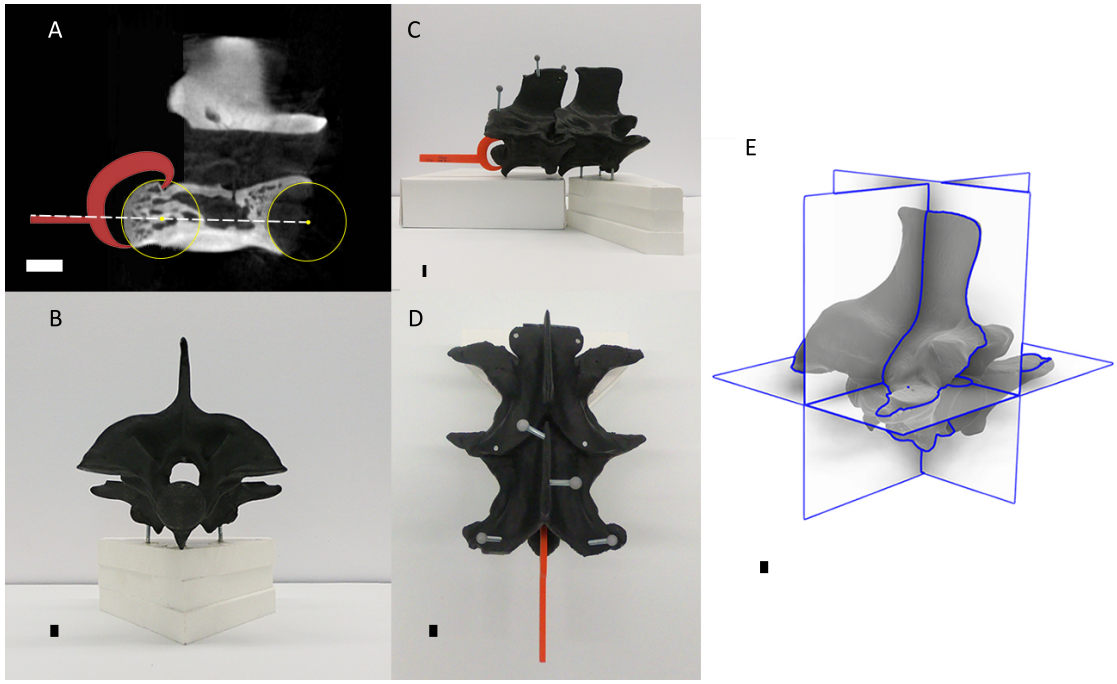

Figure 2.4: Vertebrae showing the red component and its attachment in the 3D printed vertebrae and the different axes. (A) µCT scan showing a mid-sagittal section of a corn snake (*P. guttatus*) vertebra with anterior to the right. We used circles (yellow) to estimate the axis of rotation in pitch for the cotyle and condyle to determine the slope of the neutral position of the vertebra (white dashed line). The red component was a 3D printed part designed to lock on to the vertebra (*P. guttatus*) and hold the posterior bar parallel to the neutral position axis. (B) Anterior vertebra (*B. irregularis*) showing its orientation in lab space flat with the table aligned with the pre- and post-zygapophyses. (C) Anterior and posterior vertebrae (*B. irregularis*) in lateral view with the red component attached and level with the centra and oriented in lab space by the neural spines and the table. (D) Anterior and posterior vertebrae (*B. irregularis*) in dorsal view with the red component attached and in-line with the neural spines. (E) Vertebra showing the intersections of the different anatomical planes. Scale bars = 1 mm.

hypapophyses that limited ventral pitch and thus prevented disarticulation of the cotyle-condyle. Because this is unrealistic, we used the intact dorsal and ventral pitch data from the boa constrictor and corn snake measurements to define their ventral pitch limits. Once we obtained the maximum isolated value of dorsal pitch based on the printed vertebrae, we removed points from the dataset that would have exceeded the

dorsoventral pitch ROM from the intact snakes. Reported maximum and minimum yaw angles for the altered isolated vertebrae were restricted to values within the range of roll reported from normal vertebrae to prevent high roll angles influencing yaw. Values reported for ROM refer to only one side.

To quantitatively characterize and compare ROM between species (both between normal vertebrae and altered vertebrae between species) and between normal and altered vertebrae of the same species, we created a custom-written MATLAB script to calculate overlap of the areas in two-dimensional (yaw and pitch) kinematic space. First, we used the `boundary` function with a shrink factor of 0.8 to create a boundary that conforms to the shape of the point cloud of pitch and yaw values. These boundaries were then converted to polygons using the `polyshape` function. Finally, the `intersect` function was used to determine overlap. If two separate regions of overlap occurred, the data were analyzed using the above steps in two parts: one for positive yaw and one for negative yaw, and the resulting areas were then added together. Using these tools, we conducted two separate tests. First, to assess if values of increased roll in altered vertebrae occurred at pitch and yaw combinations within the pitch and yaw ROM of normal vertebrae, we compared the overlap between the pitch and yaw ROM of normal vertebrae and the pitch and yaw values of altered vertebrae at which roll > 2.5 deg (Appendix B). Second, in order to assess shape similarity of ROM across species, the overlap between the pitch and yaw ROM was computed for all interspecific pairs of both normal and altered vertebrae after being normalized by area for each combination of snakes (Appendices C-D). In altered

vertebrae, regions with high roll were eliminated (Appendices C-D). To avoid being confounded by differences in the total ROM between species, we normalized the polygon areas of their ROM of the species being compared by equalizing their areas to each other. Thus, two highly overlapping shapes show high similarity while shapes that are highly different will show low overlap.

Results

Despite the variable shapes and proportions of the vertebrae, some general patterns of yaw, pitch, and roll were consistent for all four species (Table 2.1, Figs. 2.5-2.8, Appendix A). The normal isolated vertebrae from all species had a range of maximal yaw values from 13.9-18.5 deg, ventral pitch values from -13.5 to -8.7 deg, dorsal pitch values from 4.8-10.7 deg, and roll values < ± 2.5 deg for all species at all combinations of yaw and pitch (Table 2.1, Figs. 2.5-2.8).

After normalizing the yaw-pitch ROM areas of the normal isolated vertebrae to better analyze ROM shape space, the values of yaw-pitch ROM overlap between pairs of species ranged from 56-89% (Appendix E). The prairie rattlesnake consistently had the lowest overlap with other species (56-69%) due to asymmetries in the vertebra, whereas the other three species had quite similar overlap values with each other between 82-89% (Appendix E).

The altered isolated vertebrae had increased ROM for yaw, pitch, and roll, with most yaw and pitch combinations showing similar values of roll to unaltered vertebrae (Table 2.1, Figs. 2.5-2.8). Yaw ROM depended on pitch position and vice versa for

Table 2.1: Values (Figs. 2.5-2.8) of vertebral range of motion (in deg).

Vertebrae Type	Yaw Max	Max Yaw at 0 deg Pitch	Ventral Pitch Min.	Min. Ventral Pitch at 0 deg Yaw	Dorsal Pitch Max	Max Dorsal Pitch at 0 deg Yaw	Roll Max
Intact *B. irregularis*	16.9	-	-11.4	-	8.9	-	-
Normal *B. irregularis*	13.9	13.4	-13.5	-13.5	6.7	6.7	1.7
Altered *B. irregularis*	19.8	14.4	-14.7	-12.6	11.2	10.5	25.3
Normal *C. viridis*	15.2	14.6	-8.7	-8.6	4.8	4.6	1.7
Altered *C. viridis*	18.8	13.0	-11.6	-10.8	7.7	6.6	12.5
Intact *B. constrictor*	16.4	-	8.0	-	9.0	-	-
Normal *B. constrictor*	16.2	15.5	-	-	6.6	6.4	1.3
Altered *B. constrictor*	22.3	17.6	-	-	6.5	6.3	-
Intact *P. guttatus*	22.5	-	-16.0	-	11.3	-	-
Normal *P. guttatus*	18.5	18.4	-	-	10.7	10.6	1.7
Altered *P. guttatus*	26.9	23.9	-	-	15.9	15.0	-

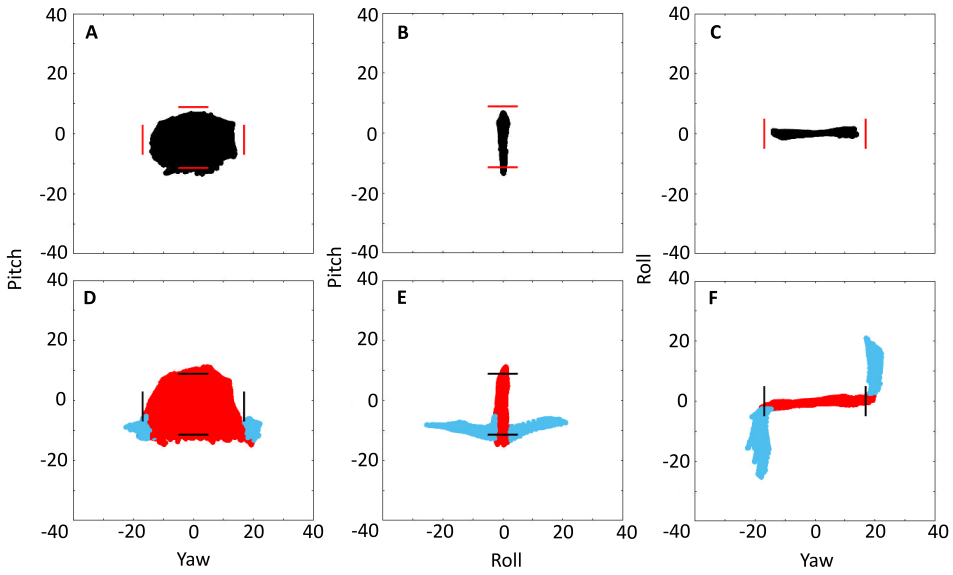

Figure 2.5: Vertebral ROM of the brown tree snake (*B. irregularis*). Red/black borders show limits obtained from an intact brown tree snake for yaw and pitch respectively. (A-C) Normal vertebra. (D-F) Altered vertebra. Red and black represent roll ≤ ±2.5 deg and blue represents roll > ±2.5 deg, respectively.

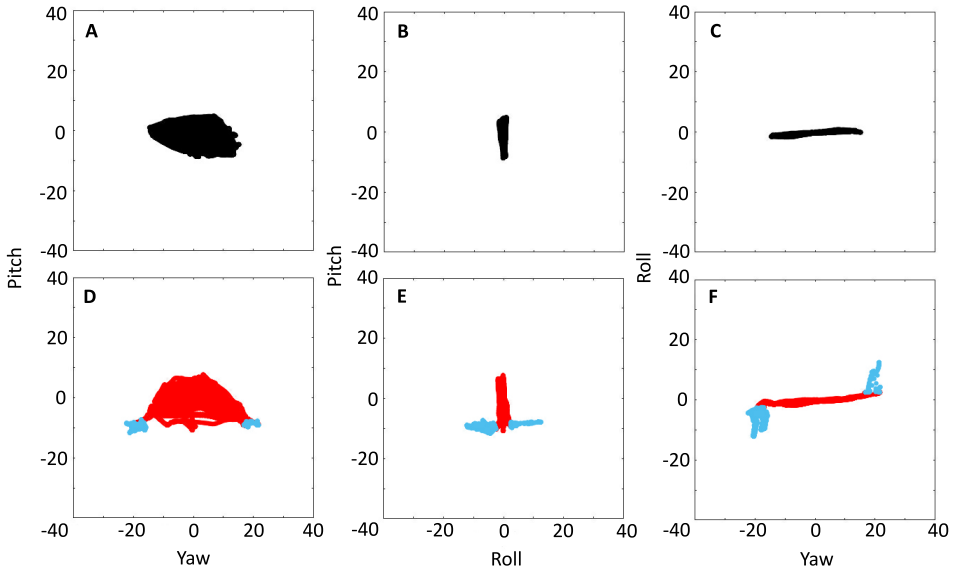

Figure 2.6: Vertebral ROM of the prairie rattlesnake (*C. viridis*). (A-C) Normal vertebra. (D-F) Altered vertebra. Red and black represent roll ≤ ±2.5 deg and blue represents roll > ±2.5 deg, respectively. A subtle asymmetry in the zygosphene morphology produced asymmetric ROM at combinations of ventral pitch and high yaw in the normal vertebra (A).

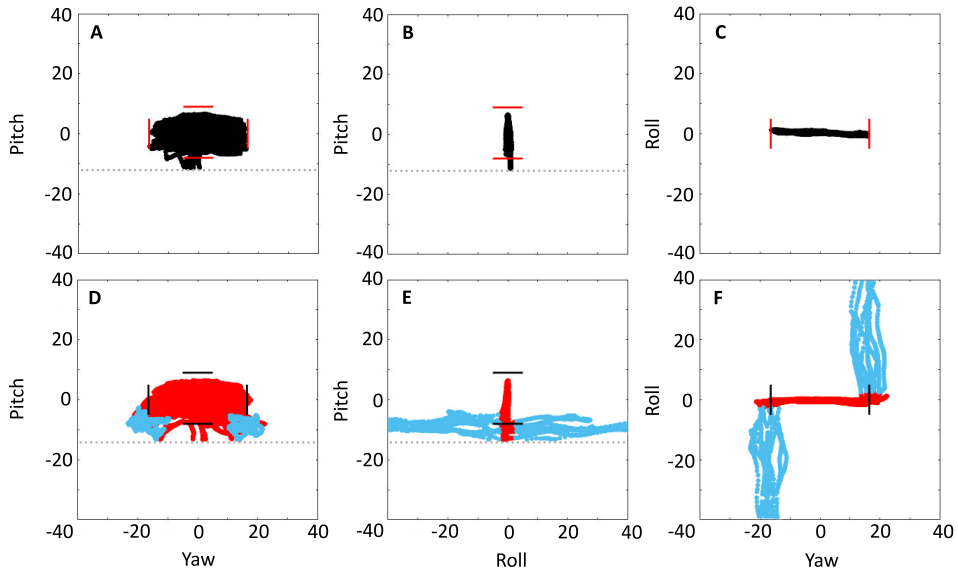

Figure 2.7: Vertebral ROM of the boa constrictor (*B. constrictor*). Red/black borders show limits obtained from an intact boa constrictor for yaw and pitch respectively. (A-C) Normal vertebra. (D-F) Altered vertebra. Red and black represent roll ≤ ±2.5 deg, blue represents roll > ±2.5 deg, respectively. The gray dotted line highlights the arbitrary ventral cutoff.

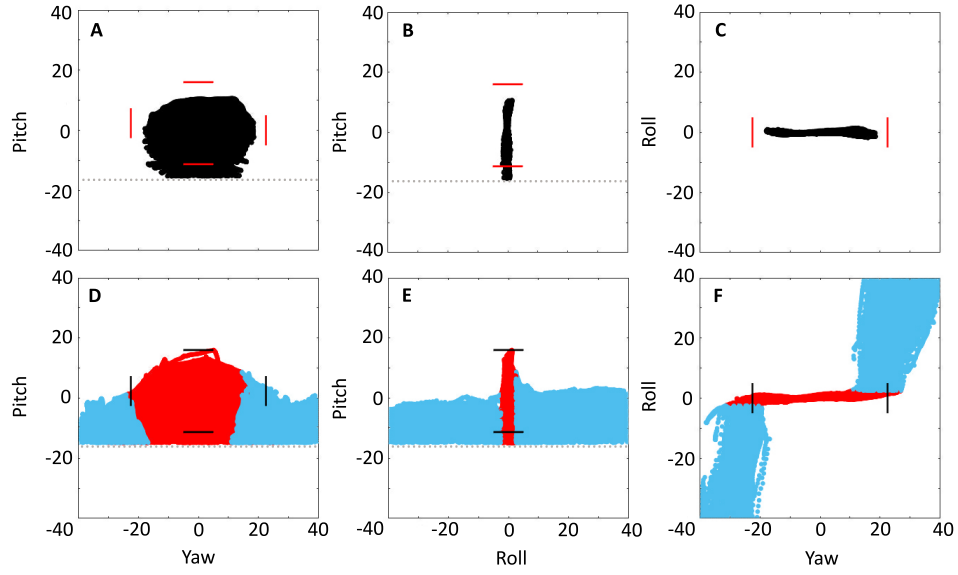

Figure 2.8: Vertebral ROM of the corn snake (*P. guttatus*). Red/black borders show limits obtained from an intact corn snake for yaw and pitch respectively. (A-C) Normal vertebra. (D-F) Altered vertebra. Red and black represent roll ≤ ±2.5 deg, blue represents roll > ±2.5 deg. The gray dotted line highlights the arbitrary ventral cutoff.

normal and altered vertebrae. The normalized areas of the altered vertebrae all had very similar overlap values ranging between 79-89% (Appendix F). The prairie rattlesnake overlap percentage increased to be similar to the other three snakes analyzed in the altered vertebrae compared to the normal vertebrae (Appendices E-F).

The maximal bending in yaw of the intact vertebrae for all species agreed closely with values obtained from the normal isolated vertebrae with a difference in range between 0.7-4.1 deg and an average difference of 2.4 deg (Table 2.1, Figs. 2.5-2.8). Yaw increased for all species in the altered vertebrae (Table 2.1, Figs. 2.5-2.8). Yaw values for normal isolated vertebrae ranged from ±13.9-18.5 deg but increased to ±18.8-26.9 deg for the altered vertebrae. For the altered vertebrae, the smallest increase was 27% for the prairie rattlesnake, and the largest increase was 42% for the brown tree snake. The corn snake and boa constrictor had increases of 31% and 38%, respectively.

The maximal values of bending in ventral pitch for the intact vertebrae of the brown tree snake agreed closely with values obtained from the normal isolated vertebrae with a difference of only 2.1 deg (Table 2.1, Fig. 5). Compared to the normal isolated vertebrae, ventral pitch of the altered vertebrae increased for both the brown tree snake and prairie rattlesnake (Table 2.1, Figs. 2.5-2.8). We could not determine maximal ventral pitch angles for 3D printed vertebrae of the boa constrictor and corn snake because they pitched ventrally indefinitely. In the isolated vertebrae of the brown tree snake and the prairie rattlesnake, ventral pitch was limited by the zygosphene-zygantrum articulation. Maximal values of ventral pitch for the normal isolated vertebrae ranged from -13.5 deg to -8.7 deg, and they increased to -14.7 deg and -11.6

deg in the altered vertebrae of the brown tree snake and prairie rattlesnake respectively. When the zygosphene was removed, ventral pitch increased for the brown tree snake by 10% and in the prairie rattlesnake by 36%, and ventral pitch was further limited by the hypapophyses on the anterior vertebra contacting the rim of the cotyle on the posterior vertebra (Figs. 2.3F, 2.5-2.6).

The maximal values of bending in dorsal pitch for the intact vertebrae agreed closely with values obtained from the normal isolated vertebrae with a difference in range between 0.6-2.4 deg and an average difference of 1.6 deg (Table 2.1, Figs. 2.5-2.8). Altering the isolated vertebrae increased dorsal pitch for all species in this study except for the nearly constant values for the boa constrictor (Table 2.1, Figs. 2.5-2.8). Among all of the species, maximal values of dorsal pitch for normal isolated vertebrae ranged from 4.8-10.7 deg and increased in the altered vertebrae from 7.7-15.9 deg. Maximal dorsal pitch increased for the brown tree snake by 67%, prairie rattlesnake by 58%, and corn snake by 49%.

Roll increased for all species in the altered isolated vertebrae but by different amounts (Table 2.1, Figs. 2.5-2.8). Roll increased from 1.7 deg to 25.3 deg in the brown tree snake and from 1.7 deg to 12.5 deg for the prairie rattlesnake. Roll for the corn snake and the boa constrictor was effectively unconstrained in the altered vertebrae, with values greater than the 40 deg cut off. Roll was limited in the brown tree snake and the prairie rattlesnake because roll caused the cotyle-condyle to twist and disarticulate, which is not possible in the corn snake and boa constrictor. Thus, we halted roll at values before disarticulation would occur.

Discernable roll only occurred in the altered vertebrae at combinations of high yaw and ventral pitch for all species. Roll ROM quickly shifted from <2.5 deg for a particular pitch-yaw combination to >30 deg over small changes in pitch-yaw position in the altered vertebra (Figs. 2.5-2.8). Such increased roll only occurred in the altered vertebrae at combinations of yaw and pitch of approximately ±15-20 deg and -10 deg, respectively. These extreme postures did not overlap with the normal isolated vertebrae ROM in the brown tree snake and the prairie rattlesnake. However, there was overlap of regions of increased roll in the altered vertebrae that occurred within the normal vertebrae ROM of 3% and 11% in the boa constrictor and the corn snake respectively. The pre- and post-zygapophyses prevented roll at lower yaw angles, especially in the prairie rattlesnake, which has large pre- and post-zygapophyses compared to the other species (Fig. 2.2).

Discussion

Snake vertebrae have highly variable shapes, but a prominent zygosphene is always present (Gasc, 1974; Johnson, 1955; Romer, 1956). Our experimental removal of the zygosphene increased roll in all snakes examined, but only at a combination of low ventral pitch and high yaw that could not occur when the zygosphene was present in two species, as shown by our overlap data (Appendices C-D). ROM is generally similar between species with and without a zygosphene (Appendices C-D). The overlap of the pre- and post-zygapophyses prevented roll at the other positions (Fig. 2.3). The base of the hypapophyses in the prairie rattlesnake and the brown tree snake limited ventral

pitch because they collided with the cotyle of the adjacent vertebra. The zygosphene in the normal vertebrae and the neural arch or the pre- and post-zygapophyses in the altered vertebrae limited dorsal pitch. By contrast, the neural spines did not contact each other and therefore did not limit dorsal flexion on the 3D printed models.

The ability of bony structures other than the zygosphene-zygantrum to constrain roll raises the question of why the novel zygosphene-zygantrum articulation evolved, rather than enlargement of existing processes. Perhaps the zygosphene acts as an osseous limit on the ROM of the vertebral column, particularly in yaw. An osseous limit is stronger than relying on soft tissue for restricting movement due to the ability to withstand higher forces without damage. Snake vertebrae can have a wide ROM during some normal locomotor behaviors (Jayne, 1988; Morinaga and Bergmann, 2019; Sharpe et al., 2015), and reliance on soft tissue limits could increase the propensity for injury as seen in rotator cuff injuries and their prevalence among humans (Yamamoto et al., 2010). This bony limit could be beneficial for multiple behaviors that rely upon both high forces and tight bending such as constriction, concertina locomotion, or gripping narrow arboreal substrates. The zygosphene could also reduce the need to rely on proprioception and motor control to prevent the body from reaching postures that could damage tissues similar to the antitrochanter articulating with the femur to restrict rotation in birds (Kambic et al., 2017). Thus, a bony blocker has some benefits that expanding the zygapophyses would be unable to provide (limiting yaw), potentially outweighing the reduced ROM due to the zygosphene. Additionally, snakes can still achieve high flexibility despite the limitations of the ROM via their large total number of

vertebrae compared to other vertebrates. Together, these benefits could potentially give snakes access to increased range of motion compared to legless lizards, which lack a zygosphene-zygantrum articulation (Hoffstetter and Gasc, 1969). The lack of a zygosphene in other limbless tetrapods is puzzling, and may be due to evolutionary trade-offs, constraints, or contingency. Presumably, limbless lizards must limit range of motion either using soft tissue structures, which are vulnerable to injury, or modifications of existing vertebral processes, which may reduce range of motion (Anderson et al., 2001; Johnston and Smidt, 1970; Kazar and Relovszky, 1969; Scopp and Moorman, 2001; Veeger and Van Der Helm, 2007; Zakani et al., 2017). More research is needed to determine how limbless lizards limit roll and measure how their overall range of motion compared with snakes.

Our results suggest that normal isolated snake vertebrae can roll 2-3 deg even with the zygosphene. However, we suggest caution, as such small values could be due to cumulative errors from limited CT resolution, errors in segmenting, and the 3D printing process. The error from the fixed vertebra showed errors in pitch, yaw, and roll of between 0.4-1.9 deg. Any small errors due to our process will comprise a small fraction of the total ROM of pitch and yaw due to the large values of these variables (up to 20 degrees), while small or zero values could be dominated by error. Therefore, roll *in vivo* could be minimal and not biologically important. A prior study (Moon, 1999) reported similar amounts of roll in snakes *in vivo* and in skinned body segments and suggested that roll is actively used in locomotion. However, these *in vivo* estimates of roll were determined from two-dimensional dorsal-view distances between marks along the

dorsal midline and the sides of the snake, although the author acknowledged that rib movements can alter this distance (Moon 1999). Furthermore, apparent roll across multiple joints (with no actual roll between adjacent vertebrae) can arise from combined lateral and dorso-ventral flexion without departing from planar motion (Zhen et al., 2015), which could have confounded both the *in vivo* and skinned body segments data in Moon (1999). Without more direct methods of obtaining *in vivo* data on vertebral motion, it remains unclear if substantial roll occurs *in vivo* in snake vertebrae.

Our ROM values of yaw are similar to some previously reported maximal values for snakes (Jayne, 1988; Sharpe et al., 2015) suggesting they are biologically relevant. Even though one might expect diverse species of snakes to have large differences in ROM, many values are actually rather similar. The maximal amount of realized yaw, however, does vary among the different modes of snake locomotion. For example, Jayne (1988) estimated yaw from marks on the mid-dorsal scales of *Crotalus cerastes*, *Nerodia fasciata*, and *Pantherophis obsoleta* and found less during lateral undulation (approximately 5 deg) than during sidewinding (approximately 7-10 deg). After commonly finding values of yaw between 15-16 deg in both *Nerodia fasciata* and *Pantherophis obsoleta* performing concertina locomotion in tunnels ranging from 3-10% of total snake length, Jayne (1988) suggested that snakes using this mode often may approach their maximal yaw ROM. Although our study did not include the same species, our maximal yaw for a congeneric (*Pantherophis*) reached a similar value of 16 deg (Table 1), supporting the idea that at least some snakes do indeed use their maximal yaw ROM during concertina locomotion. Morinaga and Bergmann (2019) found *Nerodia*

sipedon had inter-vertebral joint angles between 6 and 9 deg when using lateral undulation between different peg spacings. These values are higher than Jayne (1988) found for lateral undulation, but they are still below any of our observed values, supporting Jayne's (1988) conclusions that during lateral undulation, and many other locomotor activities, snakes do not bend maximally. Additionally, Sharpe et al. (2015) found that anaesthetized *Chionactis occipitalis* (165-175 vertebrae) could form an average of 6.2 complete (360 deg) coils when bent by an experimenter (though whether these are maximal values remains unclear), resulting in average yaw ROM between 12.8-13.5 deg which is similar to Jayne (1988) and our own results (Table 2.1). Thus, despite considerable phylogenetic and ecological differences among the few species studied to date, ROM appears broadly similar across snake species, suggesting that variation in overall flexibility depends primarily on variation in the total number of vertebrae.

Snake vertebral ROM values for yaw, dorsal pitch, and ventral pitch are also similar to values previously reported for crocodiles (lateral, dorsal, and ventral flexion: 18.6, 9.4 deg, and 12.7 deg, respectively) (Molnar et al. 2015), skinks (lateral flexion: 13.5 deg) (Sharpe et al. 2015), and armadillos (lateral, dorsal, and ventral flexion: 6, 7, and 8 deg, respectively) (Oliver et al., 2016). Collectively, the data suggest that the considerable flexibility of snakes is mainly from large numbers of vertebrae per unit rather than unusually high ROM.

Digitally altering bones to create hypothetical morphologies is a powerful tool to circumvent limitations of using naturally occurring biological morphologies (Kleinteich et

al., 2012; this study). In our study system, differences in vertebral form between lizards and snakes would create a confounding factor that could not be excluded via traditional analyses. Consequently, creating hypothetical morphologies provides a way to test effects of morphology that would otherwise be impossible using only natural specimens. This approach can also be applied to paleontological specimens (Shiino et al., 2012), modeling of transitional forms throughout the fossil record, and for small bones for which testing can be difficult (this study). However, caution is warranted in interpreting these results, because these are not natural morphologies, and may not represent the ancestral form of snake vertebrae prior to the development of the zygosphene. Potential sources of discrepancies include rib interactions, partial cotyle-condyle disarticulation, and soft tissue limitations (particularly in pitch). Our results have a ventral bias, which may result from an effect of soft tissue such as synovial fluid in the cotyle-condyle joint, but resolving this requires further investigation. It is also possible cartilage in the joints of the cotyle-condyle provide a slight increase in ROM of yaw and pitch. Our data obtained from the intact brown tree snake, boa constrictor, and corn snake did not include forces generated when bending the snakes, which may differ from *in vivo* ranges. Nonetheless, the data from the brown tree snake, boa constrictor, and corn snake matched closely with the observed intact values, supporting the validity of our results and suggesting minimal soft tissue influence in contrast to that observed influence of soft tissue in avian hip and limb joints (Baier, 2012; Kambic et al., 2017; Manafzadeh and Padian, 2018). Thus, biological validation should be used wherever possible.

ROM in joints relies on soft tissue and joint geometry for stability though the contribution of each differs between joints. Whether a system relies on soft tissue or joint geometry, the body typically has to constantly interact with that system, whether that is stiff connective tissue around the joint (Oliver et al., 2016), a deep joint cotyle, or articular facets such as the pre- and post-zygapophyses. However, in snakes, the zygosphene only interacts at positions of high yaw or high dorsal pitch with no effect at most other positions. Through the interaction of multiple joints (i.e., zygosphene-zygantrum and pre- and post-zygapophyses) and a process (i.e., hypapophysis) or soft tissue an overall functional response is achieved that limits yaw, dorsal pitch, and ventral pitch even though any given component listed above may not actively interact at all joint positions. Thus, the zygosphene may allow snakes to avoid certain trade-offs between mobility and stability, while also providing an additional load-bearing structure at high yaw positions. Future work investigating other joint articulations that engage only at high ROM could provide insight into whether other species employ similar mechanisms.

CHAPTER III

CORN SNAKES (*Pantherophis guttatus*) SHOW CONSISTENT SARCOMERE LENGTH RANGES ACROSS MUSCLE GROUPS AND ONTOGENY

Introduction

Sarcomeres are the fundamental component of skeletal muscle and despite their microscopic size, they can have dramatic consequences on whole animal performance (Bennett, 1985; Taylor, 2000; Gidmark et al., 2013). Sarcomeres are composed of thick and thin filaments, myosin and actin respectively, that slide past each other and generate force (Huxley, 1963). Furthermore, the sarcomere's position on the length-tension curve has a direct effect on the amount of force it can generate due to overlap and interactions between the filaments, with the maximum being across the plateau region (i.e., 2.2-2.1 µm in vertebrates) (Gordon et al., 1966). Within vertebrates, sarcomeres are typically found to operate over lengths from 3.6-1.2 µm (Burkholder & Lieber, 2001).

Initial position on the length-tension curve and subsequent length change has important implications for animal biomechanics in a variety of contexts. In fish, sarcomere lengths have been shown to influence bite force at different gapes relevant to prey size (Gidmark et al., 2013; Kaczmarek & Gidmark, 2020). In frogs, sarcomeres

shorten across large length ranges during jumping, but different muscles show different sarcomere lengths in the pre-jump posture. The semimembranosus, a hip extensor, shortens across the plateau for increased force and power production during jumping (Lutz & Rome, 1996). In contrast, the plantaris muscle (an ankle extensor with an elastic tendon) shortens from the descending limb onto the plateau to match the increasing resistance while stretching the elastic tendon (Azizi & Roberts, 2010; Astley & Roberts, 2012). Additionally, sarcomere length has been shown to aid in stability during locomotion via preflexes at timescales too fast for neural feedback due to the rising force on the ascending limb (along with contributions from the force-velocity relationship) (Wagner & Blickhan, 1999; Dickinson et al., 2000; Hooper et al., 2016).

Snakes have a complex repeating sequence of muscles along their axial skeleton (Gasc, 1974, 1981) which faces multiple demands from several modes of locomotion as well as capturing and restraining prey. A snake could have sarcomeres at the plateau of the length-tension curve when the body is straight to ensure near maximum force and power generation during lateral undulation. Conversely, sarcomeres starting on the descending limb and ending on the plateau would be beneficial for constriction by providing increasing force as the coil of the snake tightens around its prey. Snake sarcomere lengths could also potentially differ between muscles and along the body to correspond to different functions such as force generation and stability. Furthermore, these muscles could also vary along with age/size, with small snakes having sarcomere lengths advantageous for speed to evade predators and adults having sarcomere lengths advantageous for constriction. This ontogenetic shift would prioritize

locomotion when predation pressure is highest in neonates and juveniles (Mushinsky & Miller, 1993). As the snakes increase in size and predation pressure declines, sarcomere lengths could shift to be advantageous for constriction to prioritize the capture of larger prey (Rush et al., 2014).

We hypothesized that an ontogenetic series of sarcomeres in corn snakes would show a shift from being centered on the plateau in small individuals to being on the descending limb in adults. To test this hypothesis, we obtained corn snakes (*Pantherophis guttatus*, Linnaeus, 1766) (n=5) across a wide size range (80-335 g), and measured sarcomere length across sizes, muscles, locations on the body, and posture (straight vs bent).

Materials & Methods

Five wild-caught corn snakes, *P. guttatus*, were obtained from a commercial provider (snout-vent length, SVL, range 69.5-101.0 cm; mass range 80-335 g). This species was chosen because they are locomotor generalists, constrictors, and wild-caught specimens are readily available. All experiments were approved by University of Akron IACUC.

Snakes were chosen to have an approximately even distribution of $\log_{10}$ transformed masses and were either euthanized upon arrival or housed and fed weekly with water ad libitum until reaching an appropriate mass. Corn snakes were euthanized using MS-222 following the two-stage injection protocol in Conroy et al. (2009). After euthanasia, snakes were measured, placed on a corrugated plastic board and positioned

with maximal lateral bending at 25% (anterior), 50% (middle), and 75% (posterior) SVL and a straight posture in all other regions (Fig. 3.1). Dissection pins adjacent to, but not piercing, the body were used to hold the posture, and small incisions were made into the skin and formalin was injected into the body cavity to ensure thorough fixation of the musculature. After fixation, we dissected the five largest epaxial muscles, the spinalis, semispinalis, multifidus, longissimus dorsi, and iliocostalis (upper and lower), and one hypaxial muscle, the levator costae (Jayne, 1985; Penning, 2018). Once the muscles were dissected, they were placed into 15% nitric acid for 3-5 days to loosen the connective tissue and allow easy separation of the muscle fibers. The muscle fibers were photographed using a MU1000 microscope camera connected to a FMA050 adaptor (AMScope, Irvine, CA, USA) under a microscope (40x magnification) and sarcomere lengths were measured using FIJI ((Schindelin et al., 2012); ImageJ 1.8.0_66 64 bit, Wayne Rasband, NIH, Bethesda, MD, USA). A minimum of 20 sarcomeres in series were measured per muscle fiber with seven muscle fibers measured per muscle and posture. A calibration slide with 0.01 mm spacing was used to convert pixels to mm. In bent segments, measurements were repeated bilaterally to quantify contracted and extended lengths. Once all measurements had been collected, an ANOVA was conducted with and without a random effect assigned to mass (equivalent to individual) and the full factorial for mass, posture (straight, extended, and contracted), position (anterior, middle, or posterior of the body), and muscle (spinalis, semispinalis, multifidus, longissimus dorsi, dorsal iliocostalis, ventral iliocostalis, and levator costae). A stepdown Bonferroni method was used to correct for multiple comparisons.

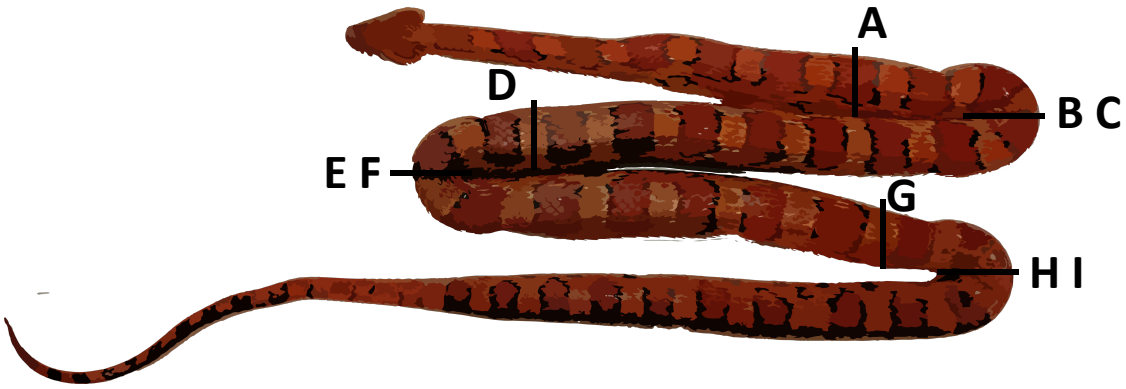

Figure 3.1: Corn snake preservation posture, showing three maximal bends at 25%, 50%, and 75% SVL. A, D, and G denote regions where straight sarcomere lengths were taken. B-C, E-F, and H-I denote regions where extended and contracted sarcomere lengths were taken.

Results

In the ANOVA with mass considered a fixed effect, all factors and interactions were found to be significant, with p-values <0.0001 (Table 3.1). In the ANOVA with mass as a random effect, only posture, mass • posture • position, mass • posture • position • muscle, mass • position • muscle, and posture • muscle were found to be significantly different (Table 3.2).

Corn snake sarcomere lengths were largely consistent across mass, position along the body, and muscle analyzed (Table 3.3). While all factors and interactions were significant with mass as a fixed effect and many were significant when mass was treated as a random effect, the effect sizes (i.e. differences between the highest and lowest least square mean values) were relatively small for main factors of mass, position, and

Table 3.1: Sarcomeres in the corn snake showing contracted, straight, and extended lengths in μm with mean±s.d. for all seven muscles. Measurements are combined for all masses and positions (i.e., anterior, middle, posterior).

Muscle	Contracted	Straight	Extended
Spinalis	1.72±0.28	2.46±0.21	3.11±0.29
Semispinalis	1.73±0.28	2.43±0.24	3.05±0.33
Multifidus	1.76±0.20	2.41±0.20	3.25±0.30
Longissimus dorsi	1.76±0.28	2.47±0.31	3.45±0.22
Iliocostalis 1-upper	1.84±0.29	2.50±0.21	3.36±0.25
Iliocostalis 2-lower	1.87±0.29	2.50±0.18	3.32±0.24
Levator costae	1.88±0.23	2.42±0.22	3.29±0.22

Table 3.2: ANOVA for snake sarcomere measurements without random linked to mass (or individual). All variables came out significant.

Variable	$F_{314,1893}$ Ratio	P-value	Range of Least-squared Means
Mass	46.25	<0.0001	2.43-2.58
Posture	13317.63	<0.0001	1.79-3.26
Mass•Posture	35.61	<0.0001	1.73-3.39
Position	21.27	<0.0001	2.47-2.53
Mass•Position	6.89	<0.0001	2.38-2.62
Posture•Position	4.12	<0.0001	1.76-3.31
Mass•Posture•Position	19.11	<0.0001	1.68-3.41
Muscle	49.44	<0.0001	2.40-2.57
Mass•Muscle	20.53	<0.0001	2.25-2.71
Posture•Muscle	19.97	<0.0001	1.72-3.45
Mass•Posture•Muscle	7.02	<0.0001	1.44-3.63
Position•Muscle	7.42	<0.0001	2.36-2.64
Mass•Position•Muscle	9.28	<0.0001	2.17-2.82
Posture•Position•Muscle	6.49	<0.0001	1.67-3.46
Mass•Posture•Position•Muscle	4.78	<0.0001	1.34-3.79

muscle excluding posture (0.06-0.17 μm) (Tables 3.1-3.2). Interactions among these three factors can result in larger effects, up to 0.65 μm, but the largest of these effects are interactions with muscle and thus are comparing different muscles at different positions and/or sizes, making these comparisons of limited value. In contrast, posture

Table 3.3: ANOVA for snake sarcomere measurements with mass (or individual) as a random factor. Bolded variables denote significance. Range of least-squared means is identical to Table 3.2.

Variable	$F_{314,1893}$ Ratio	P-value
Posture	**374.02**	**<0.0001**
Mass&Random•Posture•Position	**4**	**<0.0001**
Mass&Random•Posture•Position•Muscle	**4.78**	**<0.0001**
Mass&Random•Position•Muscle	**1.94**	**0.003**
Posture•Muscle	**2.85**	**0.005**
Mass&Random•Muscle	1.78	0.0481
Mass&Random•Posture•Muscle	1.47	0.0566
Muscle	2.41	0.0578
Position	3.09	0.1015
Posture•Position•Muscle	1.36	0.1508
Mass&Random•Posture	1.67	0.1715
Mass&Random	1.43	0.3465
Position•Muscle	0.8	0.6493
Posture•Position	0.22	0.9259
Mass&Random•Position	0.29	0.9614

had a much larger effect size (1.47 μm), with interactions producing still larger effects (up to 2.45 μm) (Table 3.1). Thus, while all factors were significant, the effects are so small without posture that they are hardly meaningful in regard to sarcomere lengths and the larger scale effects of muscle shortening. The ANOVA with a random effect assigned to mass (or individual) has broadly similar results and showed five factors and interactions as significant, four of which involved posture. As seen in the first ANOVA, the variation in the highest and lowest values was small in the significant factorial without posture and unlikely to be meaningful in the large-scale muscular contractions of the animal (Table 3.2). Posture (i.e., straight, extended, or contracted) is the strongest signal found in our data and all other variables are relatively minor in their effects on sarcomere lengths.

Discussion

Corn snake sarcomeres had large differences between extended, straight, and contracted lengths (Fig. 3.2, Table 3.3). Different muscles, body sizes, and positions on the body showed only minor differences in sarcomere lengths and thus were combined in Fig. 3.2. Straight and extended lengths of sarcomeres for every muscle were on the descending limb of the length-tension curve. Contracted lengths of sarcomeres for most muscles were on the ascending limb, with only a few exceptions on the plateau of the length-tension curve (Fig. 3.2).

We found the sarcomere positions on the length-tension curve (Fig. 3.2) are consistent with being advantageous for a snake that constricts its prey. As the muscles contract and the body bends, they generate higher forces and make it more difficult for the prey to escape the constricting coils. However, while this is consistent with constriction performance, we cannot say it evolved for that reason based on only a single species (Gould & Lewontin, 1979; Felsenstein, 1985; Garland & Adolph, 1994). However, contrary to our hypothesis, sarcomere length did not change with size, so the sarcomeres are not shifting during ontogeny to optimize from one function (i.e. locomotion) to another (i.e. constriction). However, there could be other beneficial aspects of sarcomeres on the descending limb that we are currently unaware of, potentially in locomotion or strike performance. There may also be non-selective reasons including evolutionary history or developmental constraints.

Having muscles on the descending limb of the length-tension curve could have

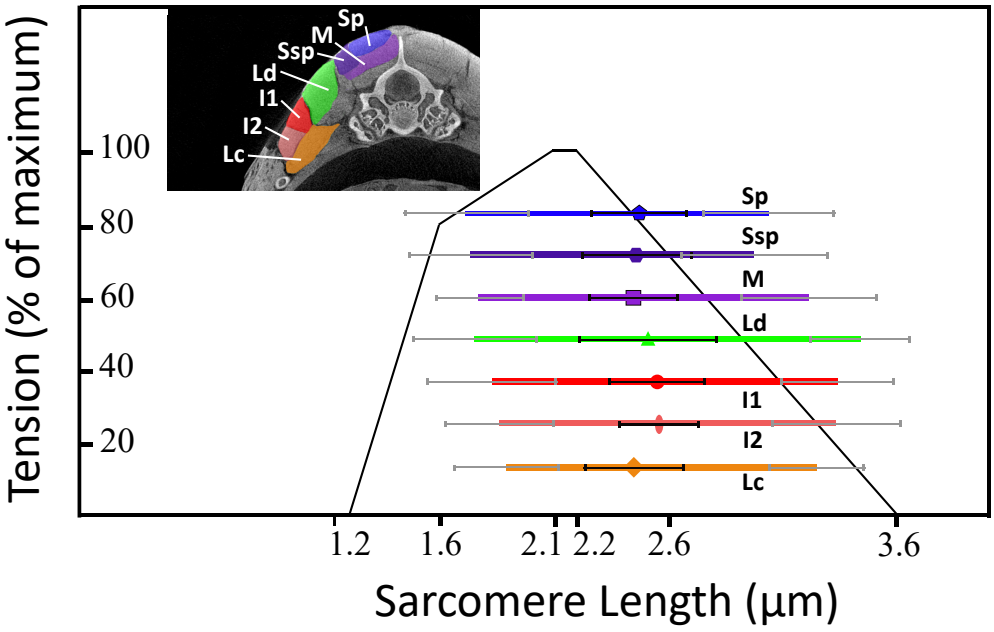

Figure 3.2: A length-tension curve showing all snake muscles analyzed in this study from five corn snakes. Shapes are placed at straight lengths and the ends of the color bars represent extended and contracted sarcomere lengths respectively. Smaller gray and black bars represent standard deviation for each element. Inset in the top left shows a µCT scan of a corn snake body segment stained with PMA with relevant muscles highlighted and labeled (Sp, blue, pentagon-spinalis; Ssp, dark purple, hexagon-semispinalis; M, light purple, square-multifidus; Ld, green, triangle-longissimus dorsi; I1, red, circle-upper iliocostalis; I2, light red, oval-lower iliocostalis; and Lc, orange, diamond-levator costae).

complex effects on locomotion. For example, if a snake is perturbed in the direction of an active contraction, it will increase the contraction force further and assist the motion. If the perturbation is in the opposite direction of the contracting segment, the body would stretch as the muscle would lose force due to the effects of the length-tension curve (though this would be partially counteracted by the force-velocity relationship). This could harm the snake's ability to maintain its posture during locomotion, but could also help the snake passively conform to the substrate. However, our results only show

the change in force due to length-tension relationships in snake muscle, and during active locomotion multiple other factors influence force production, including the force-velocity relationship and activation-deactivation dynamics (Josephson, 1985).

This is the first study to analyze sarcomere lengths in snake musculature. Accordingly, it is unclear if this pattern is conserved among snakes or if variation exists based on a multitude of factors including phyletic history, constrictors versus non-constrictors, habitat type (e.g., terrestrial, arboreal, aquatic, and burrowing), and taxa that have developed venom. However, sarcomere lengths have been reported in a variety of other taxa including frogs, mice, rats, rabbits, fish, cats, birds, and humans (Burkholder & Lieber, 2001). The majority of these taxa have highly variable sarcomere lengths (see Burkholder and Lieber, 2001, and references therein) but two exceptions included bird (pectoralis, patagialis, and surpracoracoideus) and fish (red and white axial muscle) sarcomeres that were both positioned almost entirely on the plateau and the ascending limb (Cutts, 1986; Ashmore et al., 1988; Mathieu-Costello, 1991; Rome & Sosnicki, 1991; Lieber et al., 1992). Both of these groups operate in dynamic habitats that prioritize power production that would benefit from sarcomeres with short excursions near the plateau of the length-tension curve. These restricted sarcomere lengths are unsurprising in these habitats. For birds, power production is important to produce fast wing beats to maintain flight, whereas fish benefit from the plateau of the length-tension curve by activating fewer motor units and the associated energetic savings (Cutts, 1986; Rome & Sosnicki, 1991). However, it is relatively unclear why corn snake sarcomeres are highly consistent across mass/age, position of the body, and even

different muscles. More generally, it is unclear what factors govern the ranges of sarcomere lengths a muscle operates over. Muscles perform a wide variety of tasks from force production to stabilization (Dickinson et al., 2000) and one muscle can perform multiple functions, depending upon stimulation (Full et al., 1998). Thus, functional inferences based on sarcomere length should be regarded tentatively.

The consistent sarcomere length range across postures in a variety of snake muscles, despite highly variable distances from the vertebrae, is puzzling. Theoretically, muscles close to the vertebral midline, such as the spinalis and semispinalis, should have a shorter muscular excursion compared to muscles further away from it, such as the iliocostalis (Full et al., 1998) (see inset in Fig. 3.2). However, we found a surprising consistency in muscular excursions regardless of distance from the center of rotation. This is unlikely to be a result of mistakes in preservation or other methodological errors due to the high consistency regardless of mass, muscle, position on the body, or tendon length (because muscles with short and long tendons still showed consistent values). One possible explanation for these values could be muscle and tendon length ratios. For example, the iliocostalis is predicted to undergo large length changes due to its distance from the center of rotation, and since it has relatively long muscle fibers with short tendon lengths (Jayne, 1988), the relative length change of the muscle fiber will closely match that of the whole muscle-tendon unit (Ruben, 1977; Lawing et al., 2012; Astley, 2020). In contrast, the semispinalis-spinalis is located close to the midline of the snake and thus expected to undergo only modest length change during lateral bending, but because the anterior tendon comprises over 70% of the length of the muscle-tendon

unit (Jayne, 1982), the relative length change of the muscle fiber would be correspondingly amplified (Ruben, 1977; Lawing et al., 2012; Astley, 2020). However, future work investigating snake muscular lever arms will explore this quantitatively to better understand how these muscles undergo similar excursions regardless of their distances from the center of rotation.

CHAPTER IV

GENERATION OF PROPULSIVE FORCE VIA VERTICAL UNDULATION IN SNAKES

Introduction

All animals achieve locomotion by applying force to the environment, thereby generating reaction forces which propel the animal (Dickinson et al., 2000). Limbed vertebrates typically have discrete propulsive contact points (feet) which must simultaneously generate forces to support the body weight, provide propulsive force, and maintain stability. However, in terrestrial limbless vertebrates, any individual body segment can be propulsive while stability and support needs are minimal in most environments. Additionally, frictional forces overwhelm inertial effects (Gray, 1946; Hu et al., 2009). Terrestrial limbless vertebrates propel themselves using a wide range of locomotor modes, depending upon the type of environment they encounter; however, lateral undulation is the most common across and within taxa (Gans, 1962). Lateral undulation uses posteriorly propagating horizontal waves of bending that contact and push against asperities in the environment (e.g., grass, rocks, sticks), generating reaction forces that propel the animal forward (Gans, 1962; Gray and Lissmann, 1950; Jayne, 1986).

Snakes are also capable of generating propagating vertical waves, observed during lateral undulation and sidewinding to reduce friction on certain body segments (Hu et al., 2009; Marvi et al., 2014) and during gliding for stabilization (Yeaton et al., 2020). However, the ability of snakes to generate propulsive reaction forces from vertical waves in terrestrial environments has never been tested. We hypothesize that snakes can use vertical waves to generate propulsive forces via a similar mechanism to lateral undulation when in contact with vertical asperities in the substrate at suitable angles (Fig. 4.1A-D). To test our hypothesis, we measured substrate reaction forces and kinematics as snakes traversed an experimental setup designed to elicit this behavior while impeding other modes of locomotion and confounding factors. Furthermore, our hypothesis predicts that snakes should only be able to generate net propulsive forces from surfaces with a vertical slope beyond the angle of frictional slipping (Fig. 4.1B-D). Thus, our experimental setup tested the snake with only a single potential propulsive surface oriented at an angle predicted to be either sufficient or insufficient for propulsion via vertical undulation. Finally, we attempted to replicate propulsion via vertical undulation in a robotic model to show that observed propulsion in the snake is not attributable to unobserved mechanisms, and that the proposed mechanism is mechanically sound even in the absence of snake musculoskeletal anatomy and neural control.

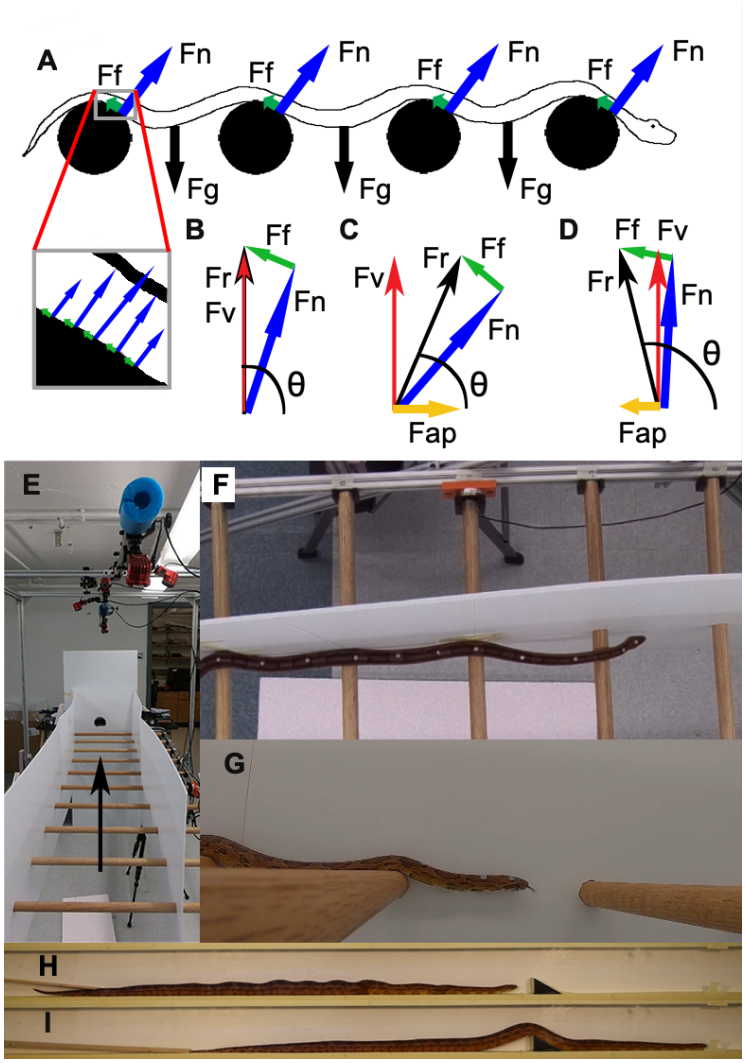

Figure 4.1: A) A lateral-view diagram of a snake using vertical undulations across multiple dowels (black circles) showing idealized forces. Inset shows the force distribution across the contact surface, which is summed into an overall reaction force in the main image. Fap-anteroposterior force, Ff-frictional force, Fn-normal force, Fr-resultant force, Fv-vertical force, θ-angle of F_r. B) Diagram of reaction forces for a snake progressing at constant velocity. Because there is no net acceleration, there is also no net force. C) Diagram of reaction forces if the snake is accelerating, generating a net forward force. D) Diagram of reaction forces if the snake is decelerating, generating a net braking force. E) Experimental setup showing cameras overhead and the horizontal ladder setup, with an arrow depicting the direction the snake is moving. F) Dorsal view of a corn snake using vertical undulations. The body is close to but not in contact with the side wall. G) Lateral view of a corn snake using vertical undulations. H and I) Side views of a corn snake moving through a tunnel with a single potential contact for vertical undulations. The snake initially performs concertina locomotion (H), indicated by the tight body waves, but switches to vertical undulations (I) once it has sufficient contact with the wedge.

Methods & Materials

Four adult wild-caught corn snakes (*Pantherophis guttatus)* were obtained from a commercial provider (mean +/- s.d.: snout vent length (SVL) = 102.4 +/- 9.3 cm, range 92.6-114.3 cm, mass = 463 +/- 62.6 g, range 340-550 g). This species was chosen because they are locomotor generalists and thus likely to elicit the desired behavior. All experiments were approved by University of Akron IACUC. Locomotion trials were conducted after warming the snakes to 29-32˚C, the field active temperature of a congeneric (Brattstrom, 1965).

We constructed a 248 cm long trackway consisting of a frame of 80/20 longitudinal supports with eleven horizontal oak dowels (91 cm long, 2.5 cm diameter) placed perpendicular to the longitudinal supports and spaced at 20 cm intervals, much like the rungs of a ladder laid horizontally (Fig. 4.1E). Walls were placed 45 cm apart on either side of the dowels (walls extend 36.5 cm above the dowels and 22.0 cm below) and the trackway was raised 88 cm above the ground to dissuade the snakes from leaving the trackway. Oak dowels were sanded and treated with a polyurethane sealant. Snakes were induced to move along the length of the trackway and thus perpendicular to the dowels (Fig. 4.1F-G). Trials were performed in sets of three per 24 hours and individuals were allowed a minimum of five minutes rest between trials to prevent fatigue. A dark enclosure was placed at the end of the trackway to encourage movement in the desired direction and to allow for a location of rest between trials. Light tapping, rubbing with fingers, or touching with a snake hook were used on the tail to encourage movement though we did not attempt to induce maximal speed from the

animals. Snakes were not tested for 24 hours after feeding occurred. To provide an experimental control and clear contrast between the forces produced in active versus passive systems, and to show that our data are not an artefact of our measurement system, we dragged a braided nylon rope (229 g, 144 cm long, 1.7 cm diameter) across the dowel array, as this should produce only braking force and braking impulse. The coefficient of friction was measured using a standard tilting plane method, in which snakes were conscious and alert. The snakes were oriented with most body segments parallel to the slope with anterior downwards (the presence of body segments at other angles would slightly over-estimate the coefficient of friction due to scale anisotropy) on a plane of oak prepared identically to the dowels and tilted until they began to slide (Astley and Jayne, 2007; Gray and Lissmann, 1950; Sharpe et al., 2015); the average coefficient of friction was 0.17 (+/- 0.02, range 0.14-0.19) for the snakes (n=4) and 0.28 (+/- 0.03, range 0.23-0.32) for the rope based on three trials per individual/object. While there were some trials in which only braking force was recorded, to streamline analysis, only trials with propulsive force were analyzed (see Results).

Two six-axis force/torque sensors (Nano 43, ATI Industrial Automation, Apex, NC, USA) were connected on either end of a single dowel mid-way along the trackway (dowel 6 of 11). Outputs of the force sensors were collected using 12 channels (six per sensor) on a NIDAQ N1-USB-6218 (16 bits, National Instruments, TX, USA) and recorded using the software IGOR Pro (WaveMetrics, Tigard, OR, USA) at 1 kHz. This force-sensing dowel was calibrated using hanging masses and pulleys at different angles and locations along the dowel to apply known anterior/posterior, lateral, and vertical forces, which

were used to create a calibration matrix using the MATLAB (MathWorks, Natick, MA, USA) function linsolve. Force data were splined to smooth the data in IGOR Pro and analyzed using a custom-written script in MATLAB. Data were normalized to body weight to facilitate comparisons between individuals (Appendix G). During rope trials, forces induced by inertial motion of the end of the rope dropping from an adjacent dowel would confound analysis, thus we only included the smooth rise and steady state of the forces during these trials (Appendix H). The impulse (the time integral of force, in BW*s) is the total change in momentum of the system, and was used to determine if the overall interaction between the snake and the force-sensing dowel had a net propulsive or net braking effect, similar to limbed studies (Budsberg et al., 1987; Hodson et al., 2001).

Kinematics were recorded at 120 images s^{-1} using six motion capture cameras (Flex 13, NaturalPoint, Inc., OR, USA) placed 1 m above the dowels at varying angles (Fig. 1E). Small markers of infra-red 7610 reflective tape (3M, MN, USA) were placed at regular intervals (~10 cm) along the dorsal side of each snake. Camera synchronization, recording, calibration, point tracking, and position calculation were all accomplished using Motive Optitrack software v.2.0.2 (NaturalPoint, Inc.), which then exported 3D marker coordinates. A HERO6 Black GoPro (GoPro Inc., CA, USA) camera was also used to record video from above for visual confirmation, but not analysis. To determine how straight the snake was when moving across the force-sensing dowel (and thereby rule out lateral undulation), we analyzed motion capture data (dorsal view, fore-aft and lateral components) using a custom-written script in MATLAB to perform a linear

regression on the points within 20 cm of the force dowel throughout the trial. The captured region spanned three dowels (middle dowel with the force sensors) while the entire snake's body contacted between five and six dowels at any one time. Snakes occasionally used lateral bends prior to and after this region, however trials were discarded if any lateral bends occurred on the force-sensing dowel or adjacent dowels. We quantified the maximum residual and the 95% confidence interval of the residuals as metrics of body straightness, and the angle of the body relative to the trackway (φ = 0^o is parallel and $\varphi = 90^o$ is perpendicular). To quantify the vertical undulations along the captured region, we analyzed the motion capture data (lateral view, vertical and fore-aft components) by splining along the captured region, normalized the splines by height at the force-sensing dowel, and ran both an ANOVA and Tukey's (5% probability) *post-hoc* statistical tests using custom-written scripts in MATLAB. Overall velocity was calculated from Motive Optitrack data in the horizontal plane, fore-aft and lateral components. The snake exerts a net normal and frictional force on the dowel, with the normal force being perpendicular to the substrate and the frictional force being tangent and equal to the magnitude of the normal force multiplied by the coefficient of friction (μ) (Fig. 4.1B-D). The vector sum of the normal force and frictional force is the net substrate reaction force, the angle of which determines whether there is net propulsive or braking force (Fig. 4.1B-D). The force sensors in our study provide us the antero-posterior (F_{AP}) and the vertical (F_V) components of this reaction force (Fig. 4.1A-D). Based on these relationships, one can calculate the magnitude of the normal force (F_N):

$$\|F_N\| = \frac{\|F_{AP}\|}{\cos(\theta)\sqrt{1+\mu^2}} \quad (4.1)$$

where θ_{F_R} is the angle of the resultant force (F_R),:

$$\theta = tan^{-1}\left(\|F_V\| \Big/ \|F_{AP}\|\right) \quad (4.2)$$

From these equations (and those easily derived from them), the magnitude and orientation of any of the vectors can be derived (Fig. 4.1B-D), however, we report the antero-posterior (F_{AP}) and the vertical (F_V) forces (particularly F_{AP}), as these components directly test our hypothesis.

To test whether single vertical asperities of the appropriate orientation could be used to generate propulsion in a terrestrial setting (despite drag on many body segments), we constructed a trackway made of 1.27 cm thick expanded PVC boards, a common construction material consisting of foamed PVC interior with a smooth surface finish. This trackway was 5 cm wide and 180 cm long with a sloped wedge three-quarters of the way along the trackway (Fig. 4.1H-I). All horizontal surfaces were covered with masking tape, which had an average coefficient of friction with the snakes of μ_{tape} = 0.21 (+/- 0.06). One lateral wall was clear acrylic, and video was recorded using a Nikon D3300 DSLR camera (Nikon, Tokyo, Japan). In one set of trials, the wedge had a slope of 30°, steeper than the predicted minimum necessary for propulsive force ($\tan^{-1}(\mu_{tape})$ = 11.3°) and thus suitable for generating propulsive forces (Fig. 4.1C, Appendix I), while in the second set of trials, the wedge had a slope of 8°, which is predicted to be insufficient for generating net propulsive force (Fig. 4.1D, Appendix I). Each snake moved through the tunnel three times, separated by rest periods of at least 15 minutes.

To test whether pure vertical undulation is sufficient to traverse our experimental setup and rule out unobserved mechanisms, a 13-link snake robot composed of twelve servo-motors (Hitec HS-85BB, Hitec RCD USA, Inc., Poway, CA) mounted in custom 3D printed brackets was constructed (total length: 73.5 cm, mass: 398.6 g, coefficient of friction: 0.47 +/- 0.03, range 0.45-0.53). The snake robot was controlled through a USB servo controller (Lynxmotion, SSC-32U, Robotshop, Mirabel, Canada) using a custom-written Python (Python Software Foundation, Wilmington, Delaware, USA) script using a serpenoid wave (Hirose, 1993) with the equation:

$$M_i = a * \sin(t + p_i) + x_i \quad (4.3)$$

where M_i is the angle of motor number i, a is the maximum angle possible, t is time, p_i is phase shift between successive motors, and x_i is an offset to ensure all links are parallel when all motors are at an angle (M) of zero. The values used for these experiments were a= 600 μs (for pulse-width modulation control) and p = 1.5 radians, which produced two waves on the body and a suitably long, shallow wave to span two or more pegs in order to support itself. The robot had no sensors and body posture was under open-loop control.

Results

Snakes were able to move across the setup using propulsive vertical undulations (velocity 0.04 SVL•s^{-1} ± 0.03, 4.1 cm•s^{-1} ± 2.6) despite minimal lateral undulation and no apparent use of other modes of locomotion. The motion capture data revealed significant vertical displacement of the body across the force-sensing dowel ($F_{5,90}$ = 4.37,

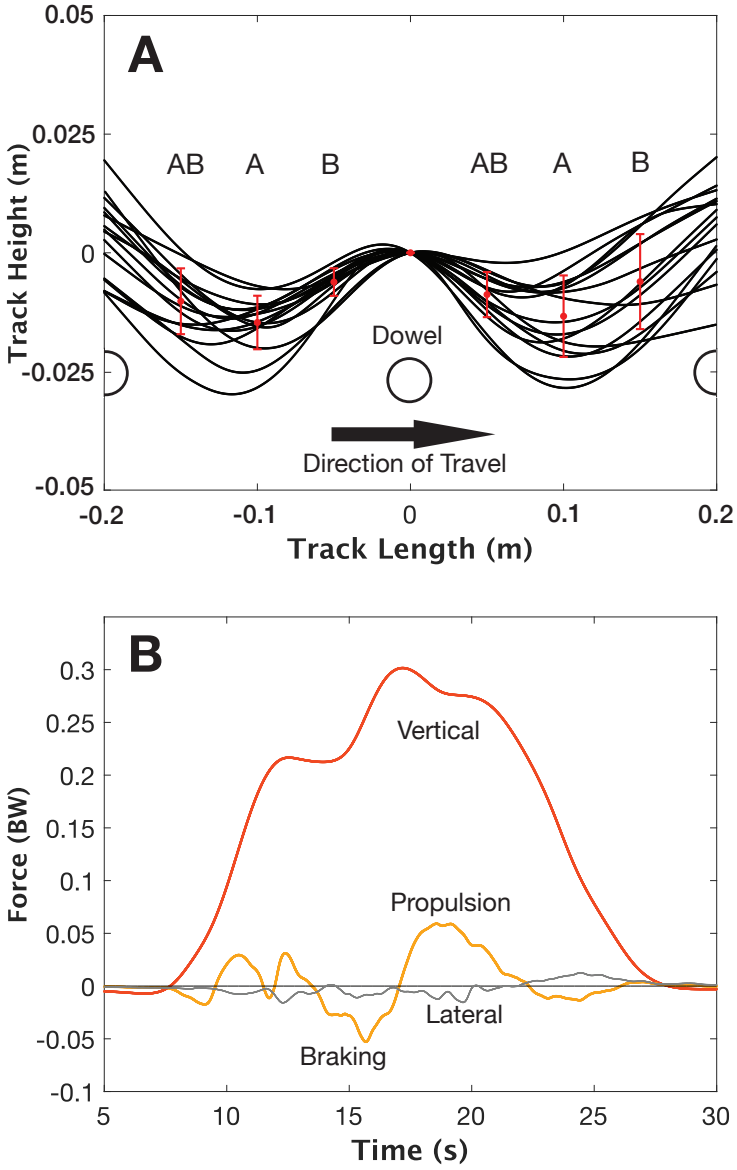

Figure 4.2. A) Splines of dorsal marker paths in all trials (lateral view). Red dots and bars indicate the mean and s.d. of vertical displacement at five cm intervals (relative to the midpoint) showing clear vertical displacement prior to and after the force-sensing dowel (zero) represented by the white circle. Letters reflect significant differences based on the Tukey's *post-hoc* test and the arrow indicates the direction of movement. B) Forces during a complete vertical undulation trial, from initial head contact (~7 s) until the tail has lost contact with the force-sensing dowel (~27 s). The corn snakes were spread over 4-6 pegs and the weight is unevenly distributed along its length. The orange line is the vertical force and the yellow line the anterior/posterior force. The gray line is the lateral force and the dashed line marks zero force. Propulsive force is positive, while braking force is negative.

p-value < 0.0013) (Fig. 4.2A) with a nearly straight horizontal posture approximately parallel to the trackway (2.18^{o} +/- 2.26^{o} relative to the trackway) and that most points followed a nearly straight path (maximum lateral excursion = 11 cm, 95% confidence interval = 3.0 cm). Snakes applied highly variable forces to the instrumented dowel, ranging from pure braking to predominantly propulsive, without clear temporal patterns (Fig. 4.2B, Appendix G). The maximum propulsive force on a single peg (mean ± s.d: 0.08 +/- 0.04 body weight, BW) was larger than the maximum braking force on a single peg (-0.04 +/- 0.02 BW) in all trials analyzed (Table 4.1); the maximum frictional force to be overcome is 0.17 BW for the entire snake. The maximum lateral force in either direction was small (0.02 +/- 0.01 BW). For all but two trials, there was a net propulsive impulse (Table 4.1), and the average propulsive impulse was more than double the braking impulse (Table 1). The average lateral impulse was low (Table 4.1). The control trials in which a rope was dragged across the trackway generated high maximum braking force (-0.09 +/- 0.006 rope weights (RW)), consistent with the higher coefficient of friction, but never generated propulsive force (Table 4.1). The average lateral force in either direction of the rope trials was low (0.01 +/- 0.006 RW). The rope had purely braking impulse (Table 4.1) and the average lateral impulse of the rope was low (Table 4.1).

In the trials within the tunnel, the corn snakes always used concertina locomotion prior to encountering the sloped surface, but noticeably transitioned to vertical undulations shortly after encountering the 30° sloped wedge in all but two (10/12) of the trials (Fig. 4.1I). In contrast, the snakes encountering the 8° sloped wedge

Table 4.1. Summary of the maximum forces and average impulses obtained during our experiments.

	Snake		Rope	
	Maximum/average	Range	Maximum/average	Range
Force (BW or RW)	-	-	-	-
Propulsive	0.08	0.14 to 0.03	0.00	0.00 to 0.00
Braking	-0.04	-0.09 to -0.01	-0.09	-0.09 to -0.08
Lateral		-0.03 to 0.05		-0.02 to 0.02
Impulse (BW*s or RW*s)	-	-	-	-
Anterior/Posterior	0.35	-0.19 to 1.29	-2.37	-2.61 to -2.11
Braking	-0.29	-0.88 to -0.02	-2.37	-2.61 to -2.11
Propulsive	0.64	0.25 to 1.65	0.00	0.00
Lateral net	0.07	-0.61 to 0.62	-0.11	-0.22 to 0.08
Lateral positive	0.25	0.003 to 0.87	0.08	0.01 to 0.48
Lateral negative	-0.18	-0.61 to -0.003	-0.19	-0.23 to -0.13

continued to perform concertina locomotion across the wedge, and never used vertical undulations.

The snake robot successfully moved across the setup using a vertical waveform in all five trials attempted. Because the snake robot consisted of rectangular body segments connected by revolute joints, once a given segment achieved sufficient contact angle to generate propulsive force (Fig. 4.1D), the robot would slide forward until the subsequent segment (with insufficient angle) collided with the dowel. This resulted in a discontinuous velocity which, in turn, precluded effective force measurements.

Discussion

These results confirm our hypothesis that snakes can generate propulsive force via posteriorly propagating vertical waves down the body (Fig. 4.1A-D), albeit in a highly constrained, artificial system. During all trials, snakes had a relatively straight posture with minimal lateral bending across the region with the force-sensing dowel. This posture precludes the use of lateral undulation to generate the observed forces; inspection of video recordings showed no evidence of rectilinear movement. Similarly, while snakes may use rib motions or muscular connections to and within the skin to deform the ventral surface during this behavior, the robotic trials show that the proposed mechanism can function effectively even in a highly simplified system without these anatomical benefits.

Several lines of evidence suggest that snakes can generate considerable

propulsive force per contact via vertical undulations. In several un-analyzed trials, no propulsion was captured by the force-sensing dowel, but steady forward progression was nonetheless occurring without obvious lateral undulation (Appendix J). Since we were only able to measure forces at a single dowel, this suggests that snakes do not need to use every contact point to propel themselves using vertical undulations and trials without measured propulsion were generating propulsion using other contact points. Consistent with this, the mean peak propulsive force across trials was 0.08 BW, almost half the force necessary to propel the snake (given a coefficient of friction of 0.17), with one trial showing a force of 0.14 BW, indicating that snakes were capable of generating sufficient force for propulsion from as few as two contact points. Similarly, during the tunnel trials, the entire snake was propelled via a single contact area on the 30° inclined wedge.

While snakes are unlikely to use purely vertical undulations to move through their environment, propulsive vertical undulations (as opposed to drag-reducing vertical motion in sinus lifting and sidewinding (Hu et al., 2009; Marvi et al., 2014)) could be easily combined with lateral undulation. Snakes might use lateral undulation until they encounter a vertical asperity, then use vertical undulations against this object while simultaneously using lateral undulation at other points on the body, as opposed to simply dragging their body across these vertical obstructions. Indeed, this has been recently shown by Fu et al. (2022) where snakes traversed a complex 3D terrain using vertical and lateral bends at the same time. This mechanism has the potential to be particularly advantageous in arboreal locomotion, where a variety of structures provide

useful contacts for vertical undulations. Similarly, rodent burrows are often spatially complex and vertical undulations could also be employed if suitable asperities are present, as in the tunnel trials, rather than using concertina locomotion as snakes typically do in narrow, flat tunnels.

Our experiments confirm that snakes can use vertical undulations to propel themselves, but whether this mechanism can be classified as a new mode of locomotion is uncertain. Jayne (2020) highlights at least eleven modes of locomotion under four specific headings (i.e., rectilinear, sidewinding, five types of lateral undulation, and four types of concertina). Vertical motion has been previously documented in lateral undulation and sidewinding for reducing friction (Hu et al., 2009; Marvi et al., 2014), during gliding for stability (Yeaton et al., 2020), and bridging height changes in arboreal environments (Byrnes and Jayne, 2012) but never previously for direct generation of propulsive force. However, while we demonstrate effective locomotion using only vertical undulations, our instrumented trackway is, by necessity, a highly constrained and artificial system, and snakes are unlikely to use purely vertical undulation in natural environments. However, whether or not this mechanism is a true “mode” of locomotion, the ability of snakes to use vertical undulations to generate propulsion dramatically expands our understanding of snake locomotor mechanics and their interactions with their habitats. By using vertical undulations, snakes demonstrate the ability to exploit the complexity of their habitat in three dimensions, generating propulsive forces from previously overlooked surfaces and allowing more effective use of cluttered habitats.

CHAPTER V

BLOOD PYTHON (*Python brongersmai*) STRIKE KINEMATICS AND FORCES ARE ROBUST TO VARIATIONS IN SUBSTRATE GEOMETRY

Introduction

Rapid impulsive behaviors (e.g., frog jumps, mantis shrimp strikes) are challenging for organisms for many reasons, including generating high force, high power, and the fast responses required (Astley and Roberts, 2014; deVries et al., 2012; Ilton et al., 2018; Patek et al., 2004). Multiple factors can influence quick actions including substrate rigidity (Astley et al., 2015; Demes et al., 1995), surface friction (Sutton and Burrows, 2008), and substrate geometry (Majumdar and Robergs, 2011). Predominately horizontal accelerations are particularly challenging on flat substrates because slip will occur if the ground reaction force angle is too shallow (due to a high ratio between horizontal and vertical force components) (Hildebrand, 1989; Wilson et al., 2013). The surface's coefficient of friction determines the angle at which slip occurs (e.g., walking on ice versus asphalt) and thus how much lateral force an animal can apply (as a fraction of body weight) before losing their grip on the surface. In addition to friction, substrate geometry can greatly enhance an organism's ability to push off the surface by providing a rigid surface closer to perpendicular to the ground reaction force

angle. For example, sprinters typically begin a race using starting blocks which provide them with inclined surfaces to apply propulsive force to, which allows them to apply higher horizontal forces without slipping (Majumdar and Robergs, 2011). The natural environment provides a wide range of variable substrate geometries which have the potential to affect an animal's performance of impulsive behaviors.

Striking snakes propel a large fraction of their anterior body forward with some of the highest accelerations seen in vertebrates (Herrel et al., 2011; Kardong, 1986; Kardong and Bels, 1998; Smith et al., 2002; Vincent et al., 2005; Young, 2010). Snakes are found on a wide range of substrates with highly variable surface friction and geometries, both of which will create challenges for striking. On flat, level, rigid ground a snake must rely on static friction to prevent slipping during mostly horizontal strikes (in which the propulsive forces are primarily oriented posteriorly to the strike direction with minimal lateral and vertical components), limiting how much force a snake can generate during a strike. Furthermore, while the low forward coefficient of friction between snake scales and the substrate is beneficial for locomotion, this exacerbates the problem of slip during striking (Baum et al., 2014; Benz et al., 2012). However, if the body can press against a rigid near-vertical surface (e.g., a rock, a log, etc.), a snake could potentially exert more force during their strike without slip.

Snake strikes consistently show high head accelerations across taxa (56.8-199 m/s^2) (Herrel et al., 2011; Kardong, 1975; Kardong and Bels, 1998; Moon et al., 2019; Penning et al., 2016; Ryerson and Tan, 2017; Ryerson and Van Valkenburg, 2021; Whitford et al., 2020). However, the substrate reaction forces that produce these rapid

accelerations are unknown. We hypothesize that snakes will strike faster and with more force on a surface with vertically-oriented features than on a featureless one. To test our hypothesis, we recorded synchronized kinematics and substrate reaction forces of the strikes for four blood pythons (*Python brongersmai*) on a custom-built platform with a high friction surface in two setups: a featureless plane and one with vertical walls that could serve as propulsive surfaces (Appendix K).

Materials & Methods

Four wild-caught blood pythons, *P. brongersmai* (Stull 1938), were obtained from a commercial provider (snout-vent length (SVL) mean±s.d. 76.1±6.2 cm, range 67.0-80.9 cm; mass 586.3±167.1 g, range 450-670 g). This species is highly suitable for strike studies because it is easily obtainable, non-venomous, and strikes defensively with particular readiness. All experiments were approved by University of Akron IACUC.

We constructed a rigid strike platform out of a 30.5 x 30.5 x 0.7 cm carbon fiber sandwich panel (DragonPlate, ALLRed & Associates Inc., Elbridge, NY, USA) covered in a rough material (Rock-on-a-Roll, Aquatica Water Gardens, Minneapolis, MN, USA; coefficient of friction = 0.30±0.09). The strike platform was attached to a six-axis force/torque sensor (Nano 43, ATI Industrial Automation, Apex, NC, USA), which was connected to a base made of expanded PVC board via two custom 3d printed ABS parts (Appendix K). Force data were collected using a NIDAQ N1-USB-6218 (16 bits, National Instruments, Austin, TX, USA) and recorded using the software IGOR Pro (Wavemetrics, Tigard, OR, USA) at 1 kHz. To dissuade the snakes from slithering off the platform, we

raised it 83.0 cm off the ground using a frame of 80/20 supports and clamps to attach the pvc board to the 80/20 supports anchored with sandbags. The walled setup was made by adding two adjacent walls made of rigid insulation foam attached to corrugated plastic board and screwed into the carbon fiber sheet on two adjacent sides (Appendix K). High-speed video was recorded at 500 images s^{-1} in dorsal view using an overhead SC1 Edgertronic high-speed camera (Sanstreak Corp, San Jose, CA, USA) 1.4 m above the strike platform. The trigger signal from the cameras was simultaneously recorded in IGOR via the NIDAQ, providing a method to synchronize the force and video recordings. Trials were performed in sets of three to five per 24 h and individuals were allowed a minimum of five minutes rest between trials to prevent fatigue. Snakes were not tested for 24 h after feeding occurred.

Strike trials were conducted after warming the snakes to 29-30°C, within the field active temperature of this species (Brattstrom, 1965, listed as *P. curtus*). After a snake was warmed and placed onto the strike platform, we induced strikes by either moving side to side and/or quickly moving our hands to one side of the snake's head and back because one method failed to achieve strikes from all individuals. A total of 47 trials were recorded among four individuals (24 for the open setup followed by 23 for the walled setup) with five to seven trials per individual per setup. We digitized the locations of the heads and tails of our snakes using the MATLAB application DLTdv8a (Hedrick, 2008). Next, we used coordinate transformation to reorient both the force sensor axes and the axes of the digitization to align with the strike direction (defined as

the overall direction of the snake's head movement after ten frames from when the strike begins) using the following two equations:

$$x' = x * \cos(\theta) + y * \sin(\theta) \quad (5.1)$$

$$y' = -x * \sin(\theta) + y * \cos(\theta) \quad (5.2)$$

where θ is the angle between the original axis (i.e. force sensor or digitization) and the new axis (direction of the snake strike). Force and kinematic data were splined and processed using a custom-written MATLAB script (MathWorks, Natick, MA, USA). We measured 12 variables: maximum fore-aft force, maximum lateral force, maximum vertical force, maximum total force, maximum head velocity in x and y, maximum head acceleration in x and y, strike duration (from beginning of the strike until forward progress ends or left the camera field of view), fore-aft impulse (the integral of fore-aft force from the beginning of the strike until forward progress ends), strike distance, maximum tail velocity in the strike direction, maximum tail acceleration in the strike duration, and maximum tail displacement in the strike direction. Maximum values (e.g., maximum force and velocity) were calculated using the built-in MATLAB peak function. Impulse was calculated using the built-in MATLAB trapz function.

Statistical tests were performed using JMP Pro 15 (SAS Institute Inc., Cary, NC, USA). To test whether variables differ between the open and walled setups we ran a mixed model ANOVA for each variable with setup, individual, and setup•individual as factors with a random effect assigned to both the individual and setup•individual. Additionally, to test whether one setup was more variable than another, we also ran a Brown-Forsythe coefficient of variance (CV) test by setup and not individual via a one-

way ANOVA. Finally, we applied a stepdown Bonferroni correction to both our ANOVA and multivariate tests to correct for multiple comparisons.

Results

Snakes displayed high strike performance in both setups with maximum fore-aft force of 0.64 ± 0.52 body weights (BW), maximum total force of 1.79±0.48 BW, maximum head velocity of 3.32 ± 0.81 m/s, maximum head acceleration of 95.84 ± 28.05 m/s^2, strike distance of 0.22 ± 0.08 m, and strike duration of 60±10 ms (Table 5.1, see Appendices L-M for all values). Our results displayed high individual variability within and between individuals and setups. As a result, the open and walled setups were statistically indistinguishable in most variables measured (Table 5.1, see Appendix M for all values) (Figs. 5.1-5.2). Only maximum lateral force and maximum tail distance were significantly affected by setup (Table 5.1). Individual and individual • setup effects were common, emphasizing the high variability of striking behavior (Table 5.1), and multiple variables showed substantial differences in CV between setups (Table 5.2). The CV for maximum fore-aft force almost tripled in value between the open and walled setup (open: 0.23, walled: 0.70) and the CV for fore-aft impulse was almost double between the open and walled setup (open: 0.42 and walled: 0.74), both of which were statistically significant (p-values <0.0001 and 0.0003) (Table 5.2). We also noticed that the snakes never fell off the platform in the open setup but frequently fell off the platform in the walled setup.

Table 5.1: Average values for each variable by setup (open versus walled) and pooled alongside statistical model values (of a mixed model ANOVA) showing significant variables based on a stepdown Bonferroni test (bold denotes significance).

				Whole Model		Setup		Ind. & Random		Ind. Setup & Random	
Variable	open (mean±s.d.)	walled (mean±s.d.)	overall (mean±s.d.)	$F_{7,39}$ Ratio	p-value	$F_{7,39}$ Ratio	p-value	$F_{7,39}$ Ratio	p-value	$F_{7,39}$ Ratio	p-value
Max. Lat. Force (BW)	0.28±0.09	0.83±0.49	0.55±0.44	**6.06**	**<0.0001**	**21.92**	**0.02**	1.16	0.45	1.54	0.22
Max. Vert. Force (BW)	1.70±0.55	1.63±0.38	1.67±0.47	**6.72**	**<0.0001**	0.8	0.44	**59.71**	**0.004**	0.26	0.86
Max. Fore-aft Force (BW)	0.37±0.09	0.92±0.64	0.64±0.52	**6.79**	**<0.0001**	6.98	0.08	1.30	0.42	**3.63**	**0.02**
Fore-Aft Impulse (BW•s)	0.14±0.06	0.36±0.27	0.25±0.22	**6.94**	**<0.0001**	5.22	0.11	1.13	0.46	**4.53**	**0.01**
Max. Velocity (m/s)	3.18±0.68	3.47±0.91	3.32±0.81	**6.16**	**<0.0001**	0.78	0.44	3.27	0.18	**3.22**	**0.03**
Strike Distance (m)	0.19±0.05	0.24±0.09	0.21±0.08	**12.22**	**<0.0001**	2.21	0.23	3.90	0.15	**5.24**	**0.004**
Max. Total Force (BW)	1.74±0.54	1.85±0.43	1.79±0.48	**4.87**	**0.0005**	2.34	0.22	**20.24**	**0.02**	0.53	0.67
Max. Tail Distance (m)	0.07±0.05	0.02±0.02	0.05±0.05	**4.14**	**0.0017**	**23.94**	**0.016**	1.79	0.32	0.89	0.45
Max. Tail Accel. (m/s^2)	42.56±46.57	14.41±19.47	28.79±38.32	**3.54**	**0.0048**	2.62	0.20	0.63	0.65	**3.26**	**0.03**
Max. Tail Velocity (m/s)	1.18±0.99	0.51±0.49	0.86±0.85	3.45	0.0057	5.18	0.11	1.39	0.40	1.94	0.14
Strike Duration (ms)	50±10	60±10	60±10	2.71	0.0217	3.38	0.16	0.77	0.58	2.32	0.09
Max. Acceleration (m/s^2)	99.27±29.86	92.27±26.21	95.84±28.05	1.17	0.3431	0.96	0.40	1.46	0.38	1.06	0.38

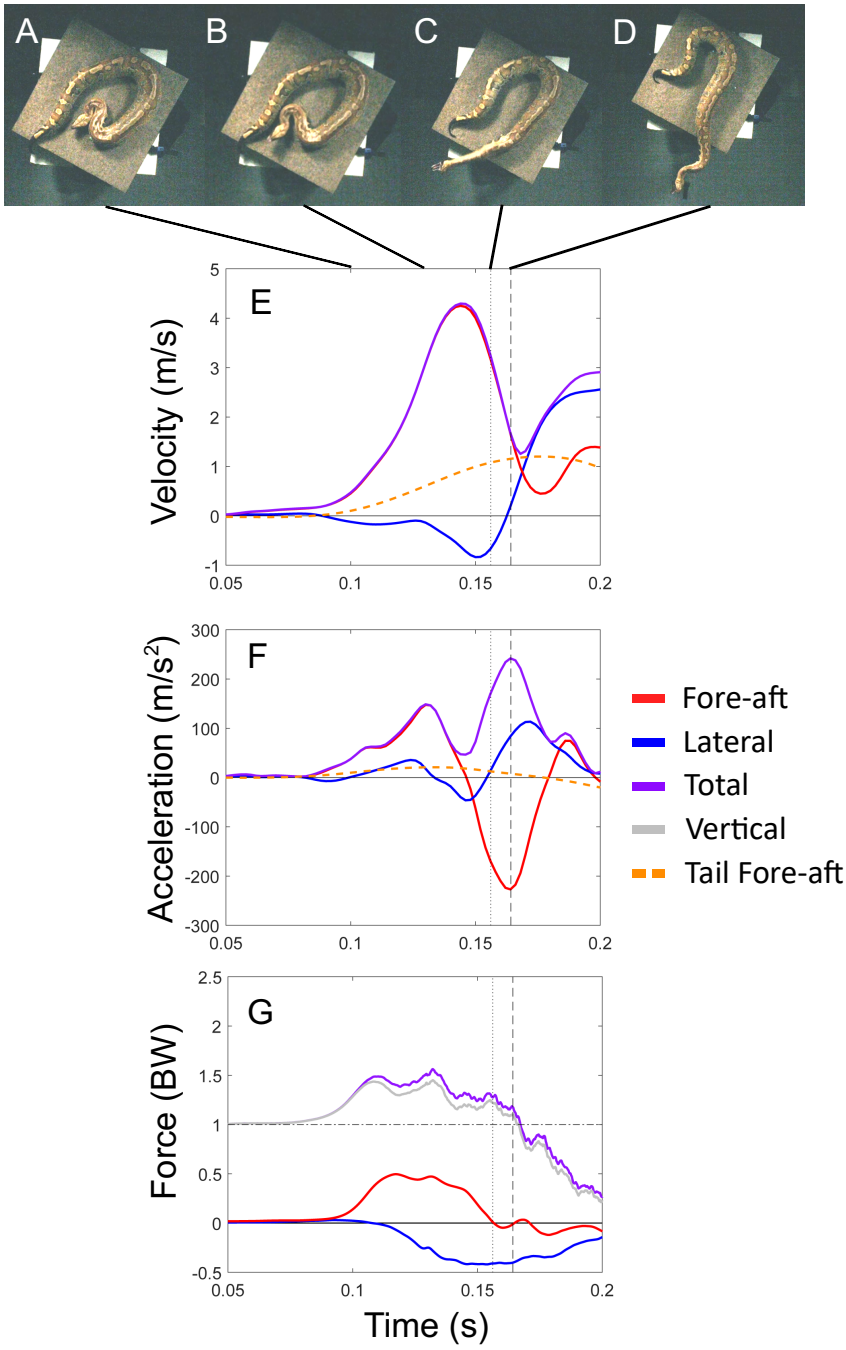

Figure 5.1: A-D still images of the snake strike in the open setup at various stages of the strike including the beginning (A), point of maximum fore-aft force (B), point when the snake's neck is straight (C), and point when forward progress ends (D). E-G are the corresponding graphs for the same strike of velocity (E), acceleration (F), and force (G). Solid red line is fore-aft, solid blue line is lateral, solid purple line is total, solid gray line is vertical, and dashed orange line is tail fore-aft.

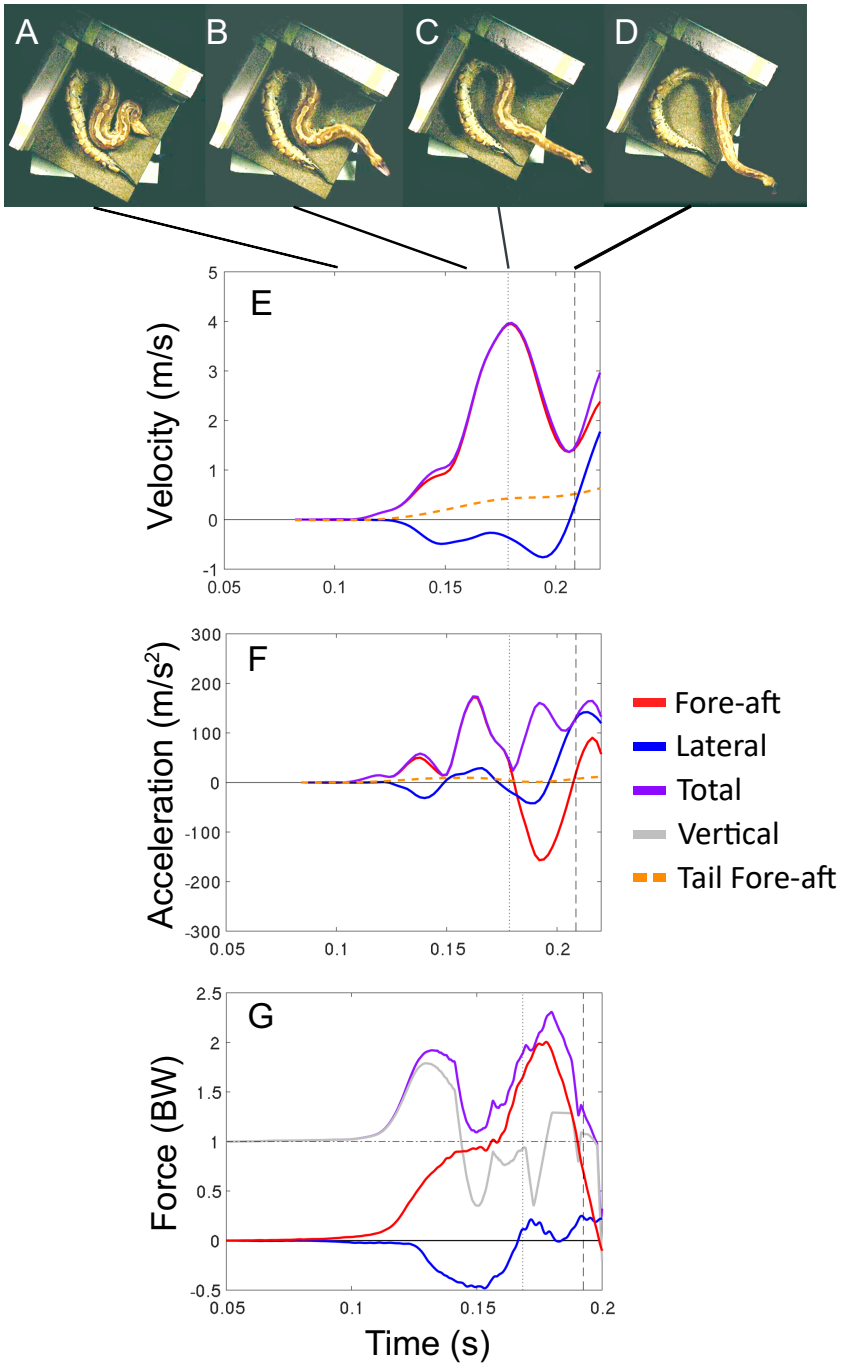

Figure 5.2: A-D still images of the snake strike in the walled setup at various stages of the strike including the beginning (A), point of maximum fore-aft force (B), point when the snake's neck is straight (C), and point when forward progress ends (D). E-G are the corresponding graphs for the same strike of velocity (E), acceleration (F), and force (G). Solid red line is fore-aft, solid blue line is lateral, solid purple line is total, solid gray line is vertical, and dashed orange line is tail fore-aft.

Table 5.2: Coefficient of variation by setup (open versus walled) based on a one-way ANOVA (bold denotes significance).

	Coefficient of Variation			
Variable	Open	Walled	$F_{1,45}$ Ratio	p-value
Max. Fore-aft Force (BW)	0.23	0.70	**28.57**	**<0.0001**
Max. Lateral Force (BW)	0.33	0.58	**28.52**	**<0.0001**
Fore-aft Impulse (BW)	0.42	0.74	**15.70**	**0.0003**
Max. Tail Dist. (m)	0.71	1.01	**6.94**	**0.01**
Strike Distance (m)	0.29	0.38	**6.28**	**0.016**
Max. Tail Acceleration (m/s^2)	1.09	1.35	2.70	0.11
Max. Tail Velocity (m/s)	0.84	0.95	2.12	0.15
Max. Velocity (m/s)	0.21	0.26	1.21	0.28
Max. Acceleration (m/s)	0.30	0.28	0.24	0.63
Max. Vertical Force (BW)	0.32	0.23	0.05	0.82
Max. Total Force (BW)	0.31	0.23	0.01	0.92
Strike Duration (ms)	0.19	0.18	0.001	0.97

Discussion

We recorded velocities and accelerations (Table 5.1) similar to previously reported values in various snake taxa (Ryerson and Van Valkenburg, 2021, Table 4 and references therein). Our data adds further support to previous studies showing snakes across a variety of families and body forms strike with similar fast kinematics. In addition to recording kinematic data, our study is the first to record force data during snake strikes (Figs. 5.1-5.2, Table 5.1). The blood pythons in our study generated almost 1.0 BW horizontally and up to 1.7 BW vertically (Fig. 5.2). Our results show striking similarities to the ground reaction forces measured during a human punch by Lenetsky et al. (2020). They found force was just below 0.5 BW in both the fore-aft and lateral directions with roughly 1.5 BW in vertical force (Lenetsky et al., 2020). While there is support for the role of trunk rotation converting vertical ground reaction force to horizontal force during a punch (Tong-Iam et al., 2017), another study showed fatiguing

lower-body exercise diminished punch performance highlighting the importance of the ground reaction forces generated during a punch (Dunn et al., 2021). Future work exploring the ground reaction forces in other systems with rapid movement of body parts, such as chameleons tongue projection and heron predatory strikes, would provide a stronger basis for broad, comparative conclusions.

Strike kinematics have been measured in a variety of snakes (Herrel et al., 2011; Penning et al., 2016; Penning et al., 2020; Ryerson and Tan, 2017; Ryerson and Van Valkenburg, 2021; Whitford et al., 2020; Young, 2010). However, the kinetics applied to the environment are essential to understanding the kinematics of the snake's head. In order to impart momentum to the head of the snake, equal and opposite momentum must be imparted to the ground, the tail, or a combination thereof. The force sensor detects only the momentum imparted to the ground, thus if there is momentum imparted in the opposite direction by the movement of the tail, the impulse computed from the ground reaction force will provide a lower value than the true momentum imparted to the head. In contrast, if the snake is backed against a solid substrate and the tail moves little, then ground reaction forces will accurately capture forces acting on the anterior body. Furthermore, blood pythons show a similar chronic retention of fecal mass seen in other heavy-bodied snakes, which has been hypothesized to serve as inert ballast to maximum body inertia and friction with the substrate during striking (Lillywhite et al., 2002). However, this posteriorly-located fecal mass would also be beneficial to the active use of tail and posterior body as an inertial appendage.

Our study shows remarkable robustness in the majority of variables analyzed

between different setups. We did find higher CV in maximum fore-aft force and fore-aft impulse, showing snakes were able to achieve a higher range of force values in walled setups. However, despite these significantly higher variations found in the walled setup, it had no significant effect on other parameters such as maximum velocity or strike distance. This robustness to substrate geometry could be beneficial given environments with highly variable microhabitats, especially in geographically widespread taxa, as it means that a snake does not have to sacrifice strike performance if found in the open as compared to backed against an object.

We expect this inertial mechanism is not limited to blood pythons and could be exploited by multiple other snake taxa. A large variety of snakes will encounter open habitats and this mechanism would allow them to strike with similar performance as being backed against a wall, partially buried, gripping a branch, etc. allowing them to exploit a wider range of microhabitats to successfully capture prey. The use of the tail as an inertial appendage has been studied in geckos, cheetahs, monkeys, and squirrels, showing these animals using their tails as an inertial appendage for a variety of behaviors including balance, to reorient themselves mid-air, and faster, tighter turns (Fukushima et al., 2021; Jusufi et al., 2010; Patel and Braae, 2013; Young et al., 2015). However, quantifying the momentum transfer of the continuous body of these blood pythons in frictional contact with the substrate is beyond the scope of our study. To achieve similar performance in a variety of substrates and settings could have multiple benefits for a species and could be a contributing factor to snakes success in exploiting a diverse array of habitats.

CHAPTER VI

CONCLUSION

My research was structured to develop a more comprehensive understanding of several crucial but neglected areas of snake biomechanics and offered novel intellectual contributions. I 1) studied the function of the zygosphene-zygantrum joint and whether it is involved in limiting roll, 2) analyzed sarcomere length (important in generation of force) in multiple snake muscles along a wide size range of corn snakes to determine if their position on the length-tension curve shifts over ontogeny, 3) investigated whether snakes can generate forward propulsion via vertical undulation, and 4) measured forces during the strikes of blood pythons in an open and walled setup.

Most joints tend to have a tradeoff between stability and range of motion (Anderson et al., 2001; Johnston and Smidt, 1970; Kazar and Relovszky, 1969; Scopp and Moorman, 2001; Veeger and Van Der Helm, 2007; Zakani et al., 2017). I found the zygosphene-zygantrum joint functions to prevent the vertebrae from accessing positions where roll would occur, specifically at positions where the pre- and postzygapophyses no longer overlap. This allows snake vertebrae to have a high range of motion while maintaining structural stability avoiding this tradeoff (Jurestovsky et al., 2020). Snakes are effectively composed of repeating segments of vertebrae and ribs, and thus having a

strong and flexible vertebral column is essential to navigating complex environments, capturing prey, and defending oneself.

Sarcomeres are the fundamental unit of skeletal muscle and their length-tension relationship can have consequences for the entire animals performance despite their microscopic size (Bennett, 1985; Gidmark et al., 2013; Taylor, 2000). I found sarcomeres in the corn snake are consistently on the descending limb at rest across muscles, size of the animals, and regions of the body. These sarcomere lengths are consistent with being advantageous for constriction, but there could be other as yet unknown benefits in locomotion or striking. These results need to be tested in a variety of other snakes to determine whether this pattern is consistent among constrictors, all snakes, or is influenced by other factors.

The natural world is complex and filled with obstructions in all dimensions. Snakes are known to make use of lateral obstructions to generate forward propulsion (Gans, 1962; Gray and Lissmann, 1950; Jayne, 1986). I found corn snakes can also use vertical asperities to generate forward propulsion via vertical undulation. Vertical undulation allows snakes to exploit their environments in multiple dimensions and can especially be useful in arboreal environments or tunnels (Jurestovsky et al., 2021). Subsequent work has already shown vertical and lateral bending can be combined to move through three dimensionally complex environments (Fu et al., 2022).

Fast actions are a fundamental component of multiple organisms' behaviors and ecology. These rapid impulsive behaviors present multiple challenges including the generation of high force, high power, and fast response times (Astley and Roberts, 2014;

deVries et al., 2012; Ilton et al., 2018; Nüchter et al., 2006; Patek et al., 2004; Sakes et al., 2016). I found that despite variations in their environment, the blood pythons showed similar kinematics and forces. Snakes achieve robustness to variations in their strike conditions by imparting momentum to their posterior body segments to counteract slip.

My research focuses on multiple areas of limbless locomotion and specifically snake biomechanics to show how snakes use morphological, muscular, and behavioral traits to meet functional challenges. These studies highlight how snakes make use of a limbless body plan despite the inferred limitations associated without having limbs and took initial steps in filling several prominent gaps in the snake literature. However, this work raises a multitude of other questions in biomechanics including: are there other osteological joints capable of avoiding the inherent tradeoffs between structural stability and high range of motion, are sarcomeres in other snakes at similar lengths or are there variations and limitations due to phyletic history, do snakes make use of vertical undulations in nature consistently and/or in combination with lateral undulation, and how do arboreal snakes deal with highly variable strike platforms? While this work has emphasized snakes, we know far less about limbless lizards, which would be another fruitful area of study, especially to contrast with snake biomechanics to better understand the strategies, biomechanics, muscle architecture, and sarcomere lengths used by other limbless taxa.

LITERATURE CITED

Anderson, K., Strickland, S. M. and Warren, R. (2001). Hip and groin injuries in athletes. *The American journal of sports medicine* **29**, 521–533.

Andersson, K. I. (2004). Elbow-joint morphology as a guide to forearm function and foraging behaviour in mammalian carnivores. *Zoological Journal of the Linnean Society* **142**, 91–104.

Apesteguía, S. and Zaher, H. (2006). A Cretaceous terrestrial snake with robust hindlimbs and a sacrum. *Nature* **440**, 1037–1040.

Araújo, Ms. and Martins, M. (2007). The defensive strike of five species of lanceheads of the genus Bothrops (Viperidae). *Braz. J. Biol.* **67**, 327–332.

Arnold, S. J. (1988). Quantitative genetics and selection in natural populations: microevolution of vertebral numbers in the garter snake Thamnophis elegans. In *Proceedings of the second international conference on quantitative genetics* (ed. Sunderland, M.) and Sinauer, pp. 619–638. Sinauer Sunderland, MA.

Ashmore, C. R., Mechling, K. and Lee, Y. B. (1988). Sarcomere length in normal and dystrophic chick muscles. *Experimental neurology* **101**, 221–227.

Astley, H. C. (2020). Long limbless locomotors over land: the mechanics and biology of elongate, limbless vertebrate locomotion. *Integrative and Comparative Biology* **60**, 134–139.

Astley, H. C. and Jayne, B. C. (2007). Effects of perch diameter and incline on the kinematics, performance and modes of arboreal locomotion of corn snakes (Elaphe guttata). *Journal of Experimental Biology* **210**, 3862–3872.

Astley, H. C. and Jayne, B. C. (2009). Arboreal habitat structure affects the performance and modes of locomotion of corn snakes (Elaphe guttata). *Journal of Experimental Zoology Part A: Ecological Genetics and Physiology* **311**, 207–216.

Astley, H. C. and Roberts, T. J. (2012). Evidence for a vertebrate catapult: elastic energy storage in the plantaris tendon during frog jumping. *Biology letters* **8**, 386–389.

Astley, H. C. and Roberts, T. J. (2014). The mechanics of elastic loading and recoil in anuran jumping. *Journal of Experimental Biology* **217**, 4372–4378.

Astley, H., Haruta, A. and Roberts, T. (2015). Robust jumping performance and elastic energy recovery from compliant perches in tree frogs | Journal of Experimental Biology | The Company of Biologists. *Journal of Experimental Biology* **218**, 3360–3363.

Auffenberg, W. (1963). The fossil snakes of Florida. *Tulane Studies in Zoology* **10**, 131–216.

Azizi, E. and Roberts, T. J. (2010). Muscle performance during frog jumping: influence of elasticity on muscle operating lengths. *Proceedings of the Royal Society B: Biological Sciences* **277**, 1523–1530.

Baier, D. B. (2012). Mechanical properties of the avian acrocoracohumeral ligament and its role in shoulder stabilization in flight. *Journal of Experimental Zoology Part A: Ecological Genetics and Physiology* **317**, 83–95.

Baum, M. J., Kovalev, A. E., Michels, J. and Gorb, S. N. (2014). Anisotropic Friction of the Ventral Scales in the Snake Lampropeltis getula californiae. *Tribol Lett* **54**, 139–150.

Bennett, A. F. (1985). Temperature and muscle. *Journal of Experimental Biology* **115**, 333–344.

Benz, M. J., Kovalev, A. E. and Gorb, S. N. (2012). Anisotropic frictional properties in snakes. In (ed. Lakhtakia, A.), p. 83390X. San Diego, California.

Bergmann, P. J. and Irschick, D. J. (2010). Alternate Pathways of Body Shape Evolution Translate into Common Patterns of Locomotor Evolution in Two Clades of Lizards. *Evolution* **64**, 1569–1582.

Bogert, C. M. (1947). Rectilinear locomotion in snakes. *Copeia* **1947**, 253–254.

Branch, B. (1988). *Field guide to snakes and other reptiles of South Africa*. Florida: Ralph Curtis Books.

Brattstrom, B. H. (1965). Body temperatures of reptiles. *The American Midland Naturalist* **73**, 376–422.

Bruch, A. A., Utescher, T. and Mosbrugger, V. (2011). Precipitation patterns in the Miocene of Central Europe and the development of continentality. *Palaeogeography, Palaeoclimatology, Palaeoecology* **304**, 202–211.

Budsberg, S. C., Verstraete, M. C. and Soutas-Little, R. W. (1987). Force plate analysis of the walking gait in healthy dogs. *American Journal of Verterinary Research* **48**, 915–918.

Burbrink, F. T. and Crother, B. I. (2011). Evolution and taxonomy of snakes. In *Reproductive Biology and Phylogeny of Snakes* (ed. Aldridge, R. A.) and Sever, D. M.), pp. 19–53. Enfield, NH: Science Publishers.

Burkholder, T. J. and Lieber, R. L. (2001). Sarcomere length range during animal locomotion. *Journal of Experimental Biology* **204**, 1529–1536.

Byrnes, G. and Jayne, B. C. (2012). The effects of three-dimensional gap orientation on bridging performance and behavior of brown tree snakes (Boiga irregularis). *Journal of Experimental Biology* **215**, 2611–2620.

Caldwell, M. W. and Lee, M. S. (1997). A snake with legs from the marine Cretaceous of the Middle East. *Nature* **386**, 705–709.

Caldwell, M. W., Nydam, R. L., Palci, A. and Apesteguía, S. (2015). The oldest known snakes from the Middle Jurassic-Lower Cretaceous provide insights on snake evolution. *Nature communications* **6**, 1–11.

Camp, C. L. (1923). Classification of the lizards. *Bulletin of the American Museum of Natural History* **48**, 289–481.

Caputo, V., Lanza, B. and Palmieri, R. (1995). Body elongation and limb reduction in the genus Chalcides Laurenti 1768 (Squamata Scincidae): a comparative study. *Tropical Zoology* **8**, 95–152.

Cerling, T. E., Harris, J. M., MacFadden, B. J., Leakey, M. G., Quade, J., Eisenmann, V. and Ehleringer, J. R. (1997). Global vegetation change through the Miocene/Pliocene boundary. *Nature* **389**, 153–158.

Clack, J. A. (2012). *Gaining ground: the origin and evolution of tetrapods*. 2nd ed. (ed. Farlow Bloomington, IN: Indiana University Press.

Coates, M. and Ruta, M. (2000). Nice snake, shame about the legs. *Trends in Ecology & Evolution* **15**, 503–507.

Cogger, H. G. (2000). *Amphibians and reptiles of Australia*. 6th ed. Florida: Ralph Curtis Books.

Conrad, J. L. (2008). Phylogeny and systematics of Squamata (Reptilia) based on morphology. *Bulletin of the American Museum of Natural History* **2008**, 1–182.

Conroy, C. J., Papenfuss, T., Parker, J. and Hahn, N. E. (2009). Use of tricaine methanesulfonate (MS222) for euthanasia of reptiles. *Journal of the American Association for Laboratory Animal Science* **48**, 28–32.

Cundall, D. and Irish, F. (2008). The snake skull. In *Biology of the Reptilia* (ed. Gans, C.), pp. 349–692. New York: Academic Press.

Cutts, A. (1986). Sarcomere length changes in the wing muscles during the wing beat cycle of two bird species. *Journal of Zoology* **209**, 183–185.

Demes, B., Jungers, W. L., Gross, T. S. and Fleagle, J. G. (1995). Kinetics of leaping primates: influence of substrate orientation and compliance. *American Journal of Physical Anthropology* **96**, 419–429.

deVries, M. S., Murphy, E. A. K. and Patek, S. N. (2012). Strike mechanics of an ambush predator: the spearing mantis shrimp. *Journal of Experimental Biology* **215**, 4374–4384.

Dickinson, M. H., Farley, C. T., Full, R. J., Koehl, M. A. R., Kram, R. and Lehman, S. (2000). How animals move: an integrative view. *Science* **288**, 100–106.

Dunn, E. C., Humberstone, C. E., Franchini, E., Iredale, F. K. and Blazevich, A. J. (2021). The effect of fatiguing lower-body exercise on punch forces in highly-trained boxers. *European Journal of Sport Science* **0**, 1–9.

Felsenstein, J. (1985). Phylogenies and the comparative method. *The American Naturalist* **125**, 1–15.

Fu, Q., Astley, H. and Li, C. (2022). Snakes combine vertical and lateral bending to traverse uneven terrain. *Bioinspir. Biomim.*

Fukushima, T., Siddall, R., Schwab, F., Toussaint, S. L. D., Byrnes, G., Nyakatura, J. A. and Jusufi, A. (2021). Inertial Tail Effects during Righting of Squirrels in Unexpected Falls: From Behavior to Robotics. *Integrative and Comparative Biology* **61**, 589–602.

Full, R. J., Stokes, D. R., Ahn, A. N. and Josephson, R. K. (1998). Energy absorption during running by leg muscles in a cockroach. *The journal of experimental biology* **201**, 997–1012.

Gans, C. (1962). Terrestrial locomotion without limbs. *American Zoologist* **2**, 167–182.

Gans, C. (1970). How snakes move. *Scientific American* **222**, 82–99.

Gans, C. (1974). *Biomechanics: an approach to vertebrate biology*. Ann Arbor: University of Michigan Press.

Gans, C. (1975). Tetrapod limblessness: evolution and functional corollaries. *American Zoologist* **15**, 455–467.

Gans, C. (1986). Locomotion of limbless vertebrates: pattern and evolution. *Herpetologica* **42**, 33–46.

Garland, T. and Adolph, S. C. (1994). Why Not to Do Two-Species Comparative Studies: Limitations on Inferring Adaptation. *Physiological Zoology* **67**, 797–828.

Gasc, J.-P. (1974). L'interprétation fonctionelle de l'appareil musculo-squelettique de l'axe vertébral chez les serpents (Reptilia). *Mém. Mus. Nat. Hist. Nat. Paris Ser. A Zool.* **83**, 1–182.

Gasc, J. P. (1976). Snake vertebrae–a mechanism or merely a taxonomist's toy. In *Morphology and Biology of Reptiles*, pp. 177–190. London and New York: Academic Press.

Gasc, J.-P. (1981). Axial musculature. In *Biology of the Reptilia*, pp. 355–435. New York: Academic Press.

Gidmark, N. J., Konow, N., LoPresti, E. and Brainerd, E. L. (2013). Bite force is limited by the force–length relationship of skeletal muscle in black carp, Mylopharyngodon piceus. *Biology Letters* **9**,.

Gordon, A. M., Huxley, A. F. and Julian, F. J. (1966). The variation in isometric tension with sarcomere length in vertebrate muscle fibres. *The Journal of physiology* **184**, 170–192.

Gould, S. J. and Lewontin, R. C. (1979). The Spandrels of San Marco and the Panglossian Paradigm: A Critique of the Adaptationist Programme. *Conceptual Issues in Evolutionary Biology* **205**, 79.

Gray, J. (1946). The mechanism of locomotion in snakes. *Journal of Experimental Biology* **23**, 101–124.

Gray, J. and Lissmann, H. W. (1950). The kinetics of locomotion of the grass-snake. *Journal of Experimental Biology* **26**, 354–367.

Greenwald, O. E. (1974). Thermal dependence of striking and prey capture by gopher snakes. *Copeia* **1974**, 141–148.

Head, J. J. and Polly, P. D. (2015). Evolution of the snake body form reveals homoplasy in amniote Hox gene function. *Nature* **520**, 86–90.

Head, J. J., Holroyd, P. A., Hutchison, J. H. and Ciochon, R. L. (2005). First report of snakes (Serpentes) from the late middle Eocene Pondaung Formation, Myanmar. *Journal of Vertebrate Paleontology* **25**, 246–250.

Hedrick, T. L. (2008). Software techniques for two- and three-dimensional kinematic measurements of biological and biomimetic systems. *Bioinspir. Biomim.* **3**, 034001.

Herrel, A., Huyghe, K., Oković, P., Lisičić, D. and Tadić, Z. (2011). Fast and furious: effects of body size on strike performance in an arboreal viper Trimeresurus (Cryptelytrops) albolabris. *Journal of Experimental Zoology Part A: Ecological Genetics and Physiology* **315A**, 22–29.

Hildebrand, M. (1989). The quadrupedal gaits of vertebrates. *BioScience* **39**, 766.

Hirose, S. (1993). *Biologically inspired robots: snake-like locomotors and manipulators*. C. Goulden, ed. Oxford University Press.

Hodson, E., Clayton, H. M. and Lanovaz, J. L. (2001). The hindlimb in walking horses: 1. Kinematics and ground reaction forces. *Equine Veterinary Journal* **33**, 38–43.

Hoffstetter, R. and Gasc, J.-P. (1969). Vertebrae and ribs of modern reptiles. In *Biology of the Reptilia* (ed. Gans, C.), pp. 201–310. New York: Academic Press.

Holman, J. A. (2000). *Fossil snakes of North America: origin, evolution, distribution, paleoecology*. Indiana: Indiana University Press.

Hooper, S. L., Guschlbauer, C., Blümel, M., von Twickel, A., Hobbs, K. H., Thuma, J. B. and Büschges, A. (2016). Muscles: Non-linear Transformers of Motor Neuron Activity. In *Neuromechanical Modeling of Posture and Locomotion* (ed. Prilutsky, B. I.) and Edwards, D. H.), pp. 163–194. New York, NY: Springer.

Hsiang, A. Y., Field, D. J., Webster, T. H., Behlke, A. D., Davis, M. B., Racicot, R. A. and Gauthier, J. A. (2015). The origin of snakes: revealing the ecology, behavior, and evolutionary history of early snakes using genomics, phenomics, and the fossil record. *BMC evolutionary biology* **15**, 87.

Hu, D. L., Nirody, J., Scott, T. and Shelley, M. J. (2009). The mechanics of slithering locomotion. *Proceedings of the National Academy of Sciences* **106**, 10081–10085.

Ilton, M., Bhamla, M. S., Ma, X., Cox, S. M., Fitchett, L. L., Kim, Y., Koh, J., Krishnamurthy, D., Kuo, C.-Y., Temel, F. Z., et al. (2018). The principles of cascading power limits in small, fast biological and engineered systems. *Science* **360**, eaao1082.

Jayne, B. C. (1982). Comparative morphology of the semispinalis-spinalis muscle of snakes and correlations with locomotion and constriction. *Journal of Morphology* **172**, 83–96.

Jayne, B. C. (1985). Swimming in constricting (Elaphe g. guttata) and nonconstricting (Nerodia fasciata pictiventris) colubrid snakes. *Copeia* **1**, 195–208.

Jayne, B. C. (1986). Kinematics of terrestrial snake locomotion. *Copeia* 915–927.

Jayne, B. C. (1988a). Muscular mechanisms of snake locomotion: an electromyographic study of lateral undulation of the Florida banded water snake (Nerodia fasciata) and the yellow rat snake (Elaphe obsoleta). *Journal of Morphology* **197**, 159–181.

Jayne, B. C. (1988b). Muscular mechanisms of snake locomotion: an electromyographic study of the sidewinding and concertina modes of Crotalus cerastes, Nerodia fasciata and Elaphe obsoleta. *Journal of Experimental Biology* **140**, 1–33.

Jayne, B. C. (2020). What Defines Different Modes of Snake Locomotion? *Integrative and Comparative Biology* **60**, 156–170.

Jayne, B. C. and Riley, M. A. (2007). Scaling of the axial morphology and gap-bridging ability of the brown tree snake, Boiga irregularis. *Journal of Experimental Biology* **210**, 1148–1160.

Johnson, R. G. (1955). The adaptive and phylogenetic significance of vertebral form in snakes. *Evolution* **9**, 367–388.

Johnston, R. C. and Smidt, G. L. (1970). 23 Hip motion measurements for selected activities of daily living. *Clinical Orthopaedics and Related Research®* **72**, 205–215.

Josephson, R. K. (1985). Mechanical power output from striated muscle during cyclic contraction. *Journal of Experimental Biology* **114**, 493–512.

Jurestovsky, D. J., Jayne, B. C. and Astley, H. C. (2020). Experimental modification of morphology reveals the effects of the zygosphene–zygantrum joint on the range of motion of snake vertebrae. *Journal of Experimental Biology* **223**, jeb216531.

Jurestovsky, D. J., Usher, L. R. and Astley, H. C. (2021). Generation of propulsive force via vertical undulations in snakes. *Journal of Experimental Biology* **224**, jeb239020.

Jusufi, A., Kawano, D. T., Libby, T. and Full, R. J. (2010). Righting and turning in mid-air using appendage inertia: reptile tails, analytical models and bio-inspired robots. *Bioinspiration & biomimetics* **5**, 045001.

Kaczmarek, E. B. and Gidmark, N. J. (2020). The bite force–gape relationship as an avenue of biomechanical adaptation to trophic niche in two salmonid fishes. *Journal of Experimental Biology* **223**, jeb223180.

Kambic, R. E., Roberts, T. J. and Gatesy, S. M. (2017). 3-D range of motion envelopes reveal interacting degrees of freedom in avian hind limb joints. *Journal of Anatomy* **231**, 906–920.

Kardong, K. V. (1975). Prey capture in the cottonmouth snake (Agkistrodon piscivorus). *Journal of Herpetology* 169–175.

Kardong, K. V. (1986). The predatory strike of the rattlesnake: when things go amiss. *Copeia* **1986**, 816–820.

Kardong, K. V. and Bels, V. L. (1998). Rattlesnake strike behavior: kinematics. *Journal of Experimental Biology* **201**, 837–850.

Kazar, B. and Relovszky, E. (1969). Prognosis of primary dislocation of the shoulder. *Acta orthopaedica Scandinavica* **40**, 216–224.

Kelley, K. C., Arnold, S. J. and Gladstone, J. (1997). The effects of substrate and vertebral number on locomotion in the garter snake Thamnophis elegans. *Functional Ecology* **11**, 189–198.

Kleinteich, T., Maddin, H. C., Herzen, J., Beckmann, F. and Summers, A. P. (2012). Is solid always best? Cranial performance in solid and fenestrated caecilian skulls. *Journal of Experimental Biology* **215**, 833–844.

Klemmer, K. Families: Felyiniidae and Anelytropsidae. In *Grzimek's animal life encyclopedia vol. 6 reptiles* (ed. Grzimek, B.), p. New York: Van Nostrand Reinhold Company.

LaDuc, T. J. (2002). Does a quick offense equal a quick defense? Kinematic comparisons of predatory and defensive strikes in the western diamond-backed rattlesnake (Crotalus atrox). In *Biology of the Vipers* (ed. Schuett, G. W.), Höggren, M.), Douglas, M. E.), and Greene, H. W.), pp. 267–278. Utah: Eagle Mountain.

Lawing, A. M., Head, J. J. and Polly, P. D. (2012). The ecology of morphology: the ecometrics of locomotion and macroenvironment in North American snakes. In *Paleontology in ecology and conservation*, pp. 117–146. Springer.

Lee, M. S. Y. (2005). Molecular evidence and marine snake origins. *Biology Letters* **1**, 227–230.

Lee, M. S. and Scanlon, J. D. (2002). Snake phylogeny based on osteology, soft anatomy and ecology. *Biological Reviews* **77**, 333–401.

Lenetsky, S., Brughelli, M., Nates, R. J., Neville, J. G., Cross, M. R. and Lormier, A. V. (2020). Defining the Phases of Boxing Punches: A Mixed-Method Approach. *The Journal of Strength & Conditioning Research* **34**, 1040–1051.

Lieber, R. L. and Boakes, J. L. (1988). Sarcomere length and joint kinematics during torque production in frog hindlimb. *American Journal of Physiology-Cell Physiology* **254**, C759–C768.

Lieber, R. L., Raab, R., Kashin, S. and Edgerton, V. R. (1992). Sarcomere length changes during fish swimming. *Journal of Experimental Biology* **169**, 251–254.

Lillywhite, H. B. (2014). *How snakes work: structure, function and behavior of the world's snakes*. Oxford: Oxford University Press.

Lillywhite, H. B., de Delva, P. and Noonan, B. P. (2002). Patterns of gut passage time and the chronic retention of fecal mass in viperid snakes. *Biology of the vipers* 497–506.

Lissmann, H. W. (1950). Rectilinear locomotion in a snake (Boa occidentalis). *Journal of Experimental Biology* **26**, 368–379.

Longrich, N. R., Bhullar, B.-A. S. and Gauthier, J. A. (2012). A transitional snake from the Late Cretaceous period of North America. *Nature* **488**, 205–208.

Lourdais, O., Brischoux, F. and Barantin, L. (2005). How to assess musculature and performance in a constricting snake? A case study in the Colombian rainbow boa (Epicrates cenchria maurus). *Journal of zoology* **265**, 43–51.

Lutz, G. J. and Rome, L. C. (1996). Muscle function during jumping in frogs. I. Sarcomere length change, EMG pattern, and jumping performance. *American Journal of Physiology-Cell Physiology* **271**, C563–C570.

Majumdar, A. S. and Robergs, R. A. (2011). The science of speed: determinants of performance in the 100 m sprint. *International Journal of Sports Science & Coaching* **6**, 479–493.

Manafzadeh, A. R. and Padian, K. (2018). ROM mapping of ligamentous constraints on avian hip mobility: implications for extinct ornithodirans. *Proceedings of the Royal Society B: Biological Sciences* **285**, 20180727.

Marvi, H., Gong, C., Gravish, N., Astley, H., Travers, M., Hatton, R. L., Mendelson, J. R., Choset, H., Hu, D. L. and Goldman, D. I. (2014). Sidewinding with minimal slip: Snake and robot ascent of sandy slopes. *Science* **346**, 224–229.

Mathieu-Costello, O. (1991). Morphometric analysis of capillary geometry in pigeon pectoralis muscle. *American journal of anatomy* **191**, 74–84.

McCartney, J. A., Stevens, N. J. and O'Connor, P. M. (2014). The earliest colubroid-dominated snake fauna from Africa: perspectives from the Late Oligocene Nsungwe Formation of southwestern Tanzania. *PLoS One* **9**, e90415.

Mead, J. I. and Schubert, B. W. (2013). Extinct Pterygoboa (Boidae, Erycinae) from the latest Oligocene and early Miocene of Florida. *Southeastern Naturalist* **12**, 427–439.

Moon, B. R. (1999). Testing an inference of function from structure: snake vertebrae do the twist. *Journal of Morphology* **241**, 217–225.

Moon, B. R. and Candy, T. (1997). Coelomic and muscular cross-sectional areas in three families of snakes. *Journal of Herpetology* 37–44.

Moon, B. R., Penning, D. A., Segall, M. and Herrel, A. (2019). Feeding in snakes: form, function, and evolution of the feeding system. In *Feeding in vertebrates*, pp. 527–574. Springer.

Morinaga, G. and Bergmann, P. J. (2019). Angles and waves: intervertebral joint angles and axial kinematics of limbed lizards, limbless lizards, and snakes. *Zoology* **134**, 16–26.

Mosauer, W. (1935). The myology of the trunk region of the snakes and its significance for ophidiam taxonomy and phylogeny. *Publ. Univ. Calf. Los Angels* **1**, 81–120.

Mushinsky, H. R. and Miller, D. E. (1993). Predation on Water Snakes: Ontogenetic and Interspecific Considerations. *Copeia* **1993**, 660–665.

Nüchter, T., Benoit, M., Engel, U., Özbek, S. and Holstein, T. W. (2006). Nanosecond-scale kinetics of nematocyst discharge. *Current Biology* **16**, R316–R318.

Oliver, J. D., Jones, K. E., Hautier, L., Loughry, W. J. and Pierce, S. E. (2016). Vertebral bending mechanics and xenarthrous morphology in the nine-banded armadillo (Dasypus novemcinctus). *Journal of Experimental Biology* **219**, 2991–3002.

Onary, S. Y., Fachini, T. S. and Hsiou, A. S. (2017). The snake fossil record from brazil. *Journal of Herpetology* **51**, 365–374.

Pagani, M., Freeman, K. H. and Arthur, M. A. (1999). Late Miocene Atmospheric CO_2 Concentrations and the Expansion of C_4 Grasses. *Science* **285**, 876–879.

Patek, S. N., Korff, W. L. and Caldwell, R. L. (2004). Deadly strike mechanism of a mantis shrimp. *Nature* **428**, 819–820.

Patel, A. and Braae, M. (2013). Rapid turning at high-speed: Inspirations from the cheetah's tail. In *2013 IEEE/RSJ International Conference on Intelligent Robots and Systems*, pp. 5506–5511. IEEE International Conference on Intelligent Robots and Systems.

Penning, D. A. (2018). Quantitative axial myology in two constricting snakes: Lampropeltis holbrooki and Pantherophis obsoletus. *Journal of anatomy* **232**, 1016–1024.

Penning, D. A., Sawvel, B. and Moon, B. R. (2016). Debunking the viper's strike: harmless snakes kill a common assumption. *Biology letters* **12**, 1–4.

Penning, D. A., Sawvel, B. and Moon, B. R. (2020). The scaling of terrestrial striking performance in western ratsnakes (Pantherophis obsoletus). *Journal of Experimental Zoology Part A: Ecological and Integrative Physiology* **333**, 96–103.

Pough, F. H. (1980). The advantages of ectothermy for tetrapods. *The American Naturalist* **115**, 92–112.

Pough, F. H. and Groves, J. D. (1983). Specializations of the body form and food habits of snakes. *American Zoologist* **23**, 443–454.

Pough, F. H., Andrews, R. M., Cadle, J. E., Crump, M. L., Savitzky, A. H. and Wells, K. D. (2004). *Herpetology, 3rd eds*. New Jersey: Pearson Education, Inc.

Rage, J.-C. and Escuillié, F. (2000). Un nouveau serpent bipède du Cénomanien (Crétacé). Implications phylétiques. *Comptes Rendus de l'Académie des Sciences-Series IIA-Earth and Planetary Science* **330**, 513–520.

Rage, J.-C., Buffetaut, E., Buffetaut-Tong, H., Chaimanee, Y. and Ducrocq, S. (1992). A colubrid snake in the late Eocene of Thailand: the oldest known Colubridae (Reptilia, Serpentes). *Comptes rendus de l'Académie des sciences. Série 2, Mécanique, Physique, Chimie, Sciences de l'univers, Sciences de la Terre* **314**, 1085–1089.

Richards, C. T. (2019). Energy flow in multibody limb models: a case study in frogs. *Integrative and comparative biology* **59**, 1559–1572.

Richards, C. T. and Porro, L. B. (2018). A novel kinematics analysis method using quaternion interpolation–a case study in frog jumping. *Journal of Theoretical Biology* **454**, 410–424.

Ridge, R. (1971). Different types of extrafusal muscle fibres in snake costocutaneous muscles. *The Journal of physiology* **217**, 393–418.

Rieppel, O., Zaher, H., Tchernov, E. and Polcyn, M. J. (2003). The anatomy and relationships of Haasiophis terrasanctus, a fossil snake by well-developed hind limbs from the Mid-Cretaceous of the Middle East. *Journal of Paleontology* **77**, 536–558.

Rome, L. C. and Sosnicki, A. A. (1991). Myofilament overlap in swimming carp. II. Sarcomere length changes during swimming. *American Journal of Physiology-Cell Physiology* **260**, C289–C296.

Romer, A. S. (1956). *Osteology of the reptiles*. Chicago: University of Chicago Press.

Ruben, J. A. (1977). Morphological Correlates of Predatory Modes in the Coachwhip (Masticophis flagellum) and Rosy Boa (Lichanura roseofusca). *Herpetologica* **33**, 1–6.

Rush, S. A., Sash, K., Carroll, J., Palmer, B. and Fisk, A. T. (2014). Feeding Ecology of the Snake Community of the Red Hills Region Relative to Management for Northern Bobwhite: Assessing the Diet of Snakes Using Stable Isotopes. *cope* **2014**, 288–296.

Ryerson, W. G. and Tan, W. (2017). Strike kinematics and performance in juvenile ball pythons (Python regius). *Journal of Experimental Zoology Part A: Ecological and Integrative Physiology* **327**, 453–457.

Ryerson, W. G. and Van Valkenburg, T. (2021). Linking tooth shape to strike mechanics in the Boa constrictor. *Integrative and Comparative Biology*.

Sakes, A., Wiel, M. van der, Henselmans, P. W. J., Leeuwen, J. L. van, Dodou, D. and Breedveld, P. (2016). Shooting Mechanisms in Nature: A Systematic Review. *PLOS ONE* **11**, e0158277.

Schindelin, J., Arganda-Carreras, I., Frise, E., Kaynig, V., Longair, M., Pietzsch, T., Preibisch, S., Rueden, C., Saalfeld, S. and Schmid, B. (2012). Fiji: an open-source platform for biological-image analysis. *Nature methods* **9**, 676.

Scopp, J. M. and Moorman, C. T. (2001). The assessment of athletic hip injury. *Clinics in sports medicine* **20**, 647–660.

Secor, S. M., Jayne, B. C. and Bennett, A. F. (1992). Locomotor performance and energetic cost of sidewinding by the snake Crotalus cerastes. *Journal of experimental biology* **163**, 1–14.

Sharpe, S. S., Koehler, S. A., Kuckuk, R. M., Serrano, M., Vela, P. A., Mendelson, J. and Goldman, D. I. (2015). Locomotor benefits of being a slender and slick sand swimmer. *Journal of Experimental Biology* **218**, 440–450.

Shiino, Y., Kuwazuru, O., Suzuki, Y. and Ono, S. (2012). Swimming capability of the remopleuridid trilobite Hypodicranotus striatus: hydrodynamic functions of the exoskeleton and the long, forked hypostome. *Journal of Theoretical Biology* **300**, 29–38.

Smith, T. L., Povel, G. D. E. and Kardong, K. V. (2002). Predatory strike of the tentacled snake (Erpeton tentaculatum). *Journal of Zoology* **256**, 233–242.

Sumida, S. S. (1997). Locomotor features of taxa spanning the origin of amniotes. In *Amniote origins: completing the transition to land* (ed. Sumida, S. S.) and Martin, K. L. M.), pp. 353–398. London: Academic Press.

Sutton, G. P. and Burrows, M. (2008). The mechanics of elevation control in locust jumping. *J Comp Physiol A* **194**, 557–563.

Szyndlar, Z. and Rage, J. C. (2003). *Non-erycine Booidea from the Oligocene and Miocene of Europe*. Cracow: Institute of Systematics and Evolution of Animals, Polish Academy of Sciences.

Taylor, G. M. (2000). Maximum force production: why are crabs so strong? *Proceedings of the Royal Society of London. Series B: Biological Sciences* **267**, 1475–1480.

Tchernov, E., Rieppel, O., Zaher, H., Polcyn, M. J. and Jacobs, L. L. (2000). A fossil snake with limbs. *Science* **287**, 2010–2012.

Tingle, J. L., Gartner, G. E. A., Jayne, B. C. and Garland Jr, T. (2017). Ecological and phylogenetic variability in the spinalis muscle of snakes. *Journal of evolutionary biology* **30**, 2031–2043.

Tong-Iam, R., Rachanavy, P. and Lawsirirat, C. (2017). Kinematic and kinetic analysis of throwing a straight punch: the role of trunk rotation in delivering a powerful straight punch. *JPES* **17**, 2538–2543.

Veeger, H. E. J. and Van Der Helm, F. C. T. (2007). Shoulder function: the perfect compromise between mobility and stability. *Journal of biomechanics* **40**, 2119–2129.

Vidal, N. and Hedges, S. B. (2004). Molecular evidence for a terrestrial origin of snakes. *Proceedings of the Royal Society of London Series B Supplementary* **271**, S226–S229.

Vincent, S. E., Herrel, A. and Irschick, D. J. (2005). Comparisons of aquatic versus terrestrial predatory strikes in the pitviper, Agkistrodon piscivorus. *Journal of Experimental Zoology Part A: Comparative Experimental Biology* **303**, 476–488.

Vitt, L. J. and Caldwell, J. P. (2009). *Herpetology: an introductory biology of amphibians and reptiles*. New York: Academic press.

Wagner, H. and Blickhan, R. (1999). Stabilizing Function of Skeletal Muscles: an Analytical Investigation. *Journal of Theoretical Biology* **199**, 163–179.

Walton, M., Jayne, B. C. and Bennet, A. F. (1990). The energetic cost of limbless locomotion. *Science* **249**, 524–527.

Whitford, M. D., Freymiller, G. A., Higham, T. E. and Clark, R. W. (2020). The effects of temperature on the defensive strikes of rattlesnakes. *Journal of Experimental Biology* **223**, jeb223859.

Wiens, J. J. and Slingluff, J. L. (2001). How lizards turn into snakes: a phylogenetic analysis of body-form evolution in anguid lizards. *Evolution* **55**, 2303–2318.

Wiens, J. J., Brandley, M. C. and Reeder, T. W. (2006). Why does a trait evolve multiple times within a clade? Repeated evolution of snakeline body form in squamate reptiles. *Evolution* **60**, 123–141.

Wiens, J. J., Kuczynski, C. A., Townsend, T., Reeder, T. W., Mulcahy, D. G. and Sites, J. W., Jr (2010). Combining Phylogenomics and Fossils in Higher-Level Squamate Reptile Phylogeny: Molecular Data Change the Placement of Fossil Taxa. *Systematic Biology* **59**, 674–688.

Wilson, A. M., Lowe, J. C., Roskilly, K., Hudson, P. E., Golabek, K. A. and McNutt, J. W. (2013). Locomotion dynamics of hunting in wild cheetahs. *Nature* **498**, 185–189.

Yamamoto, A., Takagishi, K., Osawa, T., Yanagawa, T., Nakajima, D., Shitara, H. and Kobayashi, T. (2010). Prevalence and risk factors of a rotator cuff tear in the general population. *Journal of shoulder and elbow surgery* **19**, 116–120.

Yeaton, I. J., Ross, S. D., Baumgardner, G. A. and Socha, J. J. (2020). Undulation enables gliding in flying snakes. *Nature Physics* **16**, 974–982.

Yi, H. and Norell, M. A. (2015). The burrowing origin of modern snakes. *Science Advances* **1**, e1500743.

Young, B. A. (2010). How a heavy-bodied snake strikes quickly: high-power axial musculature in the puff adder (Bitis arietans). *Journal of Experimental Zoology Part A: Ecological Genetics and Physiology* **313**, 114–121.

Young, J. W., Russo, G. A., Fellmann, C. D., Thatikunta, M. A. and Chadwell, B. A. (2015). Tail function during arboreal quadrupedalism in squirrel monkeys (Saimiri boliviensis) and tamarins (Saguinus oedipus). *Journal of Experimental Zoology Part A: Ecological Genetics and Physiology* **323**, 556–566.

Zakani, S., Rudan, J. F. and Ellis, R. E. (2017). Translatory hip kinematics measured with optoelectronic surgical navigation. *International journal of computer assisted radiology and surgery* **12**, 1411–1423.

Zhen, W., Gong, C. and Choset, H. (2015). Modeling rolling gaits of a snake robot. In *2015 IEEE international conference on robotics and automation (ICRA)*, pp. 3741–3746. IEEE International Conference on Robotics and Automation.

Zug, G. R., Vitt, L. J. and Caldwell, J. P. (2001). *Herpetology: an introductory biology of amphibians and reptiles*. 2nd ed. San Diego: Academic Press.

APPENDICES

APPENDIX A

NORMAL (GRAY) AND ALTERED (RED) VERTEBRAE OF SNAKES

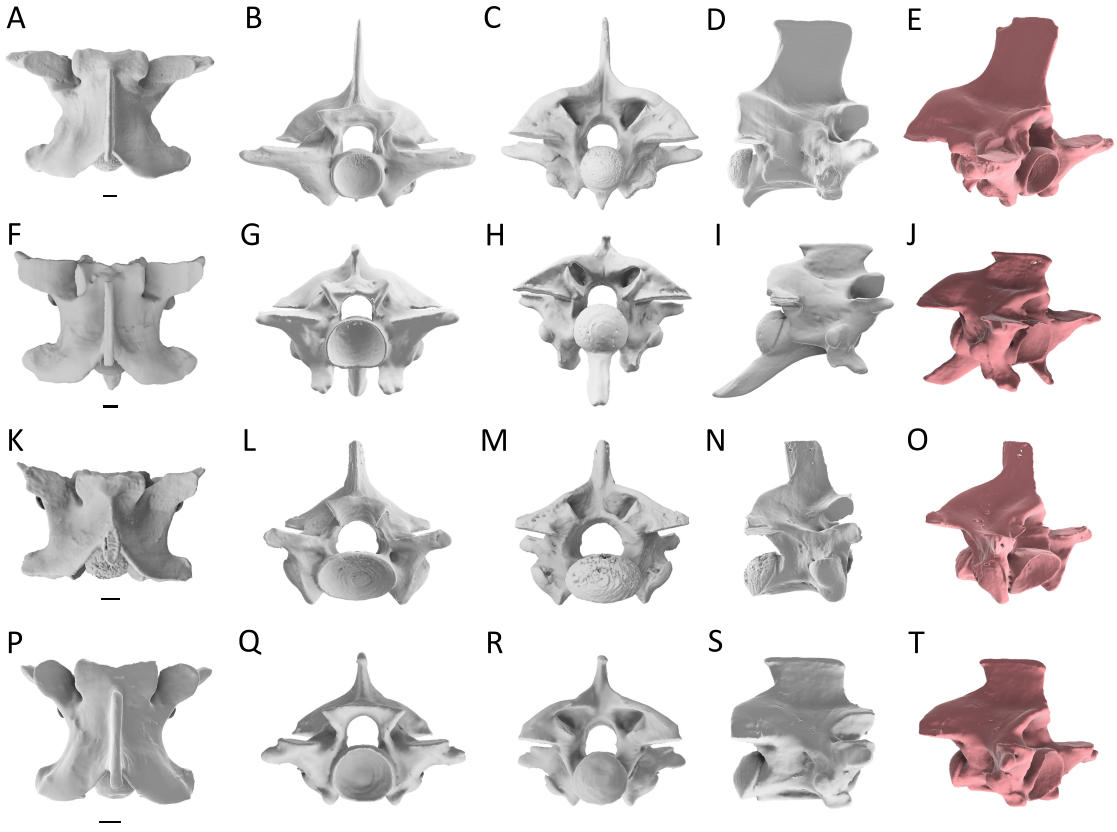

Dorsal (A, F, K, P), anterior (B, G, L, Q), posterior (C, H, M, R), and lateral (D, I, N, S) views. Posterior altered vertebrae in oblique view (E, J, O, T). *B. irregularis* (A-E), *C. viridis* (F-J), *B. constrictor* (K-O), and *P. guttatus* (P-T) respectively. Scale bars = 1 mm.

APPENDIX B

OVERLAP OF THE YAW-PITCH ROM BETWEEN THE NORMAL VERTEBRA AND THE HIGH ROLL OF ITS CORRESPONDING ALTERED VERTEBRA

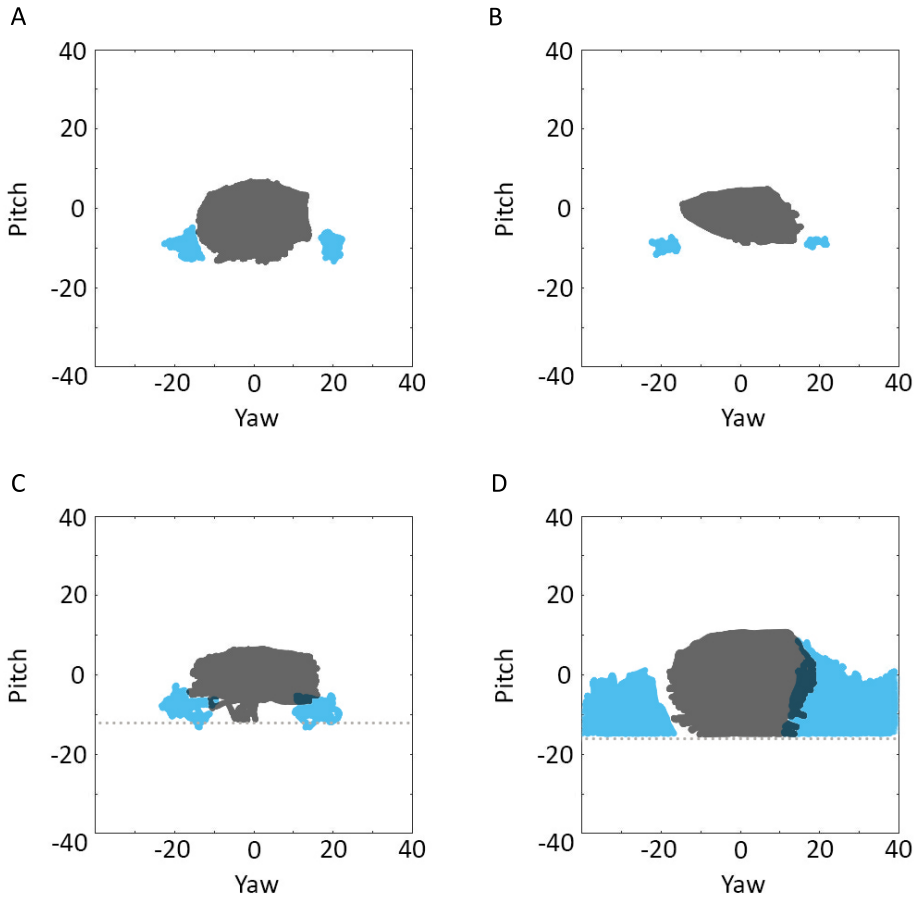

Normal ROM is black and high roll ROM is blue. (A) Brown tree snake ROM from the normal vertebra and high roll of the altered vertebra showing no overlap. (B) Prairie rattlesnake ROM from the normal vertebra and high roll of the altered vertebra showing no overlap. (C) Boa constrictor ROM from the normal vertebra and high roll of the altered vertebra showing 3% overlap. (D) Corn snake ROM from the normal vertebra and high roll of the altered vertebra showing 11% overlap. The gray dotted line highlights the arbitrary ventral cutoff of some species.

APPENDIX C

OVERLAP OF YAW-PITCH ROM BETWEEN SPECIES NORMAL VERTEBRAE

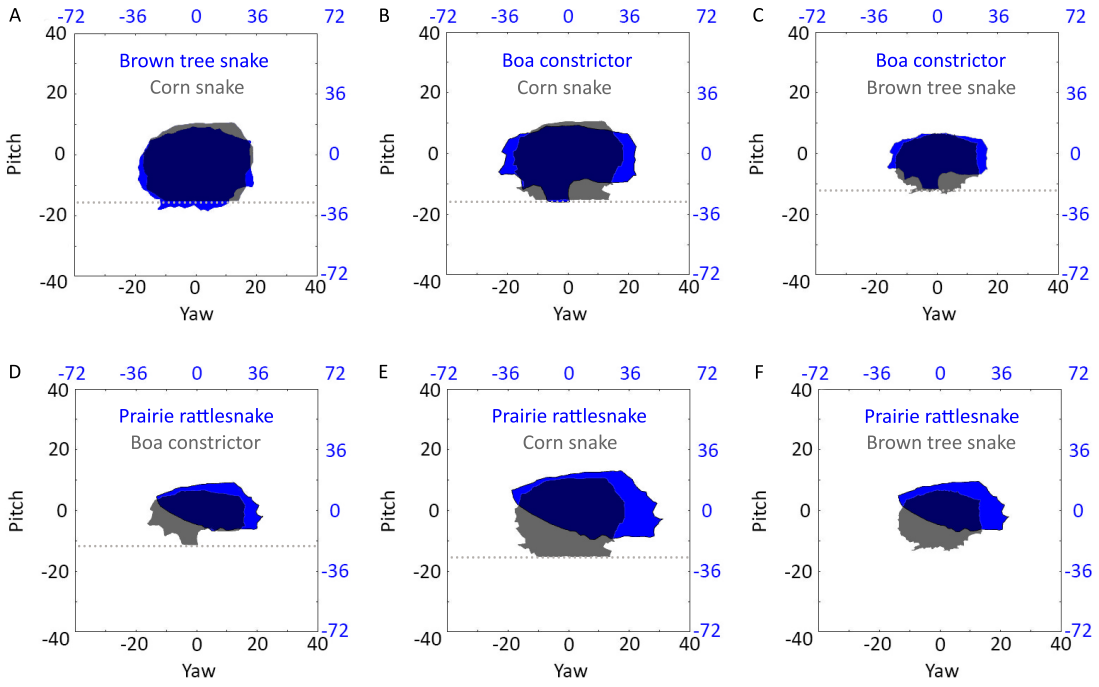

Blue ROM is always normalized to the black ROM. (A) Brown tree snake ROM normalized to the corn snake ROM. (B) Boa constrictor ROM normalized to the corn snake ROM. (C) Boa constrictor ROM normalized to the brown tree snake ROM. (D) Prairie rattlesnake ROM normalized to the boa constrictor ROM. (E) Prairie rattlesnake ROM normalized to the corn snake ROM. (F) Prairie rattlesnake ROM normalized to the brown tree snake ROM. The gray dotted line highlights the arbitrary ventral cutoff of some species.

APPENDIX D

OVERLAP OF YAW-PITCH ROM BETWEEN SPECIES ALTERED VERTEBRAE

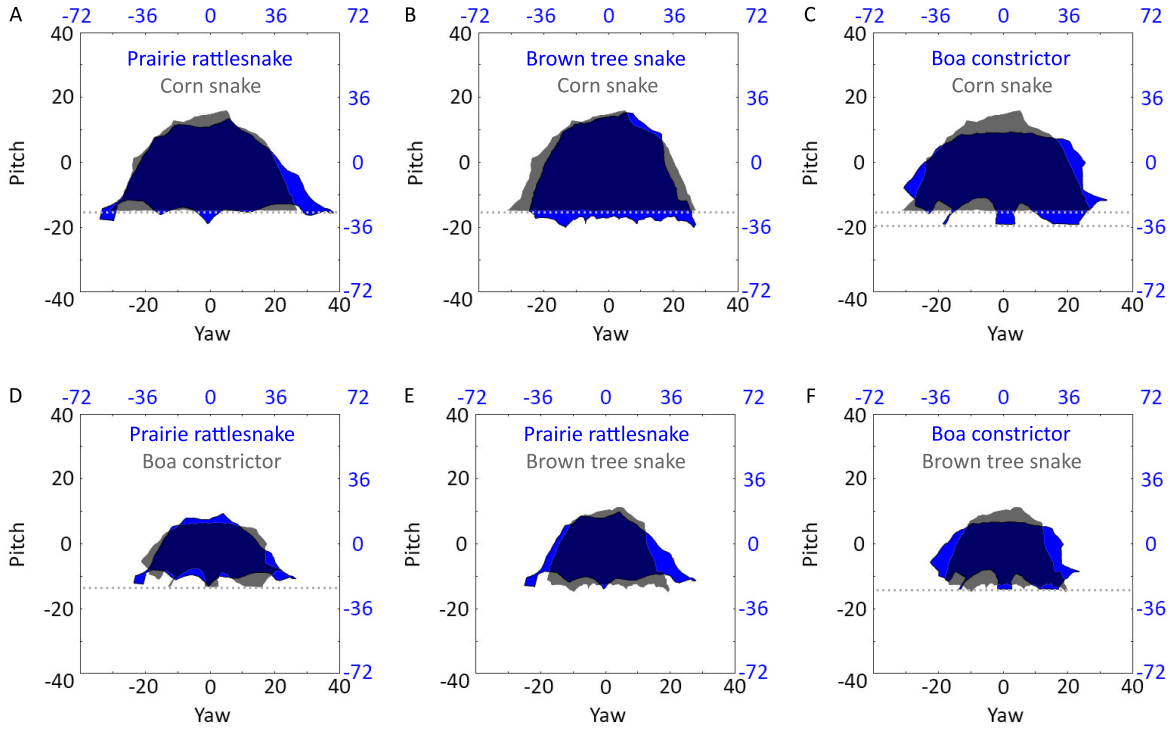

Blue ROM is always normalized to the black ROM. (A) Prairie rattlesnake ROM normalized to the corn snake ROM. (B) Brown tree snake ROM normalized to the corn snake ROM. (C) Boa constrictor ROM normalized to the corn snake ROM. Note there are two gray dotted lines due to the shifting of the boa ROM from being normalized to the corn snake ROM. (D) Prairie rattlesnake ROM normalized to the boa constrictor ROM. (E) Prairie rattlesnake ROM normalized to the brown tree snake ROM. (F) Boa constrictor ROM normalized to the brown tree snake ROM. The gray dotted line highlights the arbitrary ventral cutoff of some species.

APPENDIX E

PERCENT OVERLAP OF NORMAL YAW-PITCH ROM

	% Overlap of Normal Yaw-pitch ROM Areas			
Species	*B. irregularis*	*C. viridis*	*B. constrictor*	*P. guttatus*
B. irregularis	-	56	82	89
C. viridis	-	-	69	64
B. constrictor	-	-	-	82
P. guttatus	-	-	-	-

Values of percent overlap between yaw-pitch areas of normal isolated vertebrae normalized by areas to make the ROM areas equivalent. The top row represents a reference vertebra, and 100% overlap means it entirely engulfs the other ROM.

APPENDIX F

PERCENT OVERLAP OF ALTERED YAW-PITCH ROM

	% Overlap of Altered Yaw-pitch ROM Areas			
Species	*B. irregularis*	*C. viridis*	*B. constrictor*	*P. guttatus*
B. irregularis	-	82	79	87
C. viridis	-	-	84	89
B. constrictor	-	-	-	85
P. guttatus	-	-	-	-

Values of percent overlap between yaw-pitch areas of altered isolated vertebrae normalized by areas to make the ROM areas equivalent. Top row represents reference vertebra and 100% overlap means it engulfs the others ROM.

APPENDIX G

SUMMARY OF THE FORCE PLOTS IN ALL SNAKE TRIALS

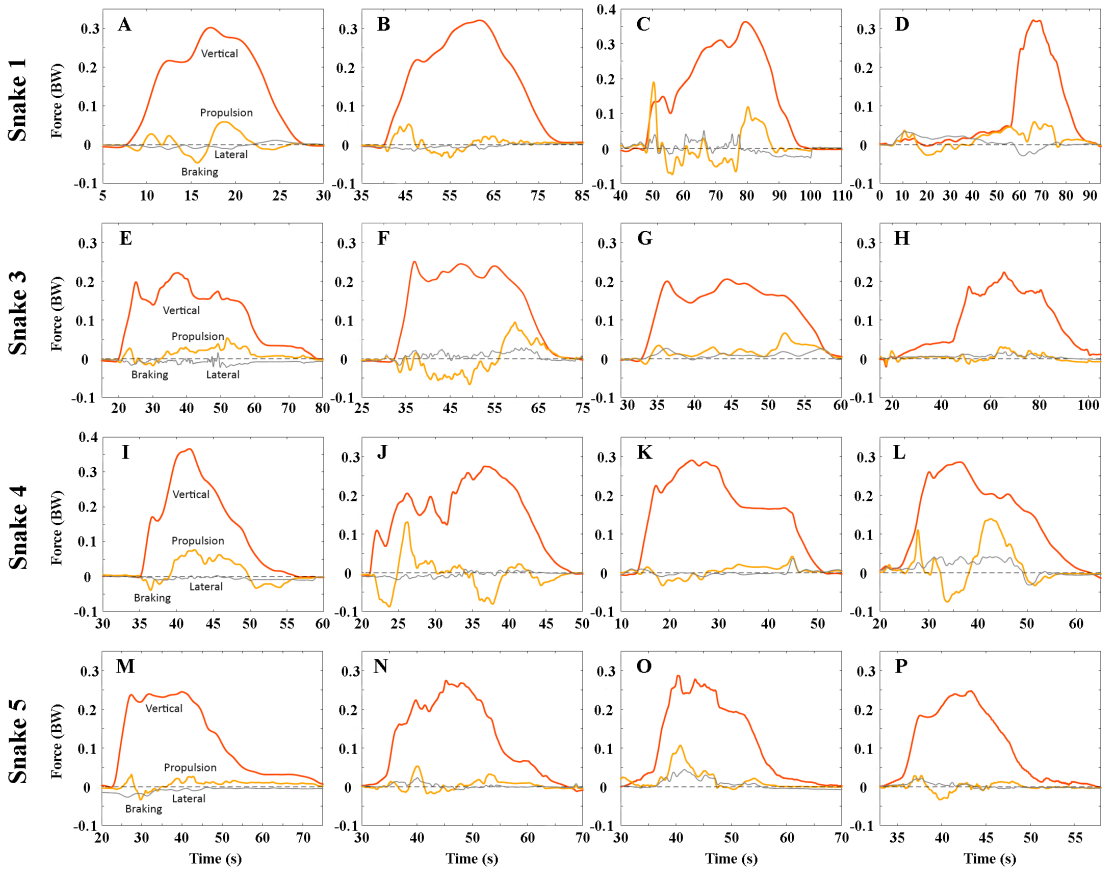

All trials we obtained showing the forces (BW) as the snake passed along the force-sensing dowel. Trials involving snake 1 are represented by A-D, snake 3 E-H, snake 4 I-L, and snake 5 M-P. Snakes 2 and 6 were not included as they would not cooperate.

APPENDIX H

SUMMARY OF THE FORCE PLOTS IN ALL ROPE TRIALS

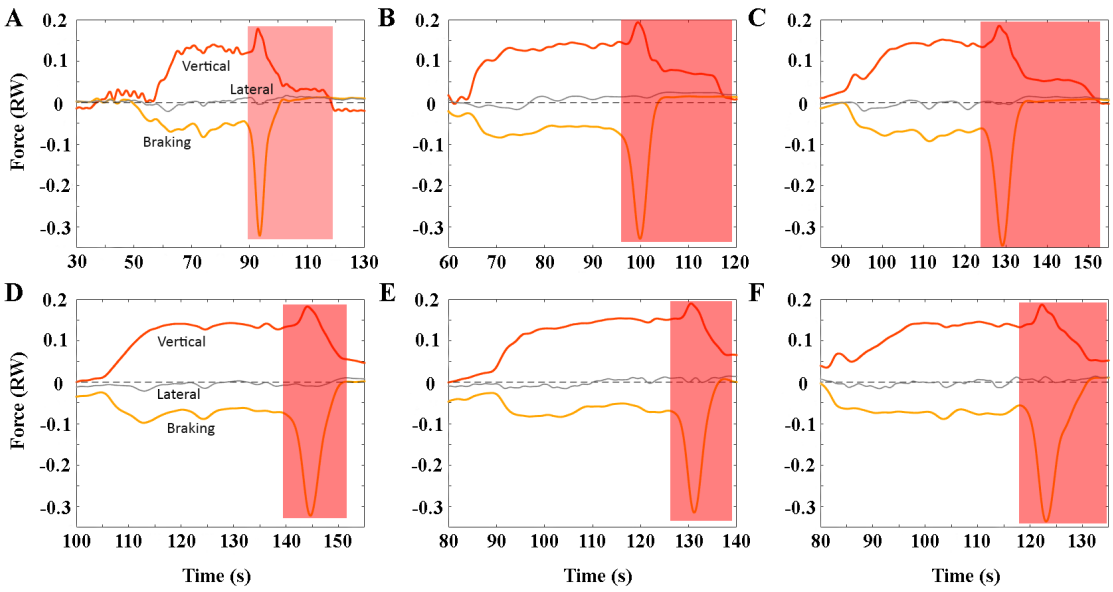

All trials obtained from the inert nylon rope dragged across the force-sensing dowel. The red region shows when the rope fell off the dowel adjacent to the force-sensing dowel, generating substantial forces due to inertial motion. This region was excluded from our analysis.

APPENDIX I

TRIALS WITH MINIMAL-TO-NO PROPULSIVE FORCE

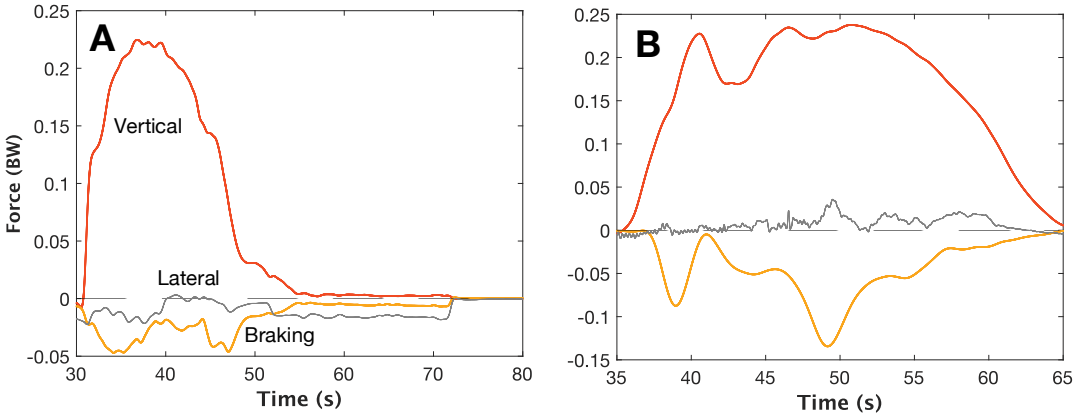

All trials obtained that have purely braking force (or nearly so). Trials are from snake 4 (A) and snake 3 (B).

APPENDIX J

REACTION FORCES OF THE CORN SNAKE ON TWO WEDGES

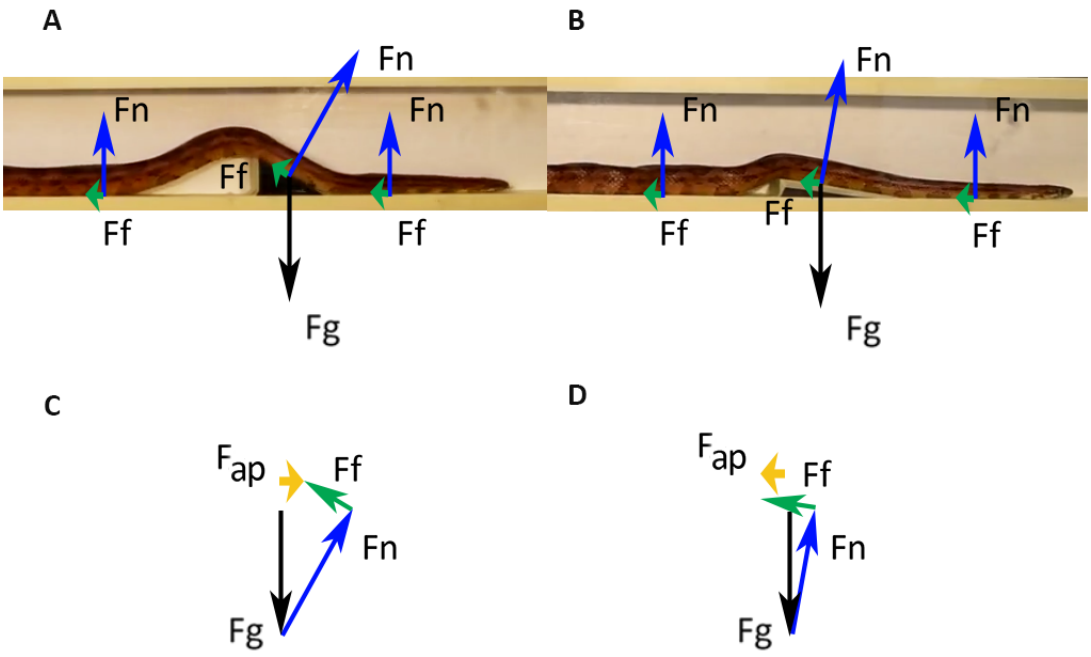

A) Reaction forces for the corn snake vertically undulating against the wedge at 30°. Fap-anteroposterior force, Ff-frictional force, Fg-gravitational force, Fn-normal force. B) Reaction forces for the corn snake using concertina against the wedge at 10°. C) Body diagram summarizing the forces from A showing a net propulsive force. D) Body diagram summarizing the forces from B showing a net braking force.

APPENDIX K

SNAKE STRIKING PLATFORM

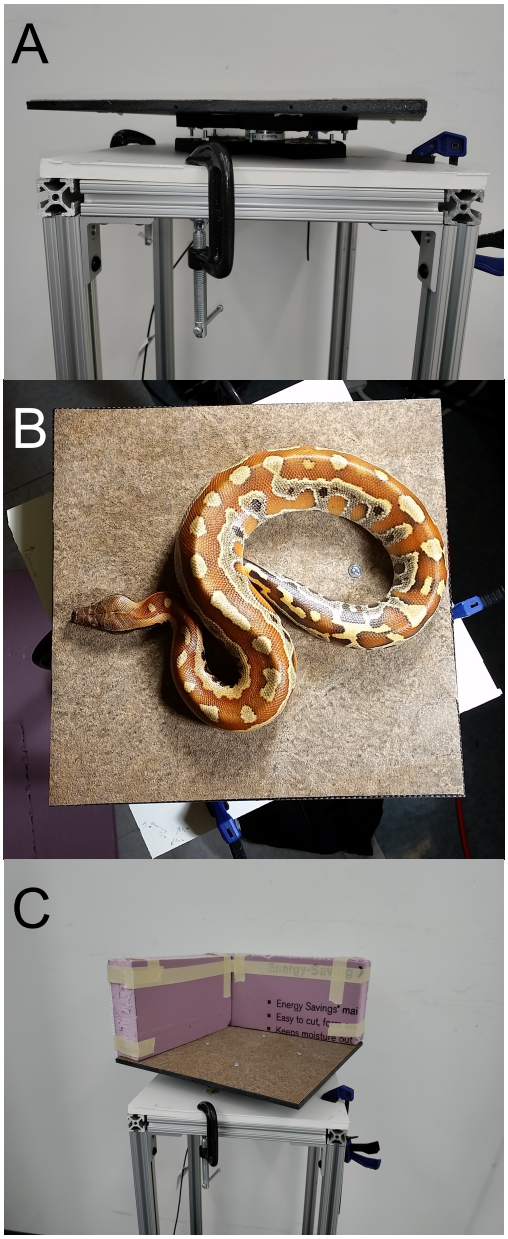

Snake striking platform showing side view (A) and our open (B) and walled setups (C).

APPENDIX L

SNAKE STRIKE DATA FROM THE OPEN SETUP FOR ALL INDIVIDUALS

Ind.	Trial	Max. Fore-aft Force (BW)	Max. Lat. Force (BW)	Max. Vert. Force (BW)	Max. Total Force (BW)	Fore-Aft Impulse (BW*s)	Max. Vel. (m/s)	Max. Accel. (m/s^2)	Str. Dist. (m)	Max. Tail Veloc.	Max. Tail Accel. (m/s^2)	Strike Dur. (ms)	Max. Tail Dist. (m)
1	1	0.33	0.14	1.58	1.60	0.15	2.48	80.16	0.22	0.73	31.48	50	0.03
	2	0.51	0.30	1.80	1.88	0.25	2.88	104.02	0.24	1.98	49.39	40	0.14
	3	0.41	0.17	3.74	3.76	0.05	3.38	119.90	0.14	1.28	28.31	60	0.06
	4	0.32	0.28	1.70	1.73	0.06	3.77	121.95	0.15	0.62	9.33	60	0.06
	5	0.51	0.33	1.86	1.94	0.21	2.20	77.18	0.16	0.67	18.42	50	0.04
	6	0.32	0.27	1.75	1.78	0.13	2.82	104.73	0.17	1.07	31.21	50	0.10
3	1	0.20	0.30	1.25	1.28	0.06	3.82	157.56	0.23	1.25	28.45	50	0.08
	2	0.42	0.35	1.03	1.14	0.19	4.26	148.62	0.18	1.20	31.30	40	0.10
	3	0.50	0.39	1.05	1.09	0.19	3.82	95.32	0.19	0.67	25.73	70	0.03
	4	0.39	0.37	1.27	1.45	0.12	4.50	122.64	0.21	0.91	46.92	70	0.07
	5	0.41	0.15	1.06	1.12	0.20	3.66	102.56	0.19	0.84	23.73	40	0.09
5	1	0.44	0.25	1.56	1.62	0.14	3.08	96.37	0.12	1.30	62.80	40	0.09
	2	0.34	0.31	1.64	1.65	0.13	3.63	118.40	0.21	0.55	14.24	60	0.03
	3	0.34	0.16	1.41	1.46	0.14	3.23	114.48	0.14	0.17	4.00	50	0.01
	4	0.25	0.15	1.59	1.60	0.11	2.54	48.89	0.15	1.66	59.27	70	0.09
	5	0.34	0.20	1.59	1.59	0.12	3.37	111.41	0.15	0.40	8.22	60	0.04
	6	0.37	0.35	1.43	1.50	0.16	3.75	136.83	0.16	0.61	25.14	70	0.06
	7	0.20	0.21	1.36	1.38	0.09	2.05	36.74	0.08	0.23	5.28	70	0.02
6	1	0.39	0.22	1.86	1.89	0.12	3.24	89.31	0.24	1.82	101.63	50	0.07
	2	0.32	0.39	2.03	2.03	0.13	3.49	108.69	0.25	0.69	21.46	50	0.05
	3	0.32	0.44	2.13	2.14	0.17	2.37	72.08	0.29	1.09	18.74	50	0.03

	4	0.31	0.37	2.01	2.04	0.08	3.19	86.09	0.32	3.89	161.88	50	0.22
	5	0.50	0.17	1.98	2.03	0.31	2.16	70.91	0.21	4.15	190.20	30	0.19
	6	0.43	0.35	2.17	2.20	0.16	2.53	57.59	0.23	0.64	24.31	50	0.03
Avg.		0.37±0.09	0.28±0.09	1.70 ±0.55	1.74 ±0.54	0.14±0.06	3.18± 0.68	99.27± 29.86	0.19± 0.05	1.18± 0.99	42.56± 46.57	50±10	0.07± 0.05

APPENDIX M

SNAKE STRIKE DATA FROM THE WALLED SETUP FOR ALL INDIVIDUALS

Ind.	Trial	Max. Fore-aft Force (BW)	Max. Lat. Force (BW)	Max. Vert. Force (BW)	Max. Total Force (BW)	Fore-Aft Impulse (BW*s)	Max. Vel. (m/s)	Max. Accel. (m/s^2)	Str. Dist. (m)	Max. Tail Vel. (m/s)	Max. Tail Accel. (m/s^2)	Strike Dur. (ms)	Max. Tail Dist (m)
1	1	1.55	0.98	1.99	2.01	0.41	3.55	78.91	0.31	0.09	2.08	78	0.03
	2	1.96	1.58	2.19	2.57	0.72	3.56	138.22	0.36	2.16	90.93	54	0.05
	3	1.86	1.39	1.84	1.94	0.84	4.68	68.29	0.37	0.64	27.69	64	0.007
	4	0.76	1.06	1.51	1.86	0.31	3.42	103.11	0.18	0.49	7.48	60	0.02
	5	0.70	0.58	2.02	2.20	0.89	4.83	81.28	0.31	0.65	6.38	94	0.09
3	1	1.70	0.94	0.99	1.98	0.50	3.96	74.85	0.22	0.68	9.61	72	0.02
	2	1.71	0.41	1.32	1.86	0.73	3.95	58.34	0.23	0.16	21.53	60	0.01
	3	0.37	0.14	1.31	1.31	0.20	3.80	129.98	0.27	0.74	9.81	52	0.01
	4	0.49	0.58	1.26	1.29	0.16	5.74	72.00	0.32	0.66	23.85	62	0.003
	5	0.38	1.32	1.09	1.51	0.15	4.13	83.16	0.28	0.91	38.96	74	0.05
	6	0.32	0.88	1.32	1.55	0.22	3.87	147.96	0.23	0.15	6.36	64	0.001
5	1	0.35	0.92	1.38	1.56	0.17	3.14	84.86	0.17	0.25	7.06	46	0.02
	2	0.27	0.17	1.54	1.54	0.11	2.99	102.84	0.12	0.15	7.54	54	0.01
	3	0.20	0.70	1.24	1.37	0.09	2.40	90.75	0.10	0.22	4.14	62	0.01
	4	0.68	0.46	2.09	2.17	0.28	2.88	97.10	0.16	0.49	13.00	54	0.02
	5	0.29	0.78	1.34	1.34	0.06	2.58	108.00	0.10	0.12	1.63	68	0.004
	6	0.33	0.43	1.38	1.43	0.14	1.82	58.82	0.08	0.17	3.60	56	0.003
6	1	1.38	0.33	1.61	1.69	0.83	3.49	70.64	0.20	1.28	20.88	62	0.02
	2	1.14	1.88	2.02	2.08	0.27	2.33	94.28	0.26	0.79	20.46	48	0.03
	3	1.45	1.51	2.21	2.43	0.31	4.22	138.29	0.37	0.03	0.02	58	0.004
	4	2.04	0.79	2.05	2.93	0.53	3.32	104.89	0.33	0.26	2.60	54	0.03

	5	0.52	0.13	1.88	1.91	0.25	2.59	63.71	0.23	0.62	5.48	56	0.03
	6	0.59	1.22	1.89	1.91	0.12	2.63	71.88	0.30	0.06	0.20	52	0.01
Avg.		0.92±0.64	0.83±0.49	1.63 ±0.38	1.85± 0.43	0.36±0.27	3.47± 0.91	92.27 ± 26.21	0.24± 0.09	0.51± 0.49	14.41± 19.47	61±1 1	0.02± 0.02